J. F. Jenkins, Jr., Ph.D., 1952

Experimental Determination of the Cross Section for Multiple Particle Production in Carbon by Cosmic Rays at Balloon Altitudes

Thesis and Abstract Approved: R. S. Myers
Professor of Physics

Date: 9 May 1952

EXPERIMENTAL DETERMINATION OF THE CROSS SECTION FOR MULTIPLE PARTICLE PRODUCTION IN CARBON BY COSMIC RAYS AT BALLOON ALTITUDES

by
J. F. Jenkins, Jr.

Thesis submitted to the Faculty of the Graduate School
of the University of Maryland in partial
fulfillment of the requirements for the
degree of Doctor of Philosophy

1953

ProQuest LLC.
789 East Eisenhower Parkway
P.O. Box 1346
Ann Arbor, MI 48106 - 1346

ACKNOWLEDGMENTS

The author is deeply indebted to the U. S. Navy Bureau of Ordnance* for support of these studies.

The balloons for these flights were made available through the courtesy of the U. S. Navy Bureau of Aeronautics and the Office of Naval Research, the latter of which also provided the flight services. He is grateful to Mr. A. T. Bauman of the General Mills Aeronautical Research Laboratories for the fine coordination of these flights and to the General Mills flight crew for their excellent cooperation.

The necessary staff and facilities for carrying out this work were provided by the Applied Physics Laboratory, The Johns Hopkins University. Within the Applied Physics Laboratory, the writer wishes to express particular indebtedness to Dr. F. T. McClure, Chairman of the Research Center, and to the writer's immediate associates: Mr. C. L. Cessna, Miss A. M. Fogelgren and Miss K. E. Pace.

The author is pleased to acknowledge as his mentors, Professor R. D. Myers, of the Physics Department of the University of Maryland, and Professor J. A. Van Allen, Head of the Physics Department of the State University of Iowa (formerly with the Applied Physics Laboratory). The writer also appreciates the many helpful suggestions and criticisms made by Professor Van Allen, who originally proposed this problem.

*This work was done under Contract NOrd 7386.

TABLE OF CONTENTS

LIST OF FIGURES

LIST OF FIGURES

LIST OF FIGURES

I INTRODUCTION

At the present time the cross sections for the interaction of neutrons and protons with various nuclei are rather well known for energies of the initiating particles up to 300 and 340 Mev (Nevis and Berkeley cyclotrons). For energies higher than this, however, it has been established only that the value of the cross section lies in the range from 20 per cent to 100 per cent of the geometric cross section. This range of values is that obtained by exposing simple and complex targets to cosmic radiation near the top of the atmosphere (20 $g\ cm^{-2}$ and less) at various latitudes (30°-60°N geomagnetic latitude where the magnetic cut-off kinetic energies for singly charged particles of protonic mass are $8 \cdot 10^{9}$ ev and 10^{9} ev respectively). The greater amount of these data has been obtained by means of nuclear emulsions (complex target) carried to altitude by balloons.[1,2,3,4]

In arriving at cross section values the complex target is divided into two categories; namely, the light nuclei, C, N and O in the gelatine and the heavy nuclei Ag, Br and I of the emulsion. Thus there

---

[1]E. O. Salant, J. Hornbostel, C. B. Fisk and J. E. Smith, Phys. Rev. 79, 184 (1950).

[2]J. Hornbostel and E. O. Salant, Phys. Rev. 76, 849 (1949).

[3]E. O. Salant, Proc. Echo Lake Cosmic Ray Symp., Paper No. 26 (1949).

[4]M. Schein, Proc. Echo Lake Cosmic Ray Symp., Paper No. 27 (1949).

are obtained the weighted mean cross sections for these two groups and their combination. Other methods for obtaining these data through the use of emulsions are: by "loading" the emulsions rather heavily with an element in the form of a powder, and by making "sandwiches" of thin metal foils between emulsion faces.[1] By the latter method Barbour and Green have shown that the cross section for the production of stars having two or more heavy prongs is proportional to $A^{2/3}$ for foils of Ni, Cu, Sn, Pt and An. Bradt and Peters[2,3] using glass "sandwiches" (mainly O and Si) have shown that the cross section for heavy primaries ($Z \geq 2$) interacting with glass is $\sim$60 per cent of the geometric value. The further work of Kaplon et al[4] using brass "sandwiches" has shown agreement with the glass case. The resulting empirical cross section is $\sigma = \pi (r_1 + r_2 - 2\,\Delta r)^2$ where r_1 and r_2 are the radii of the interacting nuclei ($r_i = 1.45 \cdot 10^{-13} A_i^{1/3}$ cm) and $\Delta r = 1.0 \cdot 10^{-13}$ cm. Van Allen[5] used a Geiger counter array as a burst detector under various thicknesses of Al and Pb to determine the transition effect for those two elements (in V-II and Aerobee rockets

---

[1] Ian Barbour and Lawrence Green, Phys. Rev. 79, 406 (1950).

[2] H. L. Bradt and B. Peters, Phys. Rev. 77, 54 (1950).

[3] H. L. Bradt and B. Peters, Phys. Rev. 80, 943 (1950).

[4] M. F. Kaplon, B. Peters, H. L. Reynolds and D. M. Ritson, Phys. Rev. 85, 295 (1952).

[5] J. A. Van Allen, Proc. Echo Lake Cosmic Ray Symp., Paper No. 28 (1949).

at 41°N geomagnetic latitude) and from the rising side of these transition curves the cross sections were calculated giving as a result nearly geometric values. The efficiency of the burst detector was estimated by comparing the increase in counting rate of a single counter in the burst detector with the increase in the number of bursts throughout the flight.

In the balloon flights of Salant et al, corrections were made to account for: heavy primaries, absorption of primary flux and secondary mesons and from this he obtained a cross section for energetic protons on emulsion materials of approximately 60 per cent of the geometric cross section.

It was proposed that an experimental determination of the absolute cross sections for multiple particle production, in various elements, by cosmic radiation at balloon altitudes be made by using Geiger counter techniques. It was felt that a counter telescope with an associated single element target and an efficient burst detection array would overcome the lack of "cleanness" of many of the experiments described above (see Fig. I-1). The main points of improvement are as follows:

(1) The use of a single element target will assure the measurement of bursts produced mainly in this target.

(2) The proposed experiment can be used to investigate a wide range of target thicknesses and hence to demonstrate that the dependance of burst production on target thickness is linear for targets thinner than $\sim$20 per cent of the geometric mean path

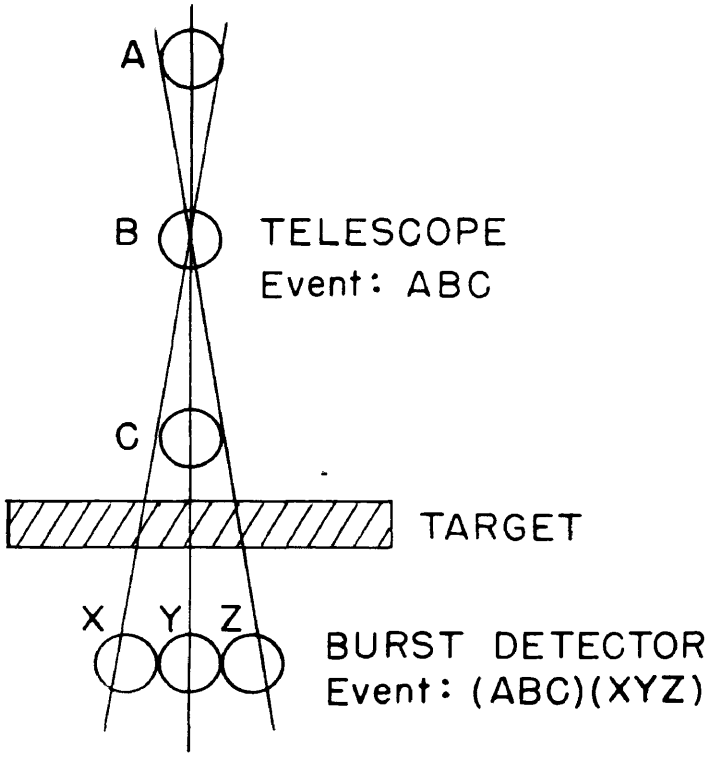
A
B
TELESCOPE
Event: ABC
C
TARGET
X
Y
Z
BURST DETECTOR
Event: (ABC)(XYZ)

Fig. I-1 [illegible]

for burst production. This investigation would include the case of no target to establish the burst production due to the equipment normally associated with the target.

(3) The measurements cited above have included an initiating flux which extends over the entire upper hemisphere and are, therefore, not characteristic of the primary flux but are characteristic of the modified primary flux at all zenith angles plus the secondary flux. It is seen that the definition of the initiating flux in a cone of approximately 30° half angle, by means of a counter telescope, will provide an improved basis for computation of the cross sections for primary cosmic radiation.

(4) The directional intensity as computed from each of the telescope counting rates obtained in one flight will serve as: an internal reliability check (internal comparison), an external reliability check (comparison with the results of other workers in the field) and a measurement of the burst producing flux.

(5) The telescope event is attributable to the passage of ionizing radiation; hence, with the consideration of the no target case, the burst production rate in any target can be determined and this must be assigned to an initiating flux of energetic charged particles.

The experiment proposed above was carried out for carbon targets. "Sky-hook" type balloons carried the equipment to 100 K ft. in two flights from Pyote Air Force Base, Texas, (41°N geomagnetic latitude) on 23 January 1952 and 2 February 1952.

II THE EXPERIMENTAL EQUIPMENT

The basic considerations in the design of equipment to be carried to high altitudes by balloons are those of weight, general reliability, and shape for ease of launching.

Of prime importance in the design of this equipment was the telescope-target-burst-detector array since the other components were only to exist as a service for the cosmic-ray end-organ.

The purpose of the telescope was two-fold in that a nearly vertical beam of incoming cosmic rays must be defined in order to insure the observation of only the nearly primary flux and a measurement of the actual burst-producing flux must be obtained. In order that the purity of the effective target be assured, it was necessary to use very thin-walled counters in the telescope. The Victoreen 1B85 Thyrode was selected as the counter to be used in the telescope. This counter has the following characteristics according to the manufacturer: maximum threshold voltage 800 v, plateau length 200 v, plateau slope 3 per cent per 100 v, recovery time 100 μ sec, life 10^9 counts, wall thickness 30 mg cm^{-2} Al, diameter 2 cm, electrode capacitance 2 $\mu\mu$ f and ambient temperature for operation - 10 to 100°C.* The effective length (see App. 2) is 5.92 cm and the intrinsic efficiency is 96 per cent (see

*The experience of other workers (private communication, E. Ney and J. Winckler, University of Minnesota) using balloons for carrying cosmic-ray equipment has shown that the temperature within a covered gondola decreases slightly during the rapid part of the balloon ascension due to convection and then increases again at floating altitudes to a value near 25°C.

App. 1). The telescope was then designed to have an effective cone of half angle 30°. The product of the above design criteria was a two-tray telescope with two contiguous 1B85 counters in each tray and a tray separation of 8 cm. To reduce the high accidental counting rate inherent to double coincidence circuits (practical resolving times), a third similar tray was interposed between the two and the telescope event was then the triple coincidence counting of the three trays. Eight "production" models of this telescope were built, one of which is shown in Figs. II-1 and -2. The 1B85 counter is fragile so in order to allow for the possible need for spare counters, the pulse height and plateau characteristics were determined for 96 of them rather than for just the 48 needed for the eight telescopes. A plateau characteristic for a typical 1B85 counter is shown in Fig. II-3.

Carbon was chosen as the target material for two reasons: it is the lightest element that is both easy to handle and to obtain and if an accurate value for the cross section were known for carbon, then the cross section for hydrogen could be determined in subsequent experiments using a hydrocarbon target. The container which held the carbon target was placed such that the upper surface of a target 6 cm thick (20% m.f.p. for burst production assuming geometric cross section) would be 2 cm from the cylindrical cases of the counters in the lowest tray of the telescope. The area of the target was such as to more than fill the aperture of the telescope. Thus any thickness of target from 0 to 6 cm could be mounted at the c.g. position of the 6

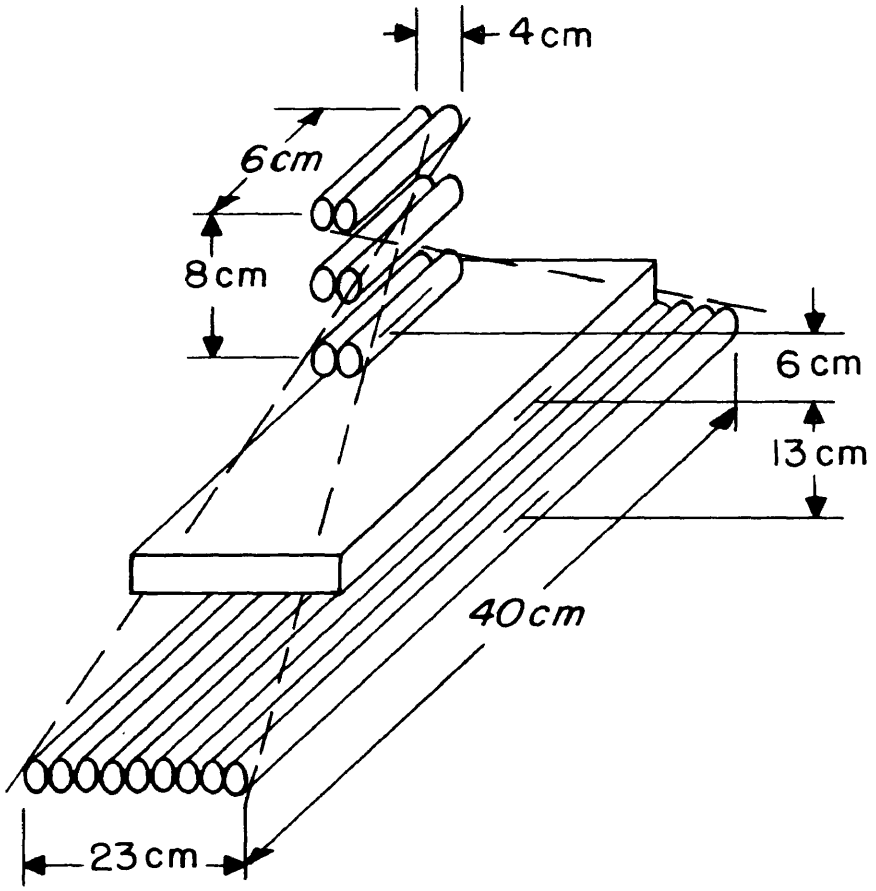

Fig. II-1 SCHEMA OF DEVICE OF THE PRESENT, PARTIAL AND MOTOR DRIVEN [illegible]

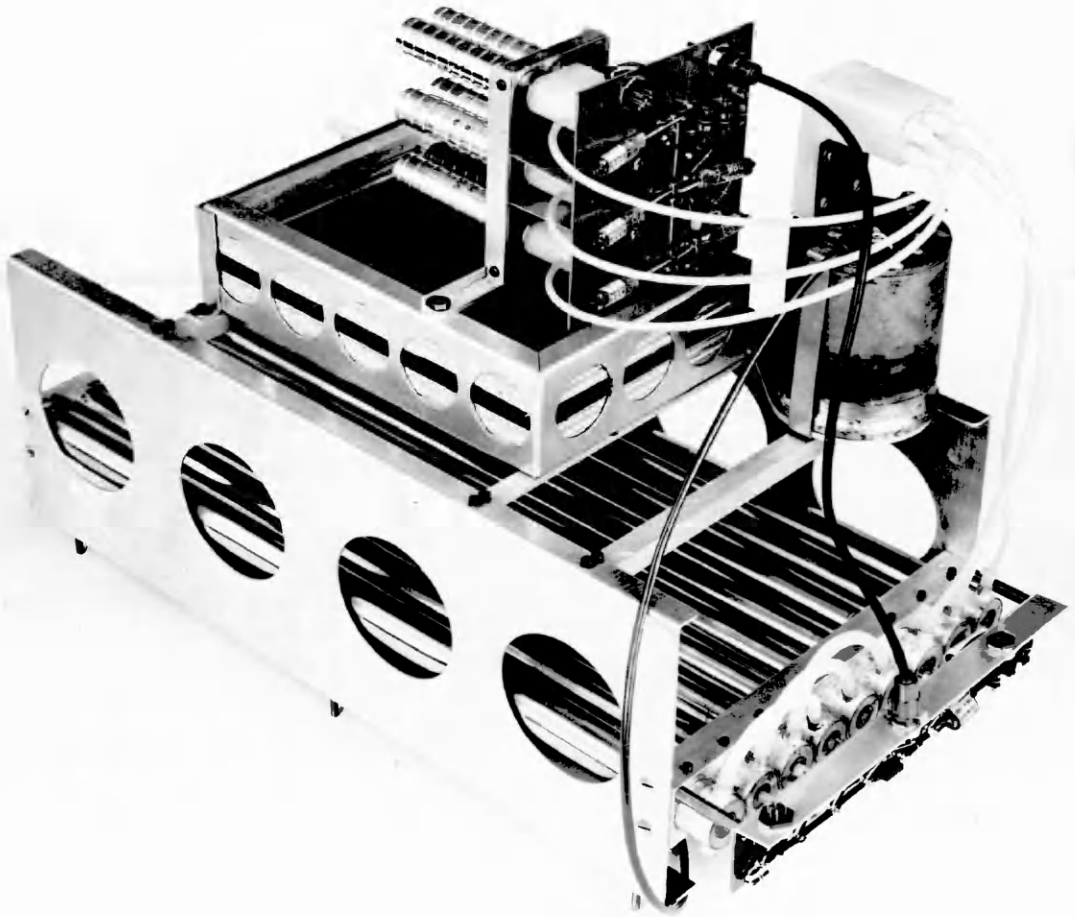

Fig. II-2 PHOTOGRAPH OF TELESCOPE, 1 cm TARGET AND BURST DETECTOR ARRAY

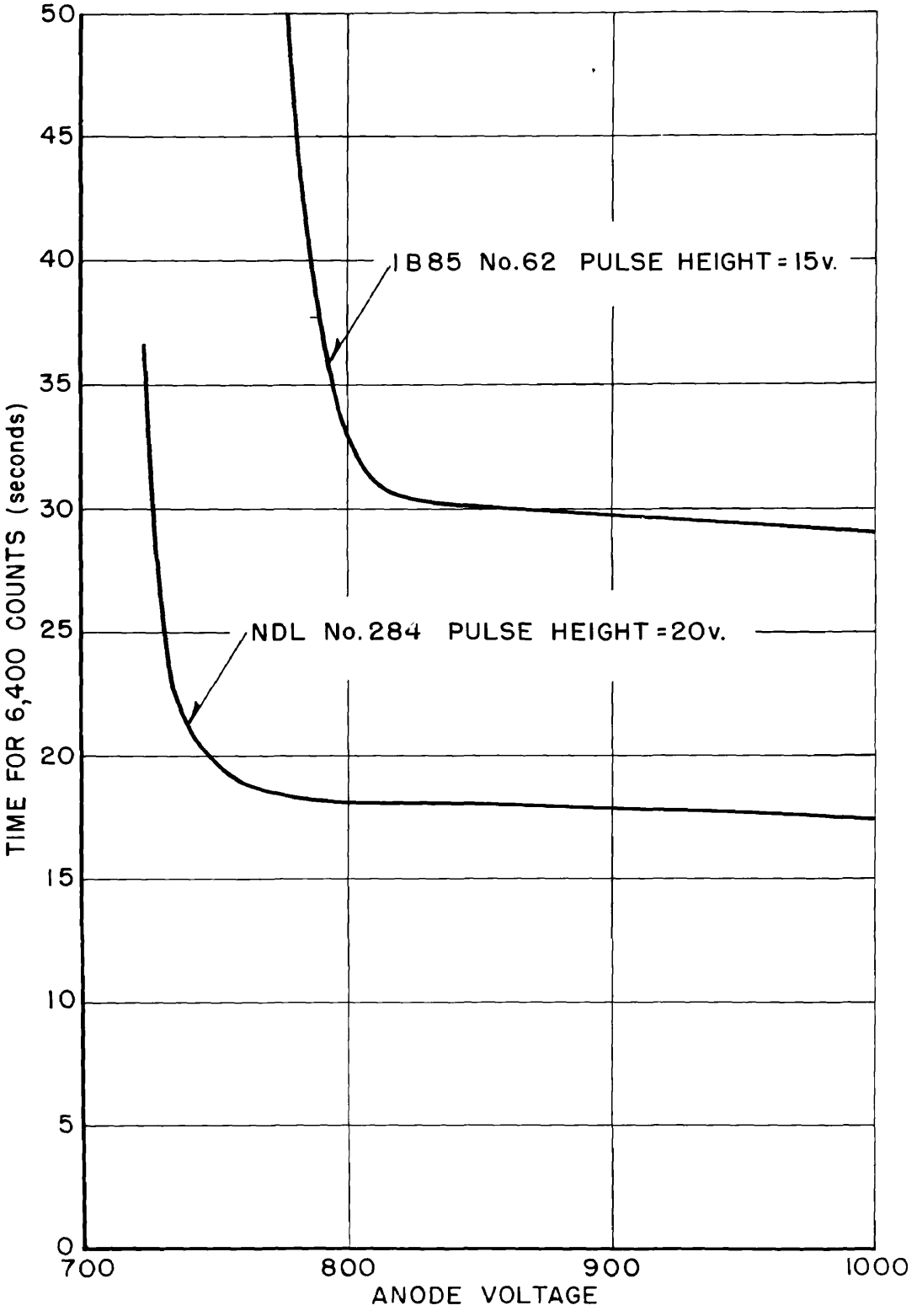

Fig. II-3 PLATEAU CHARACTERISTICS OF TYPICAL 1B85 AND NDL COUNTERS

cm target by using open wooden spacer frames (see Figs. II-2 and 4).

In the design of an ideal burst detector it would be desirable to be able to detect any event consisting of the traversal of the detector by two or more particles initiating in the target. The only known practical detectors of this type are the cloud chamber and the nuclear emulsion. From the point of view of experimental complexity, the balloon-borne cloud chamber is poor. Both of these methods suffer from the extreme difficulty of data reduction and recovery of the exposed film soon after landing.

The second choice is the scintillation burst detector in which the scintillator is used as the target. The objections to this method are that the nature of the scintillator (e.g. anthracene plus container) is that of a complex target and a limited number of compounds are efficient scintillators. The first objection might be vitiated in principle on the grounds that two such counters could be flown, one surrounded by the target material and the other with no external target and the difference between them would yield the desired events. However, for the study of thin targets this difference would be small compared to the statistical fluctuations which would be obtained in six-hour balloon flights at high altitudes and the objection obtains on practical grounds.

The third choice for a detector is a group of pulse ionization chambers in which the output is gated by the telescope event. This detector was found to be inadequate in that with present circuit designs the noise level is such that no less than five minimum ionization particles in a chamber of reasonable dimensions will yield a

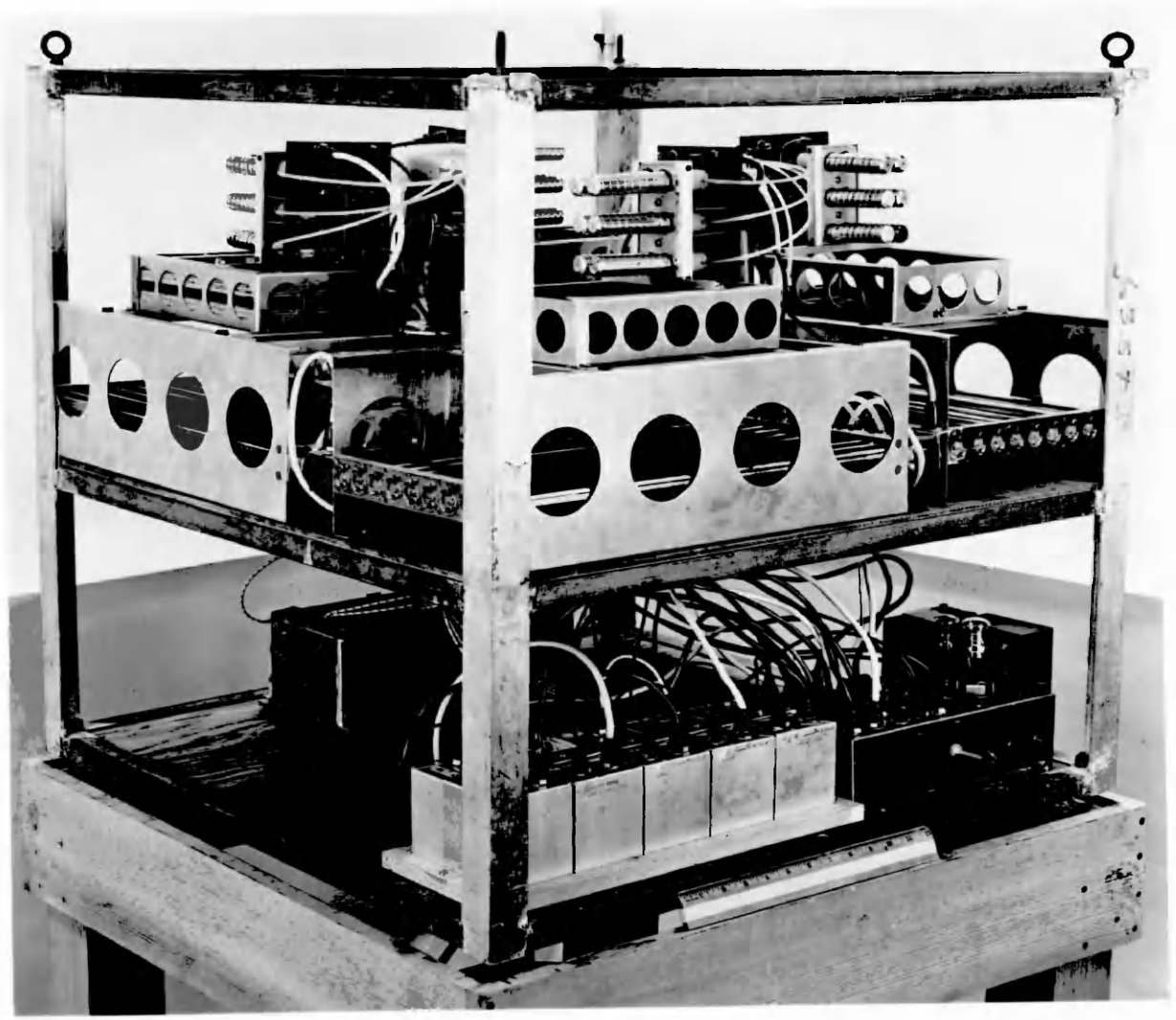

Fig. II-4 PHOTOGRAPH OF COMPLETE INSTRUMENTATION GONDOLA

detectable output.

The fourth choice is a Geiger-counter array involving multiple coincidence. This scheme is attractive in that many types of counters are commercially available and the coincidence circuitry is simple. Examination of a large number of burst events produced in nuclear emulsions suggested that fair detection efficiency could be obtained with a plane array of nine contiguous counters arranged in three coincidence groups of three counters in parallel and interlaced in such a way that two counters of each of two groups would be interposed between two counters of one group. Thus the burst detector event would consist of $(1 + 1' + 1'')\ (2 + 2' + 2'')\ (3 + 3' + 3'')$ or simply (123)* where the counters are numbered as shown in Fig. II-1. The counters selected for use in this array were obtained from Nuclear Development Laboratories, Kansas City, Missouri. The characteristics of these counters are given as follows: maximum threshold voltage 750 v, plateau length 250 v, plateau slope 2 per cent per 100 v, recovery time 150μ sec, life 10^9 counts, wall thickness .025 cm brass, diameter 2.54 cm., length $\sim$42 cm, intrinsic efficiency 99 per cent, and ambient temperature for operation -10 to 100°C. This array was then placed at such a distance below the telescope and target as to fill completely the telescope aperture. The pulse height and plateau characteristic was obtained for 96 of these counters of which 72 were used in the eight burst detectors. A plateau

---

*Notation after the algebra of Boole; thus $1 + 1'$ means 1 and/or 1' and $(1)(2)$ means 1 with 2.

characteristic for a typical NDL counter is shown in Fig. II-3.

It was decided that one high voltage supply should be used for each telescope and burst detector to enhance the reliability of the system. The basic high voltage power supply was the Eltron Vibrator Power Supply Mod. 103-D6. This supply operates on a d.c. input of from 2.5 to 3.5 v at 130 ma to give 920 v regulated for loads from 0-50 μa. These units are claimed to be hermetically sealed by the manufacturer but tests at low ambient pressures showed that the units were sparking over internally. It was then necessary to design a pressurized container which could be tested for leakage. The resulting container design incorporated a small copper pump-out tube which was swaged and soldered to effect the final seal. Eight of these containers were produced and leak tests showed the largest leakage rate to be .13 psi/hr. This is satisfactory since in a ten-hour balloon flight the container pressure would fall by only 1.3 psi. The containers were pumped down to about 25 microns for about one hour; then dry air was admitted to ambient pressure and the seal was made in the copper pump-out tube. One of the final units is shown mounted on the telescope-target-burst detector frame in Fig. II-2.

It was necessary to incase the high voltage wiring in a material with good dielectric properties to prevent corona and spark-over at low ambient pressures. The material selected for this purpose was polyethylene since an injection-molding press for this plastic was readily available. Three types of connector were designed and injection-molded to be used on the telescope counters, the burst detector counters and the high voltage supply. The first of these was a double connector for

each telescope counter tray. The 50 μμ f coupling and high voltage isolating capacitor was molded into the unit along with the 1.2 megohm anode resistor and two 1/4" grid caps for connection to the counters. The output from the 50 μμf coupling capacitor appeared on a small pin-jack molded into the connector and the polyethylene insulated high voltage lead-in wire was connected to the 1.2 megohm anode resistor and molded into the connector. The lead-in terminated at the other end in a male polyethlene plug. This is the first unit shown in Fig. II-5. The mounting plate which held the telescope counters was provided with metal partitions which shielded these connectors from each other to reduce cross-talk between trays. The seal between the counter and the connector was then made by filling the gap between the two with silicone ignition compound. The second type of connector was designed for use on the burst detector counters. This connector is similar to the first type in the input, output and lead-in features but in addition it provides for the shielding and paralleling of three separated counters. The inter-connecting leads were made of small diameter (.004") music wire and leads from different counter groups were crossed (no parallel runs) to reduce the capacity between wires and therefore reduce the cross-talk between the three groups of counters. Each connector was completely shielded, except for the inter-connecting wire and the lead-in wire, to reduce cross-talk. This connector is the second unit shown in Fig. II-5. The third polyethelene connector was to serve as a manifold for distributing the high voltage power supply output to the six lead-in

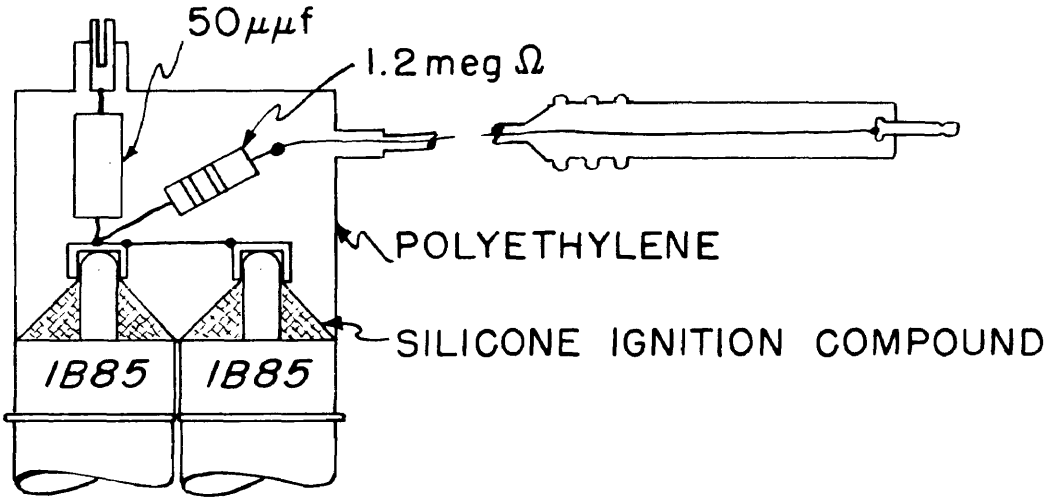
50μμf
1.2meg Ω
POLYETHYLENE
SILICONE IGNITION COMPOUND
1885
1885

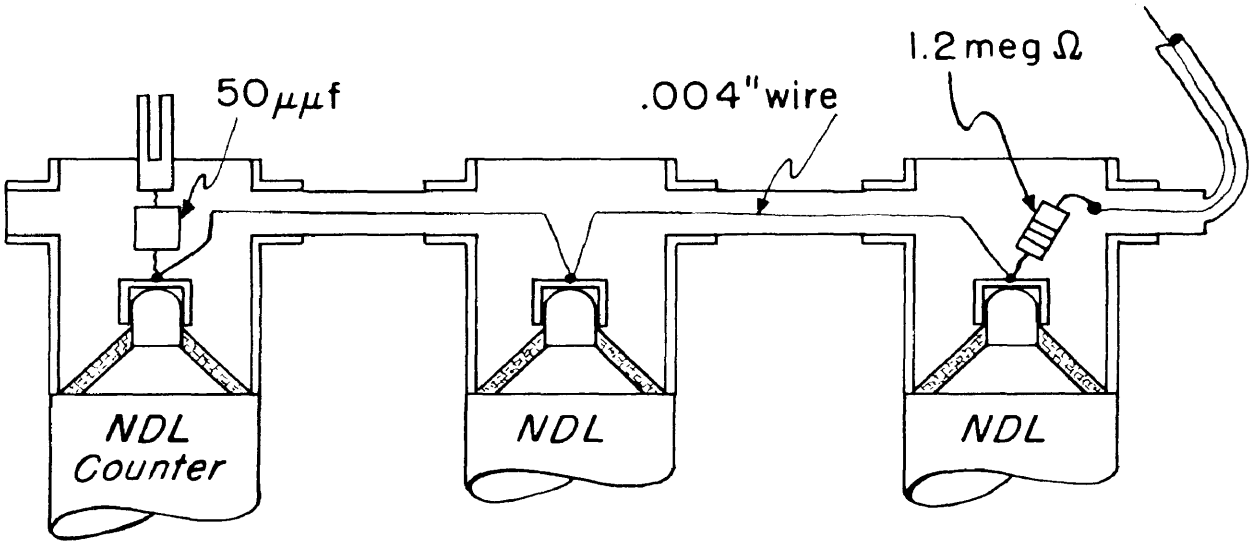
50μμf
.004"wire
1.2meg Ω
NDL Counter
NDL
NDL

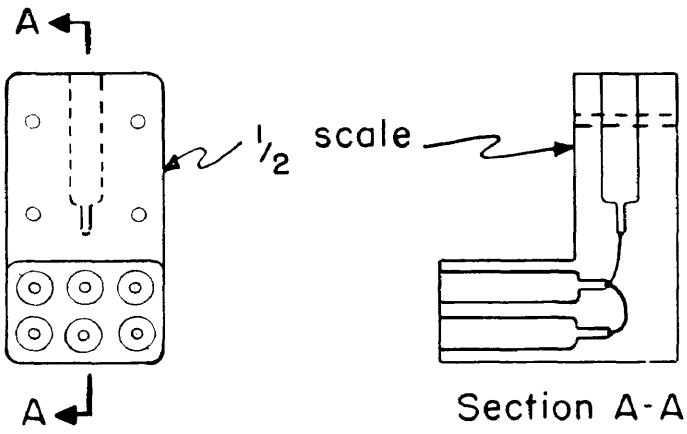
A
1/2 scale
A
Section A-A

plugs. It is shown as the last unit in Fig. II-5. The high voltage output from the power supply was terminated in a long bushing which was plugged into the manifold connector. All mating surfaces in the manifold were generously coated with silicone ignition compound so as to seal off completely the high voltage system.

The entire high voltage system was tested over the expected range of low ambient pressures and no spurious pulses were observed on any of the counter output lines. These lines were monitored with a pulse reading oscilloscope and since the counters yield pulses with characteristic shapes, any spurious pulses would be immediately obvious.

The coincidence and pulse shaping circuits used with the telescope and the burst detector were of conventional design but to save on power drain, sub-miniature pentodes and thyratrons were used throughout. Each of these units was fabricated on a bakelite board and plugged into the coupling capacitor jacks on the connectors of the individual unit. The wiring diagram is shown for the telescope coincidence circuit in Fig. II-6 and for the burst detector coincidence circuit in Fig. II-7. The system operation is briefly explained as follows: the telescope event is formed by cutting off three pentodes with the application of three pulses from the telescope counters within twice the circuit resolving time; the resulting output forms two inputs, one to an inverter-amplifier and the other to a thyratron and subsequent clippers which shape the pulse for telemetering use; the selected burst event is formed by applying three pulses from the burst detector counters

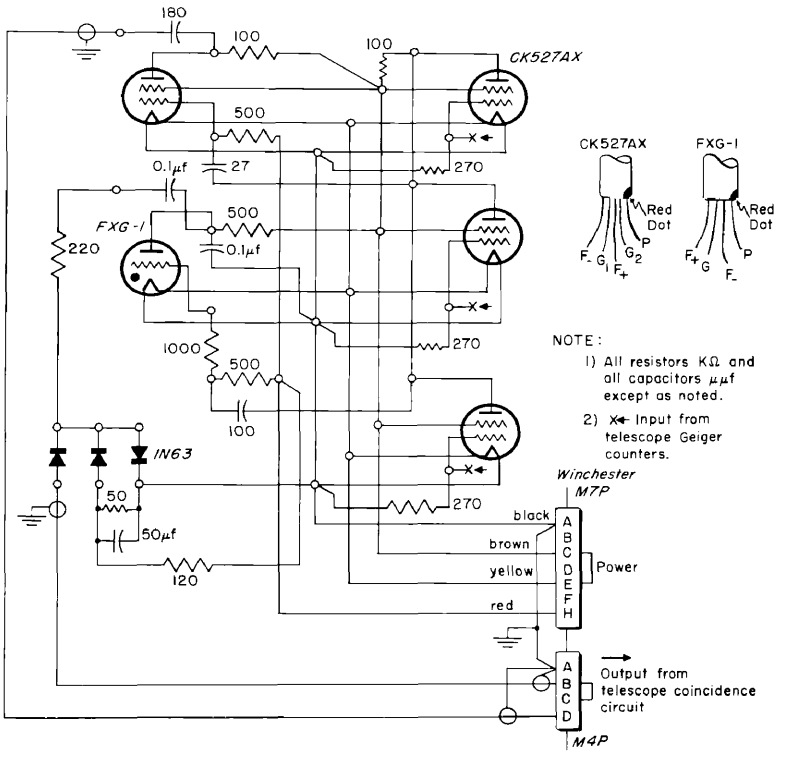

Fig. II-6 TELESCOPE COINCIDENCE CIRCUIT WIRING DIAGRAM

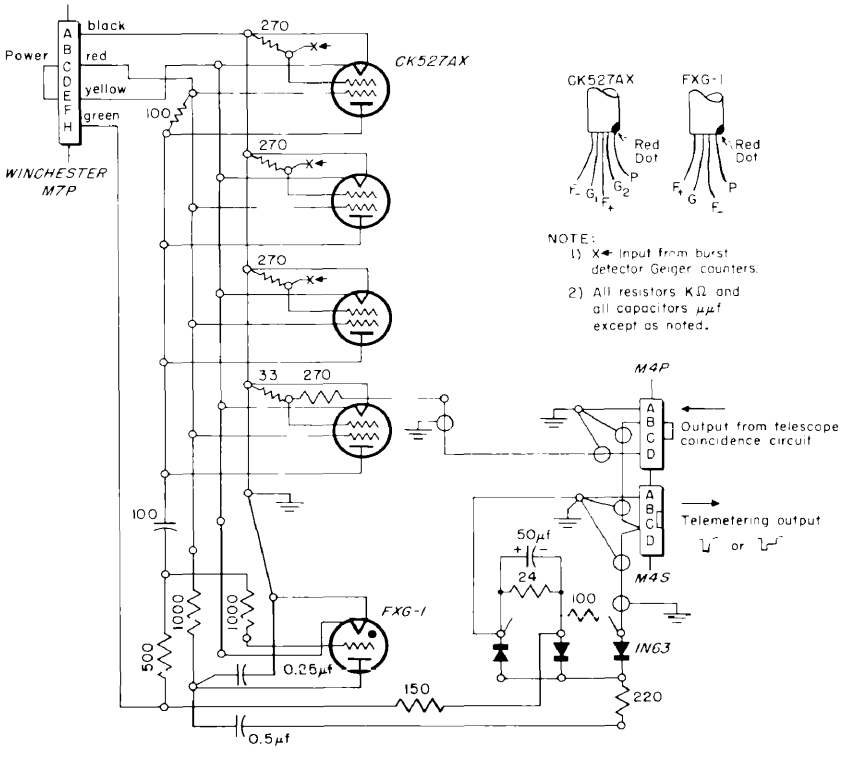

Fig. II-7 BURST DETECTOR COINCIDENCE CIRCUIT WIRING DIAGRAM

and a pulse from the inverter amplifier within twice the circuit resolving time to cut off four pentodes; the resulting output is shaped as above and the two outputs are mixed through diodes to form one channel of information. The pulse shaping circuit parameters were chosen with due regard to satisfactory pulse resolution (see App. 5).

The telemetering system used to transmit the data from the balloon gondola to the ground station was a five-channel adaptation of the standard F.M. - F.M. system developed by The Johns Hopkins University, Applied Physics Laboratory.[1] In this system each information channel frequency modulates an audio-subcarrier oscillator. The outputs of all these oscillators are isolated and additively mixed and then used to frequency modulate a radio frequency carrier. This modulated carrier frequency is transmitted to the ground station receiver where it is demodulated and the mixed subcarrier frequencies are recorded on magnetic tape for storage or further separated and demodulated for simultaneous monitoring. The five subcarrier channels were allocated as follows: 1700 cps internal gondola temperature, 2300 cps cosmic-ray end organ containing 0 cm of carbon, 3000 cps c.r.e.o. - 1 cm C, 3900 cps c.r.e.o. - 3 cm C and 5400 cps c.r.e.o. - 6 cm C. These were the only information channels that it was necessary to telemeter through this system since the complete balloon trajectory information was supplied as a part of the balloon flight service. The band width of each of the four cosmic-ray channels was set at $\pm$ 5 per cent of the

---

[1] Gene H. Melton, Electronics, Vol. 21, No. 12, 106 (1948).

center frequency since only pulses of a fixed height would be modulating these audio-subcarrier oscillators. The band width of the temperature channel, however, was set at ± 7.5 per cent of the center frequency in order to allow the measurement of a wide range of temperatures with reasonable accuracy. The 1700 cps oscillator was a free-running multivibrator with the frequency controlled by a thermistor in one grid circuit (see Fig. II-8). The square wave output of the multivibrator was filtered and amplified in a low Q tuned amplifier stage to give only the fundamental frequency. The total harmonic distortion of the subcarrier oscillator output wave form must be no greater than 6 per cent in this five-band system in order that cross-modulation products do not interfere with the intelligence to be transmitted. The resistance vs temperature characteristic for the transistor used in the flight of 2 February 1952 is shown in Fig. II-9. The frequency vs resistance characteristic for the multivibrator oscillator used in this same flight is shown in Fig. II-10. The other four subcarriers were provided by voltage controlled oscillators (V.C.O.) of a modified Hartley type. The fixed frequency oscillator tank circuit was bridged by a quadrature network which contained a tube. Thus as an amplitude modulation was applied to the grid of this tube, a reactance modulation was applied to the oscillator tank circuit and a resultant frequency modulation was obtained. The V.C.O. circuit is shown in Fig. II-11 and a typical voltage vs frequency characteristic is shown in Fig. II-12. The telemetering transmitter used was similar to the "cigarette pack" transmitter designed for use in rockets by the

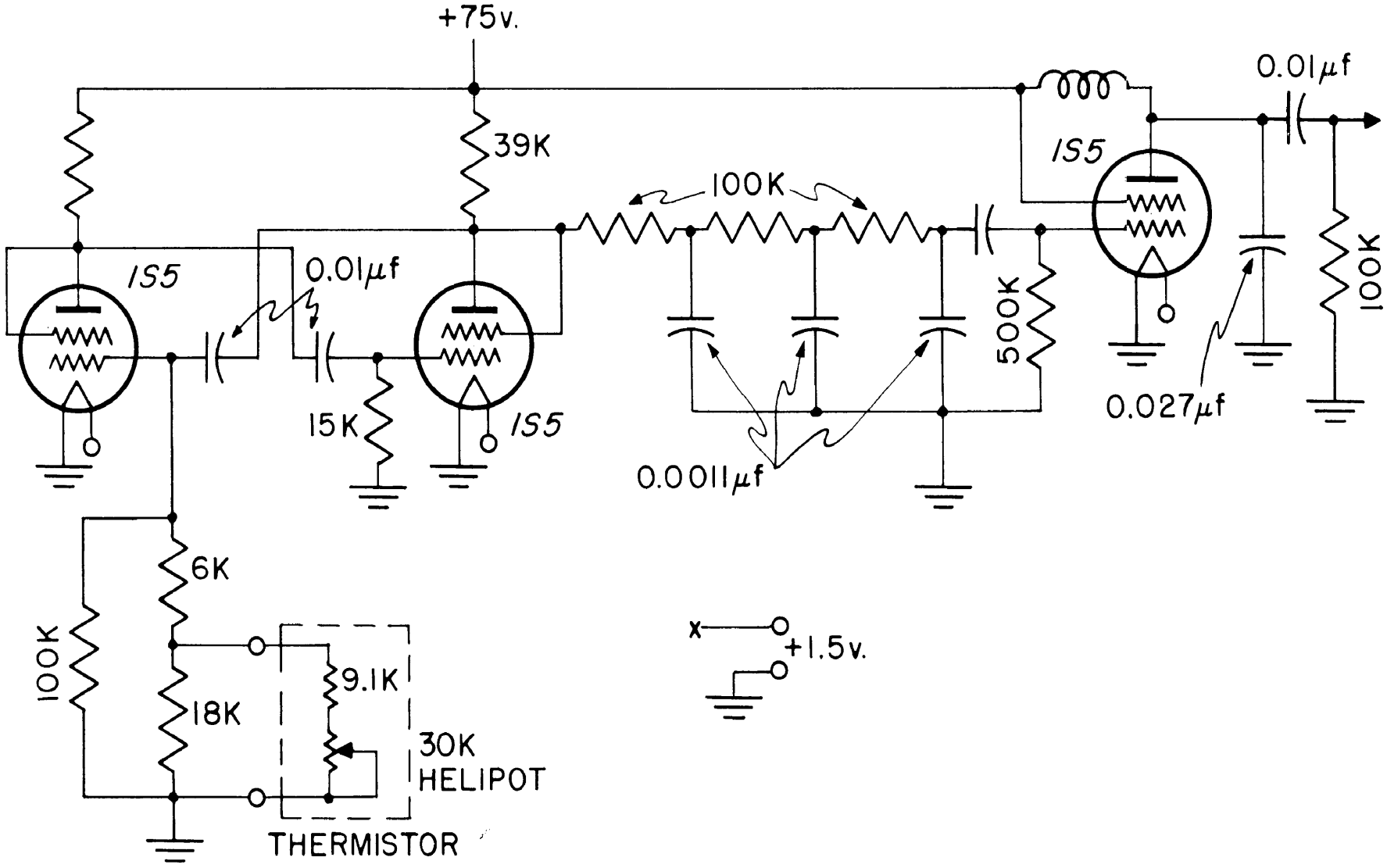
+75v.
39K
100K
0.01μf
1S5
1S5
0.01μf
15K
1S5
500K
0.0011μf
0.027μf
100K
6K
100K
18K
9.1K
30K
HELIPOT
THERMISTOR
X
+1.5v.

Fig. II-3

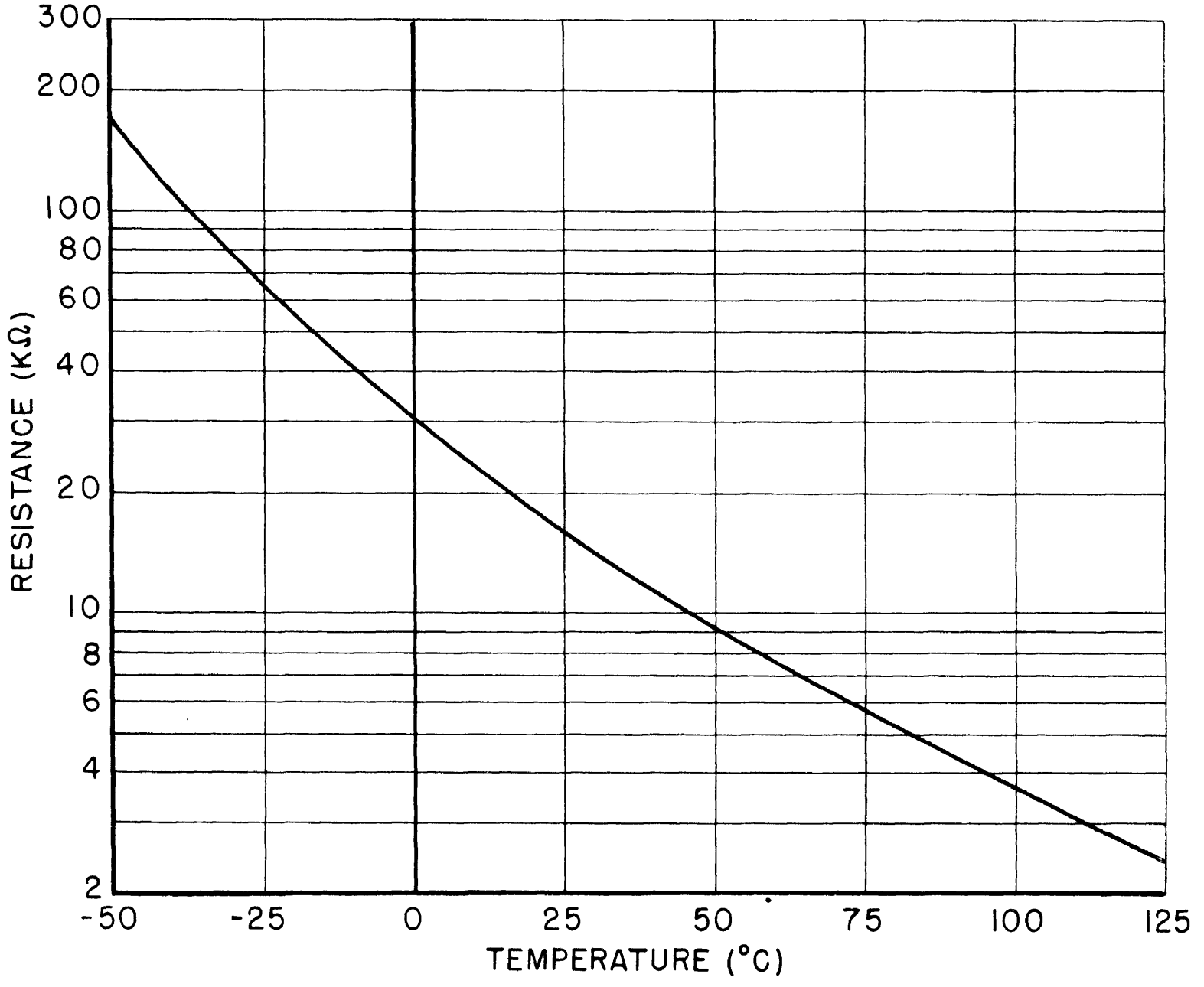
300
200
100
80
60
40
20
10
8
6
4
2
RESISTANCE (KΩ)
-50
-25
0
25
50
75
100
125
TEMPERATURE (°C)

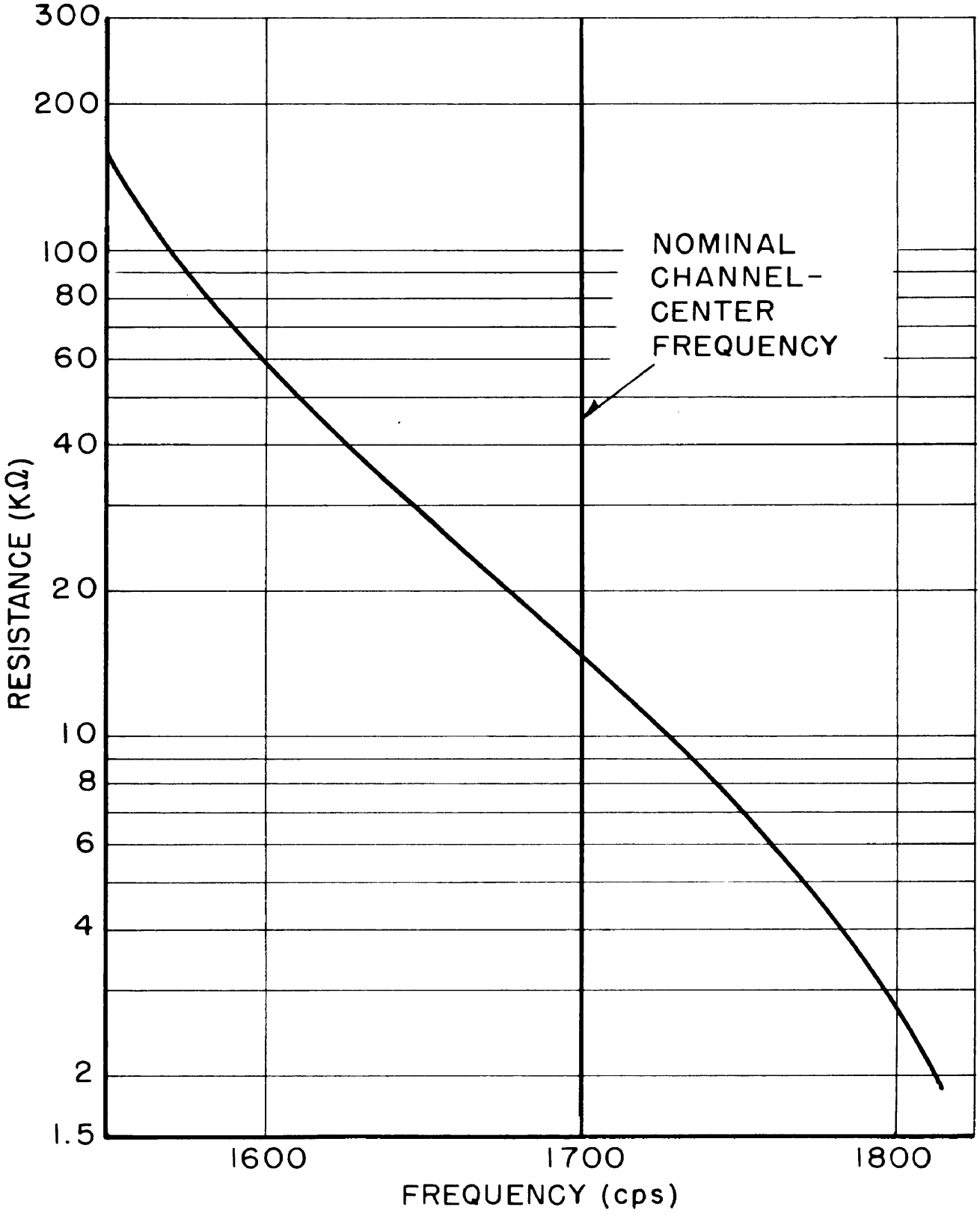
300
200
100
80
60
40
20
10
8
6
4
2
1.5
RESISTANCE (KΩ)
NOMINAL
CHANNEL-
CENTER
FREQUENCY
1600
1700
1800
FREQUENCY (cps)

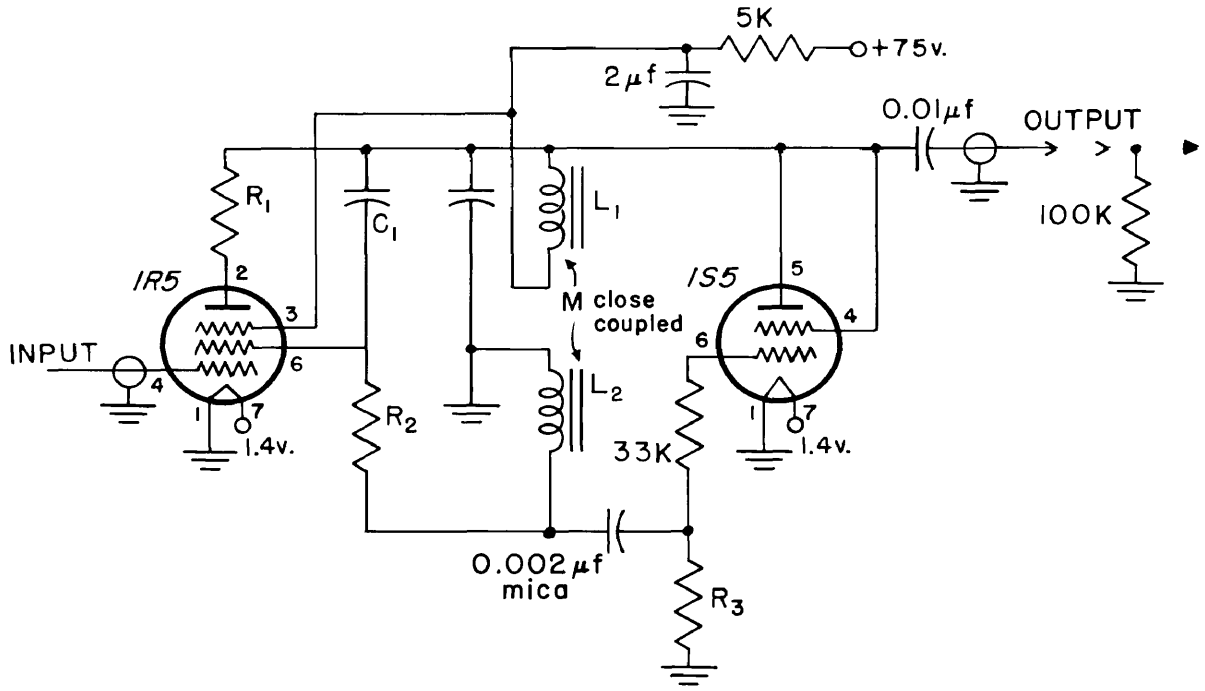

Ch.	Kc f_c	KΩ ½w			μμf (silver mica)		mhy (Budchokes)	
		R_1	R_2	R_3	C_1	C_2	L_1	L_2
2	2.3	10.0	3.0	150	8,510	19,200	125	125
2	2.3	10.0	3.3	100	8,000	21,000	125	125
3	3.0	10.0	3.8	84	5,300	6,210	125	125
3	3.0	10.0	4.7	84	5,700	10,000	125	125
4	3.9	5.1	3.9	84	3,190	6,750	125	80
4	3.9	5.1	4.1	84	3,175	6,047	125	80
5	5.4	5.1	4.3	53	2,670	4,500	80	80
5	5.4	5.1	4.3	53	2,860	6,510	80	80

Fig. II-11 VOLTAGE CONTROLLED OSCILLATOR SCHEMATIC CIRCUIT

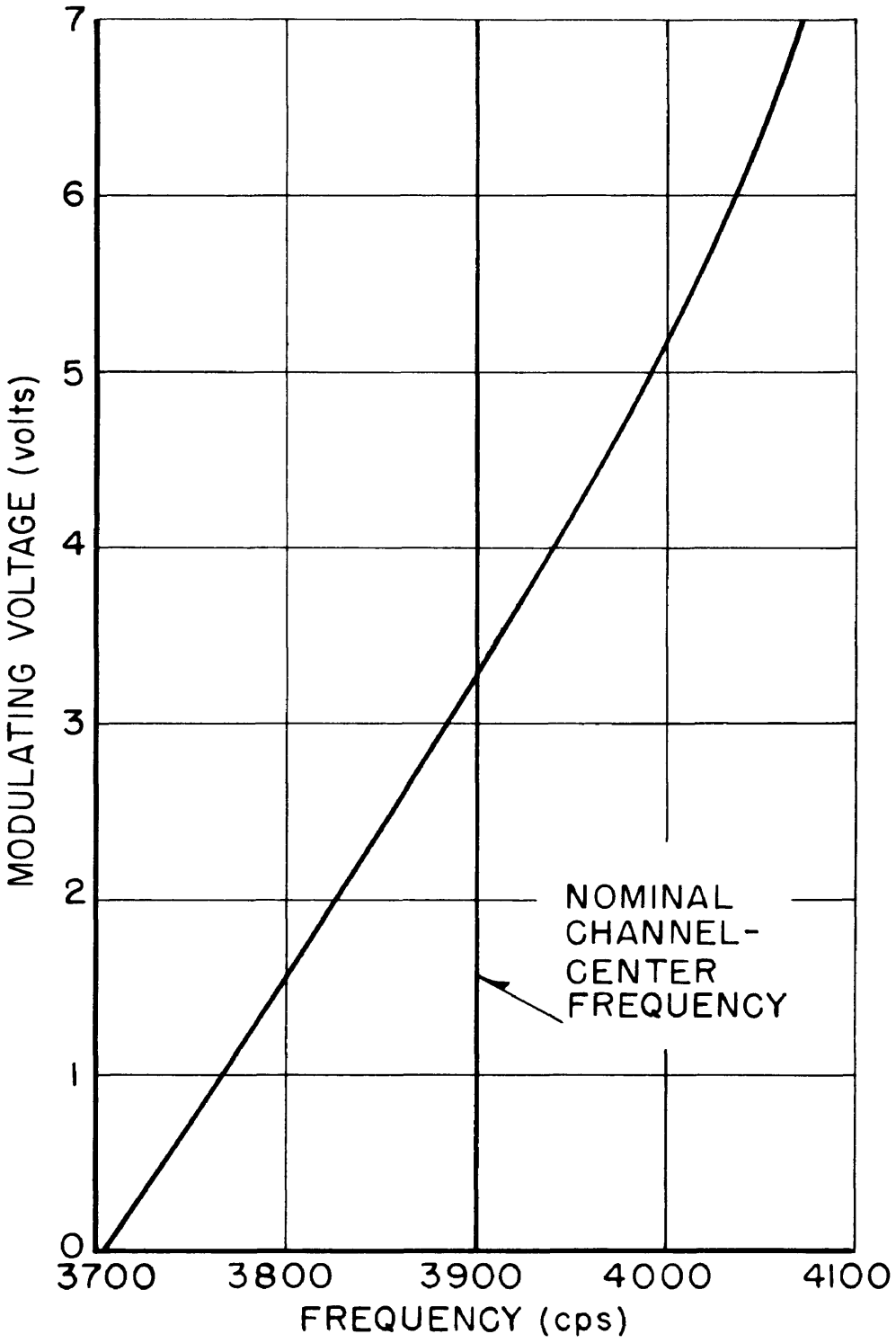
MODULATING VOLTAGE (volts)
0
1
2
3
4
5
6
7
3700
3800
3900
4000
4100
FREQUENCY (cps)
NOMINAL
CHANNEL-
CENTER
FREQUENCY

Applied Physics Laboratory. This transmitter was modified to increase the power output to 2.5 W and the useful life to 500 hrs. by changing the oscillator and final amplifier tube type. The revised circuit diagram is shown in Fig. II-13. The carrier frequency was 225 mcps and the deviation sensitivity was 55 kcps/r.m.s. volt audio (2 v r.m.s. maximum). The transmitting antenna was a folded unipole on a ground plane cut to 225 mcps (see Fig. II-14). It was necessary that the ground plane have a minimum diameter of $\lambda/2$ at the frequency in question so this determined the minimum horizontal area of the gondola. The input impedance of this antenna is 150 ohms and the transmitter output impedance was 50 ohms so a quarter-wave transformer was designed in order to obtain a good impedance match between the two. The resulting standing wave ratio on the antenna feed line was 1.3. This antenna has a 3db gain over a dipole in free space.

Five silver cells (Yardney 60 HR 45) were used in the primary power supply. These cells weigh 20 per cent as much as a lead-acid cell of the same energy capacity. The rating of these cells is 60 ahr to give 1.5 v for rates from 0-10 a. These cells mounted in a flight case weighed 10 lbs.

The secondary or plate power supply was designed around a vibrator (Airpax Products Co., Baltimore, Maryland) which has the following characteristics: input, 6 v dc; output, 110 v square wave, 30 w continuous operation, 400 cps; weight, 420 grams and efficiency, 60 per cent. The output of this vibrator supplied the input to three rectifier circuits which supplied 75 v regulated to all subcarrier oscillators, 100 v

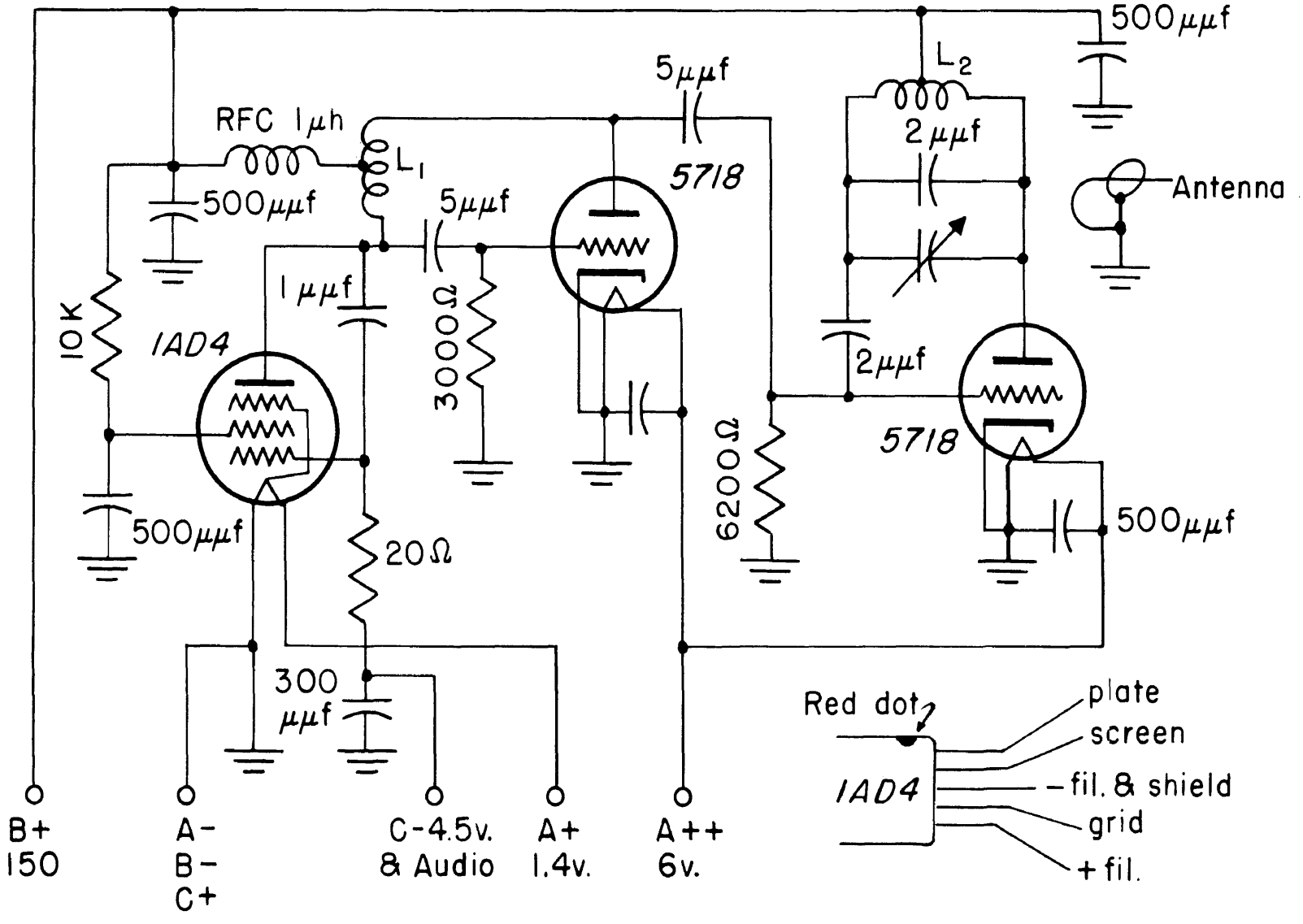
500μμf
L2
5μμf
RFC 1μh
L1
2μμf
5718
Antenna
500μμf
5μμf
1μμf
10K
1AD4
3000Ω
2μμf
6200Ω
5718
500μμf
20Ω
300
μμf
Red dot
plate
screen
1AD4
– fil. & shield
grid
+ fil.
B+
150
A–
B–
C+
C-4.5v.
& Audio
A+
1.4v.
A++
6v.

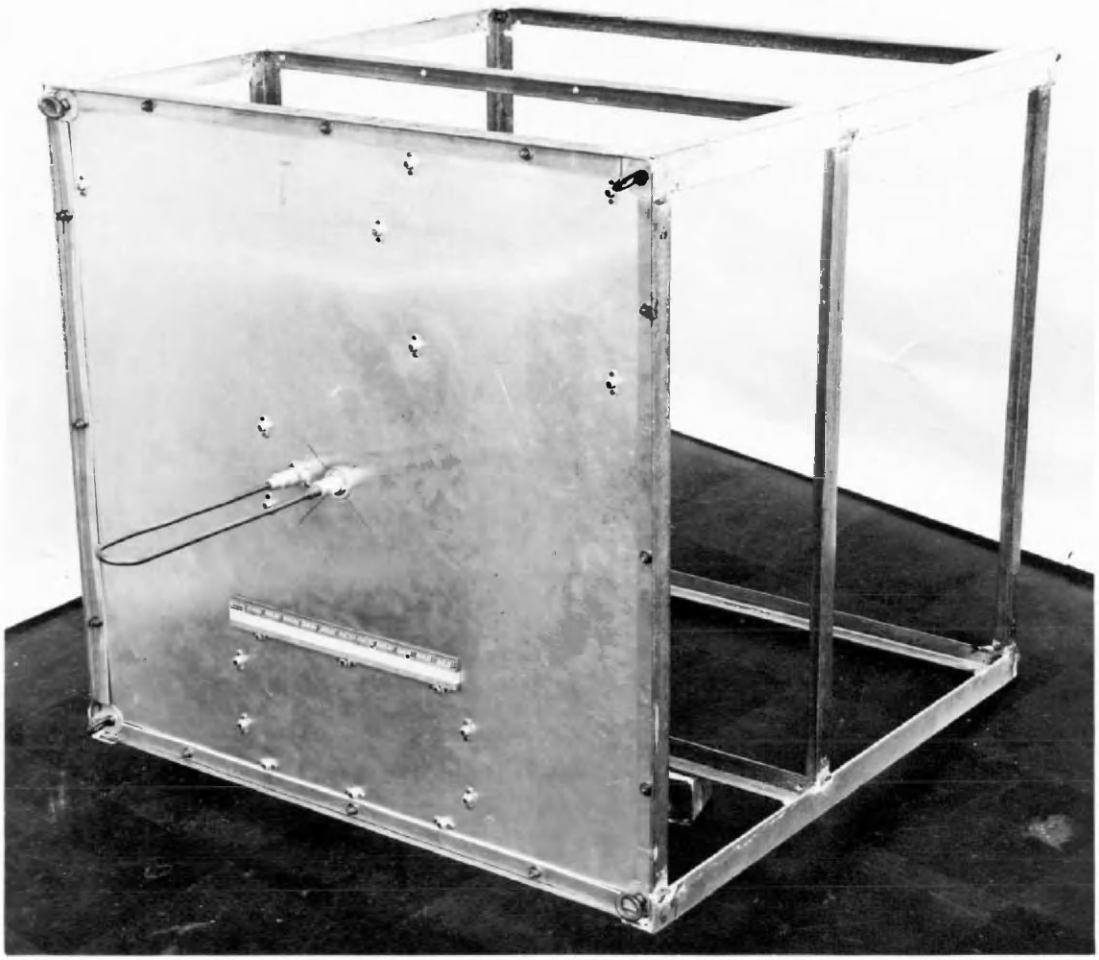

Fig. II-14 PHOTOGRAPH OF FLIGHT TRANSMITTING ANTENNA

to all coincidence circuits and 150 v regulated to the transmitter. The overall efficiency for the complete secondary power supply was 31 per cent and the weight was 13 lbs. including a 1 lb., 22.5 v bias battery. The schematic diagram for this circuit is shown in Fig. II-15. This unit was tested over a wide range of low ambient pressures and no trouble due to corona or spark-over was found.

Four of the cosmic-ray instruments along with all the other above described equipments were mounted in a two deck framework in the form of the edges of a cube 30" on an edge. Care was taken to place the four cosmic-ray instruments in this framework in such a way that the environment of each instrument was the same. The completely loaded gondola is shown in Fig. II-4. The gondola was covered with a green platicized fabric cover during actual flights. This covering served to keep the components out of the wind stream during the ascent of the balloon and to protect the instrument during landing. The total weight of the loaded gondola was 110 lbs. The block diagram is shown in Fig. II-16.

The telemetered signal was received on the ground by two helical beam antennae (10.5 db gain over a dipole in free space) and each antenna output was fed into a separate cascode preamplifier (see Fig. II-17) and thence to the two separate ground stations. The ground stations consisted of a Clarke receiver and a Magnecorder magnetic tape recorder. The noise figure for the Clarke receiver is 9 db but by using the cascode pre-amplifier this was reduced to 6 db. Time was injected into the system in the form of an interrupted 400 cps signal. The 400 cps signal was generated by an electronically driven tuning fork and a small

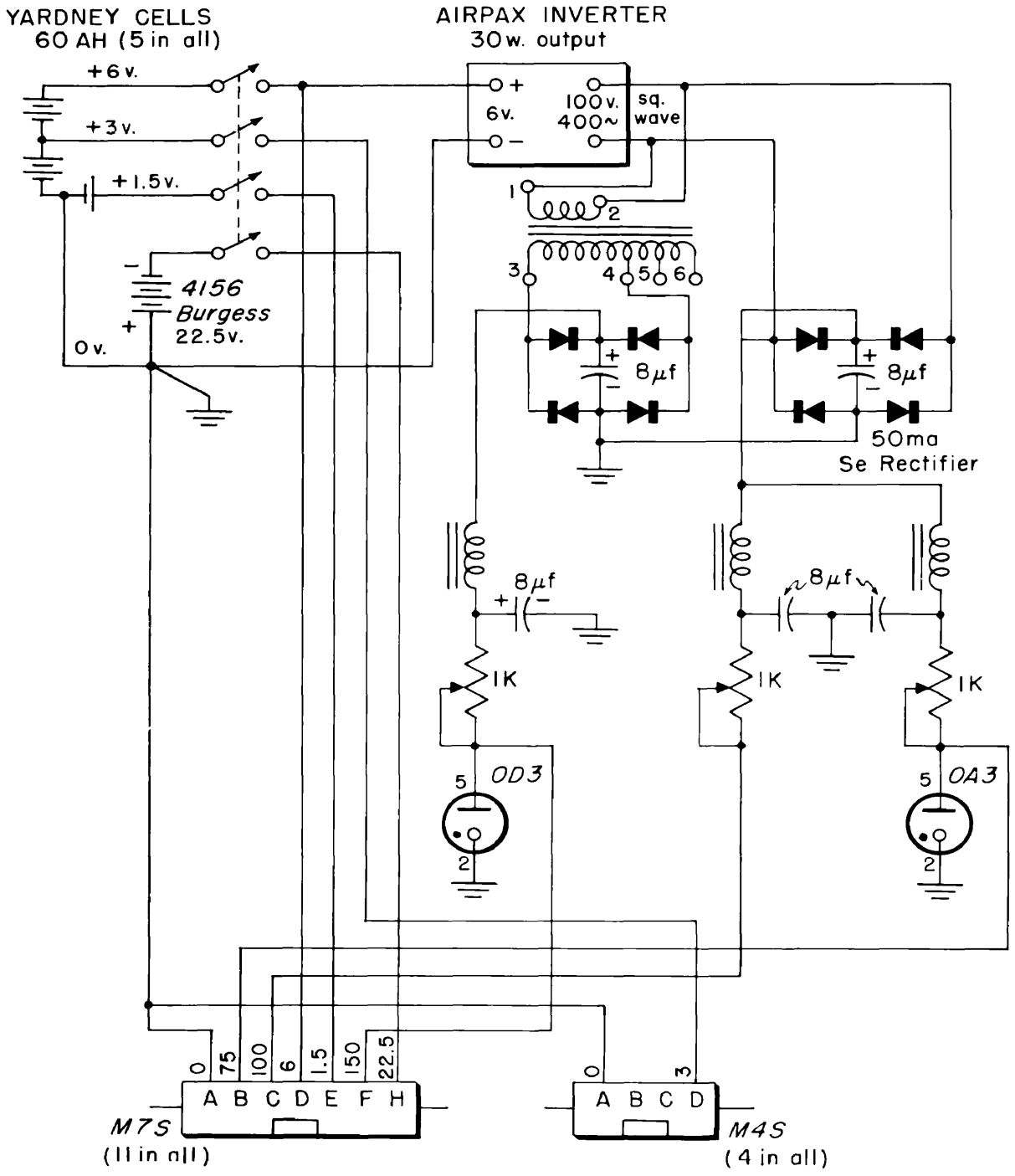

Fig. II-15 SECONDARY POWER SUPPLY SCHEMATIC CIRCUIT

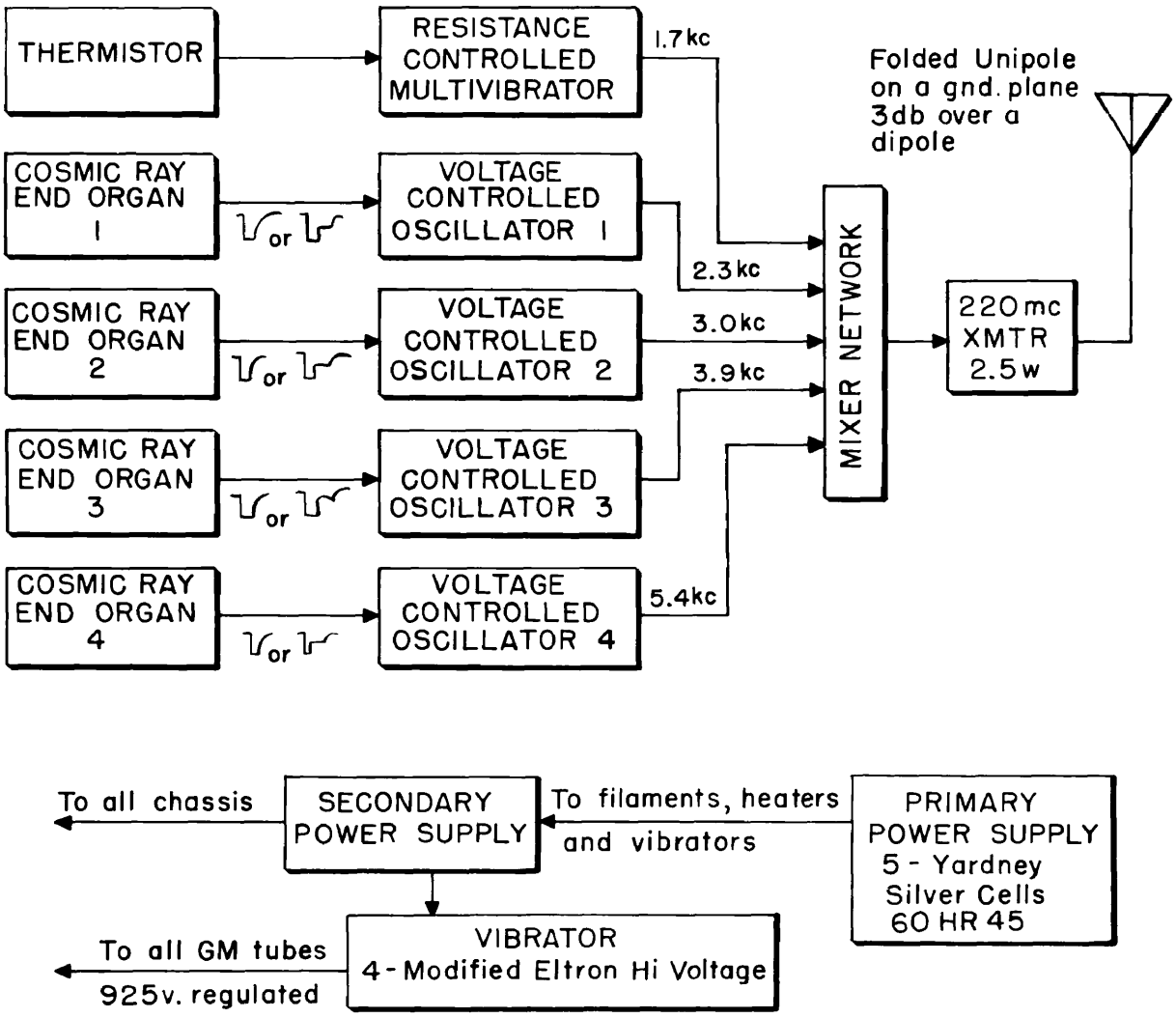

Fig. II-16 FLIGHT ELECTRONIC EQUIPMENT BLOCK DIAGRAM

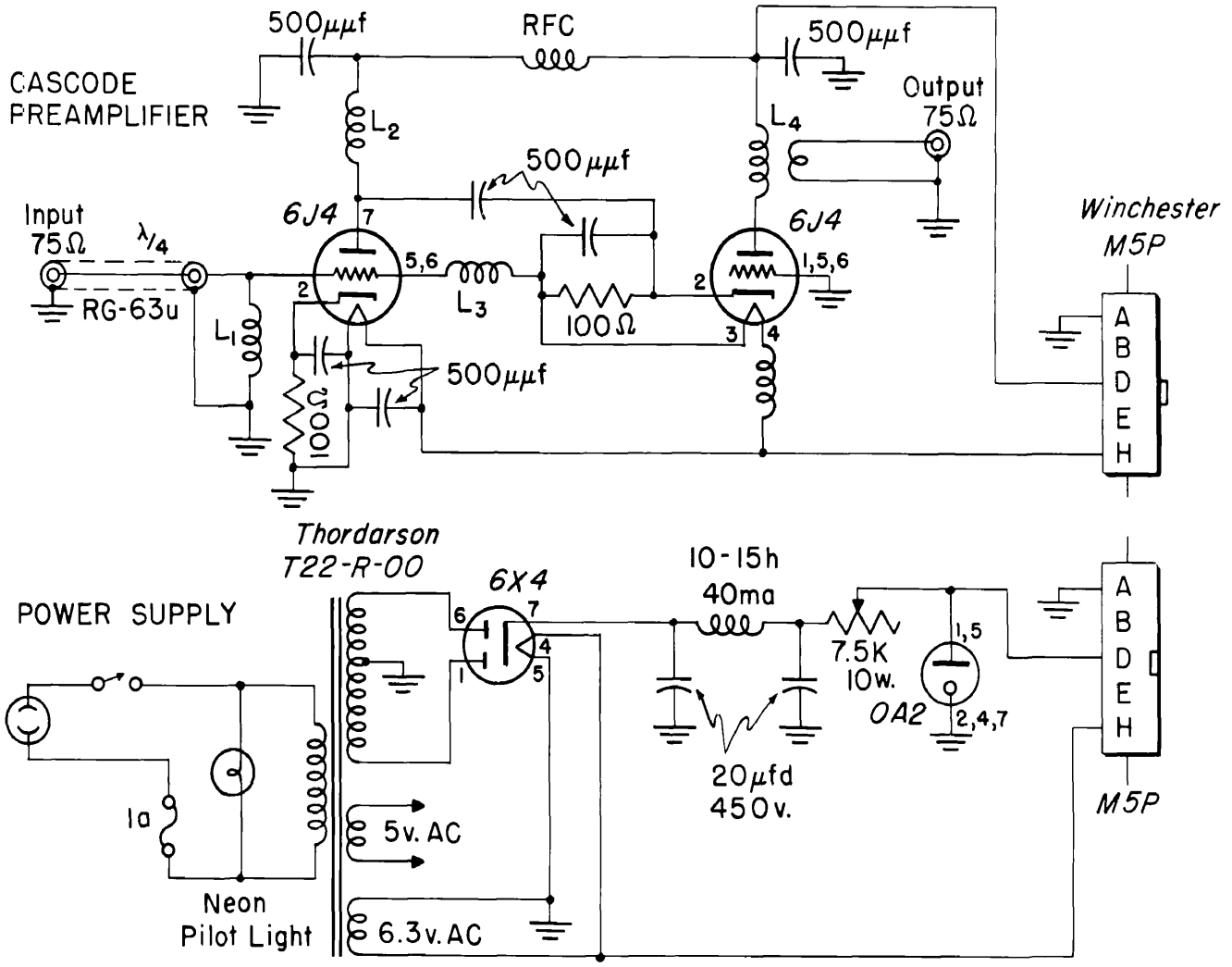

Fig. II-17 R.F. CASCODE PREAMPLIFIER SCHEMATIC CIRCUIT

synchronous motor and cam operated a microswitch to interrupt the signal once a minute. An external pushbutton switch was wired in series with the microswitch to provide for manual indexing of known times. This signal was mixed into the input to the tape recorders. A continuous record could then be made by running the tape recorder in station A (half-hour reels at 7.5 in/sec) until the reel was nearly empty, then starting the tape recorder in station B and manually indexing both records simultaneously to determine the time of overlap. The input signal to either tape recorder could also be fed into a set of six bandpass filters and discriminators to demodulate the subcarriers. The monitored signals were presented on a two-channel Brush ink and paper-tape recorder. The first discriminator output was wired directly to one channel of this recorder and the information presented on this channel was the time pulse. Any one of four of the other five channels could be switched into the second available recorder channel to record cosmic-ray pulses and the remaining discriminator was used to determine the internal temperature of the gondola. The flight record was stored on magnetic tape and later, at the home laboratory, played back through six band pass filters and discriminators into a six-channel Miller photo-galvanometer oscillograph recorder which reproduced the information on rolls of photo-sensitive paper. During a flight, frequent records were made on the field monitoring equipment in order to ascertain the status of operability of the flight equipment. The block diagram of the ground station is shown in Fig. II-18.

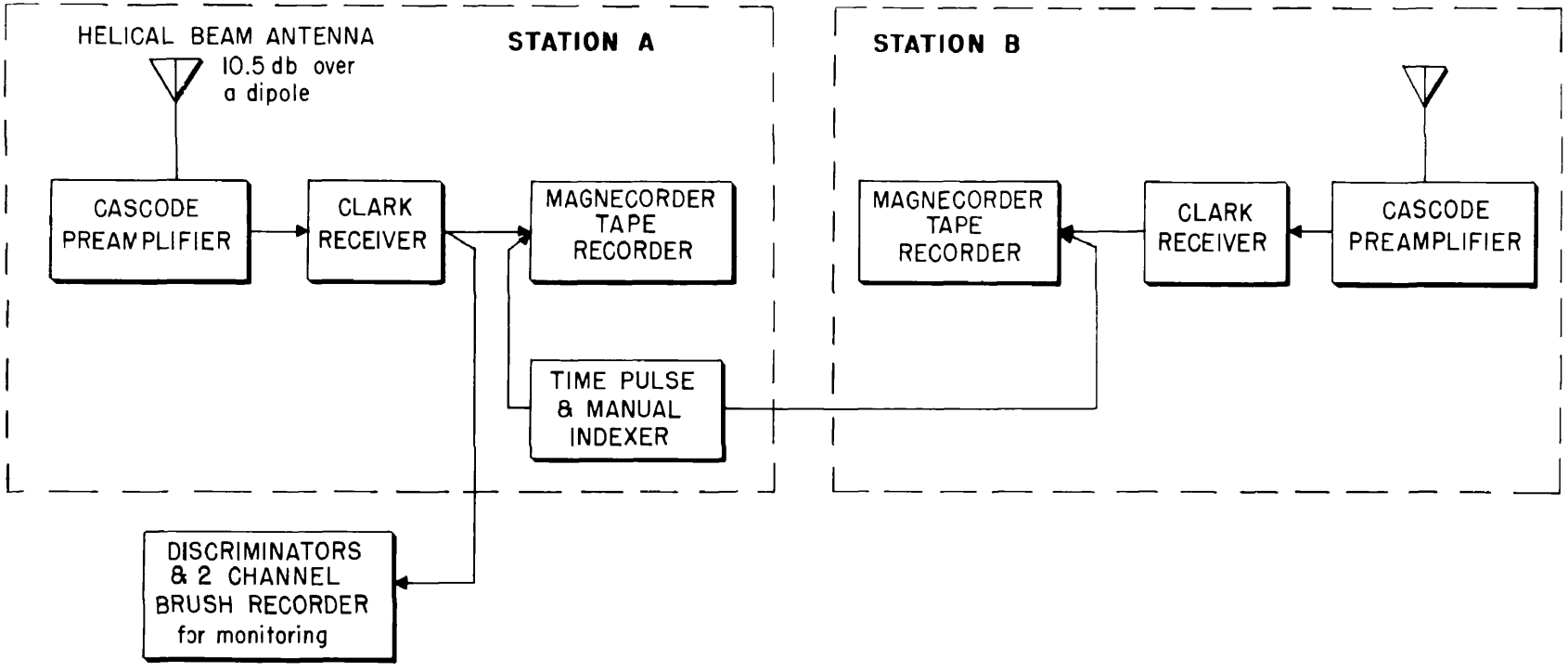

Fig. II-18 TELEMETERING GROUND STATION EQUIPMENT BLOCK DIAGRAM

III THE EXPERIMENTS, RESULTS AND DISCUSSION, AND CONCLUSIONS

A. The Experiments

In all, four balloon flights were made. The balloons used were of the "Sky-hook" type, i.e., a 0.001 to 0.002" polyethylene open neck gas bag about 80' in diameter and nearly 100' long. In each case the layout was in the following order: (1) balloon, (2) cut-down devices, (3) 24' parachute, (4) instrumentation gondola, (5) first half of beacon dipole transmitting antenna, (6) beacon and barograph and (7) second half of beacon dipole antenna with antenna weight. The entire train from the base of the balloon was about 415' long. Fig. III-1 shows this layout in flight soon after launching (flight No. 4) down to just below the gondola. For all of these flights it was necessary to wait for days on which the winds were not such as to carry the flight very far north or south so that the data would be subject to as little latitude effect as possible.[1*]

The first two flights were made from Holloman Air Force Base, New Mexico. The first of these flights, carrying gondola No. I was made

---

[1] J. A. Van Allen and S. F. Singer, Phys. Rev. 78, 819 (1950) (L).

*From the work of Van Allen and Singer[1] it is seen that the slope of the vertical intensity vs geomagnetic latitude curve is approximately 0.01 charged particles cm^{-2} sec^{-1} $steradian^{-1}$ $degree^{-1}$ at $\lambda = 41^{\circ}N$. Thus the flux changes by $10^{2}\left(\frac{0.01}{0.08}\right) = 13$ per cent for a 1° change in λ and it is desirable to maintain a nearly constant value of λ for these flights. The magnetic cut-off energy and the median energy for protons at $\lambda = 41^{\circ}N$ are $4.5 \cdot 10^{10}$ ev and 10^{10} ev respectively as deduced from this spectrum.

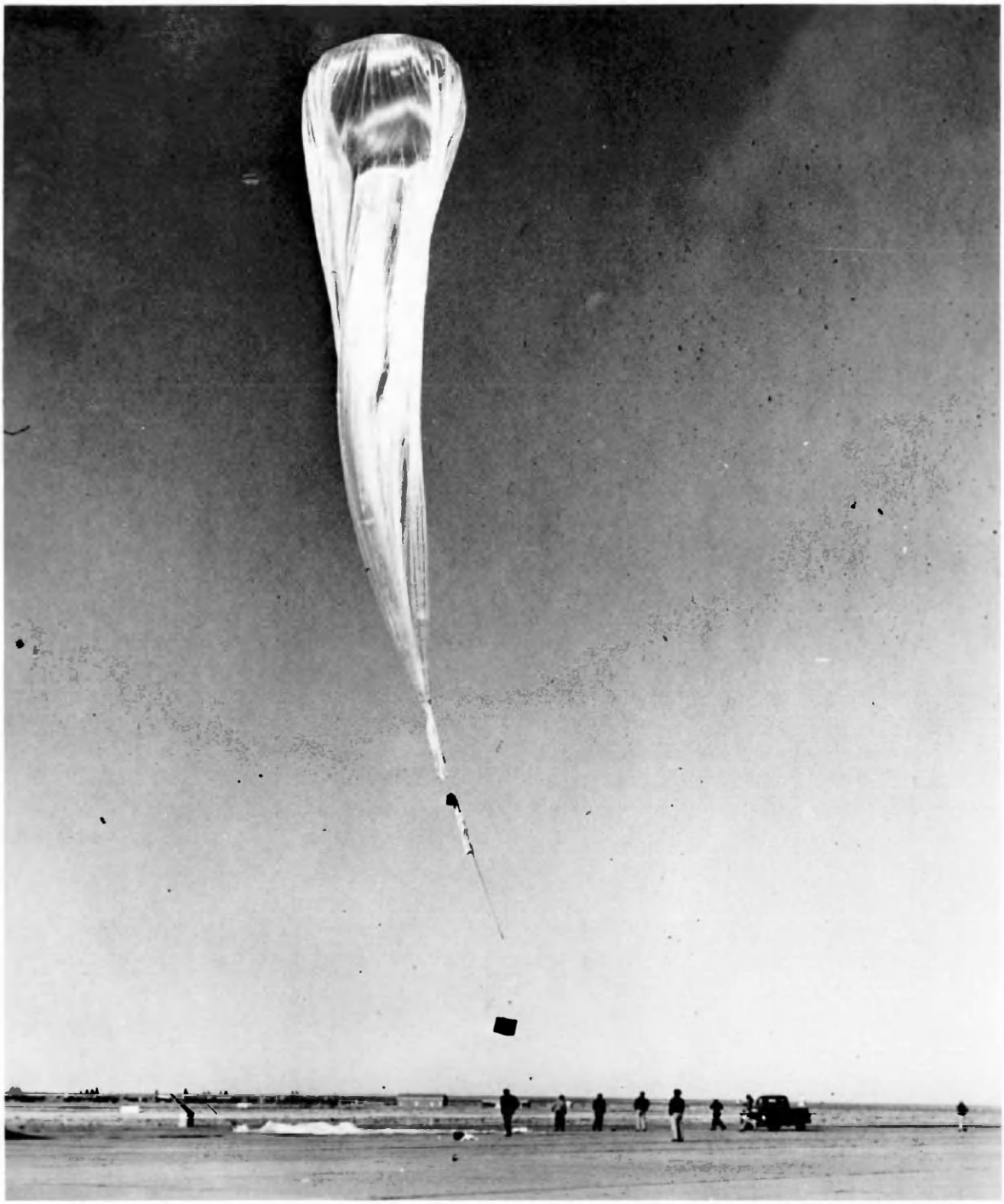

Photo Courtesy of General Mills Aeronautical Research Laboratory

Fig. III-1 PHOTOGRAPH OF BALLOON FLIGHT NO. 4 LAUNCHING

on 12 December 1951. The launching was successful and a good signal was received for approximately one hour at which time the signal was lost. It was later determined that the balloon had burst at approximately 50 K ft. and the equipment had come down somewhere on the other side of the Sacramento mountains. Recovery of the equipment was made on the next day near Hope, New Mexico (~100 mi. airline). The recovered gondola and instruments appeared to have suffered little damage and this was later borne out when the equipment was tested at the field laboratory at H.A.F.B. The second flight was also made from H.A.F.B. on 17 December 1951. This flight carried gondola No. II and proceeded along the same lines as the first flight. It differed only in the point of recovery. Recovery was again made on the following day, this time at Tatum, New Mexico (175 mi. airline). The recovery experience for this flight was even better than for the first launching since the only damage was to the transmitting antenna (it was planned that this part would have to be replaced after each recovery and the antenna was constructed of soft copper tubing so as not to cause great damage). In both of these flights it was apparent that the flight instrumentation was operating properly but that neither the altitude nor the duration was sufficient to fulfill the requirements of the proposed experiment. This then necessitated the planning of two more flights.

The next two flights were made from Pyote Air Force Base, Texas.*

---

*It is to be noted that both of the above locations are very close to the line of geomagnetic latitude which goes through the White Sands Proving Grounds in New Mexico where many cosmic-ray experiments have been performed in rocket vehicles.

The first flight of this series was launched at 0916 C.S.T. on 23 January 1952. The balloon, carrying gondola No. I reached a maximum altitude of 100 K ft. in 2.3 hrs. and descended to 90 K ft. in the next 4 hrs. at which time the cut-down mechanism operated and the balloon descended to impact at 1606 C.S.T. A quick survey of the ground monitoring recording showed that the cosmic-ray channels of the instrumentation had failed at about 90 K ft. during the ascent. The failure appeared to be due to corona on the high voltage lines. This analysis was confirmed later that day when the gondola was recovered 30 mi. east of Brady, Texas. There were evident cracks in the polyethylene which covered the fine wires of the connectors on each of the four burst detector trays. Aside from this, the gondola (which had now been recovered twice) suffered no apparent damage except for the usual crushed antenna. The data from this flight are not felt to be reliable since it can not be determined when the first spurious pulses would have appeared. None of these data were used in the text that follows.

In preparation for the next flight, the high voltage connectors in the various arrays of gondola No. II were removed and carefully examined under intense light for any evidence of cracking. Several actual and suspected cracks were located in this manner that otherwise would have gone unnoticed. For lack of molding equipment, it was decided that the cracks might be welded by using a small (1/8" dia.) soldering iron at reduced heat (polyethylene melts at 106°C) and some spare pieces of the plastic which were carved into suitable welding rods. After some amount of practice it was determined that the material could be successfully welded

and all of the cracks which had been detected in this set of high voltage connectors were welded together.

The second flight from P.A.F.B. carried gondola No. II and was launched at 0942 C.S.T. on 2 February 1952. This balloon ascended to a maximum altitude of 92.5 K ft. in 2.5 hrs. and floated between 92.5 K ft. and 82 K ft. for an estimated time of 4.8 hrs. The impact point lay some 35 mi. east of San Angelo, Texas, and the time of impact was 1700 C.S.T. The balloon flight trajectory was very nearly along the line of the geomagnetic parallel $\lambda = 41^{\circ}$N. A close check of data recorded on the ground monitoring equipment showed that excellent operation of the flight instrumentation had been obtained up to a few minutes prior to 1434 C.S.T. at which time the R.F. carrier signal had been lost. During this short time before the signal cut off, the receivers had to be retuned continuously in the direction of increasing frequency. This is direct evidence for failure of the primary battery supply since this effect had been noticed (but not so severely) in the long periods of ground testing. The four cosmic-ray channels were first to quit at 1428 followed by the temperature channel at 1431 and finally the transmitter at 1434 C.S.T. The altitude vs time curve for this flight is shown in Fig. III-2.*

The reels of magnetic tape on which the flight data were stored,

---

*The altitudes were determined from pressure data by using the standard N.A.C.A. conversion charts. These and other trajectory data were supplied as a part of the flight service by the General Mills Aeronautical Research Laboratory.

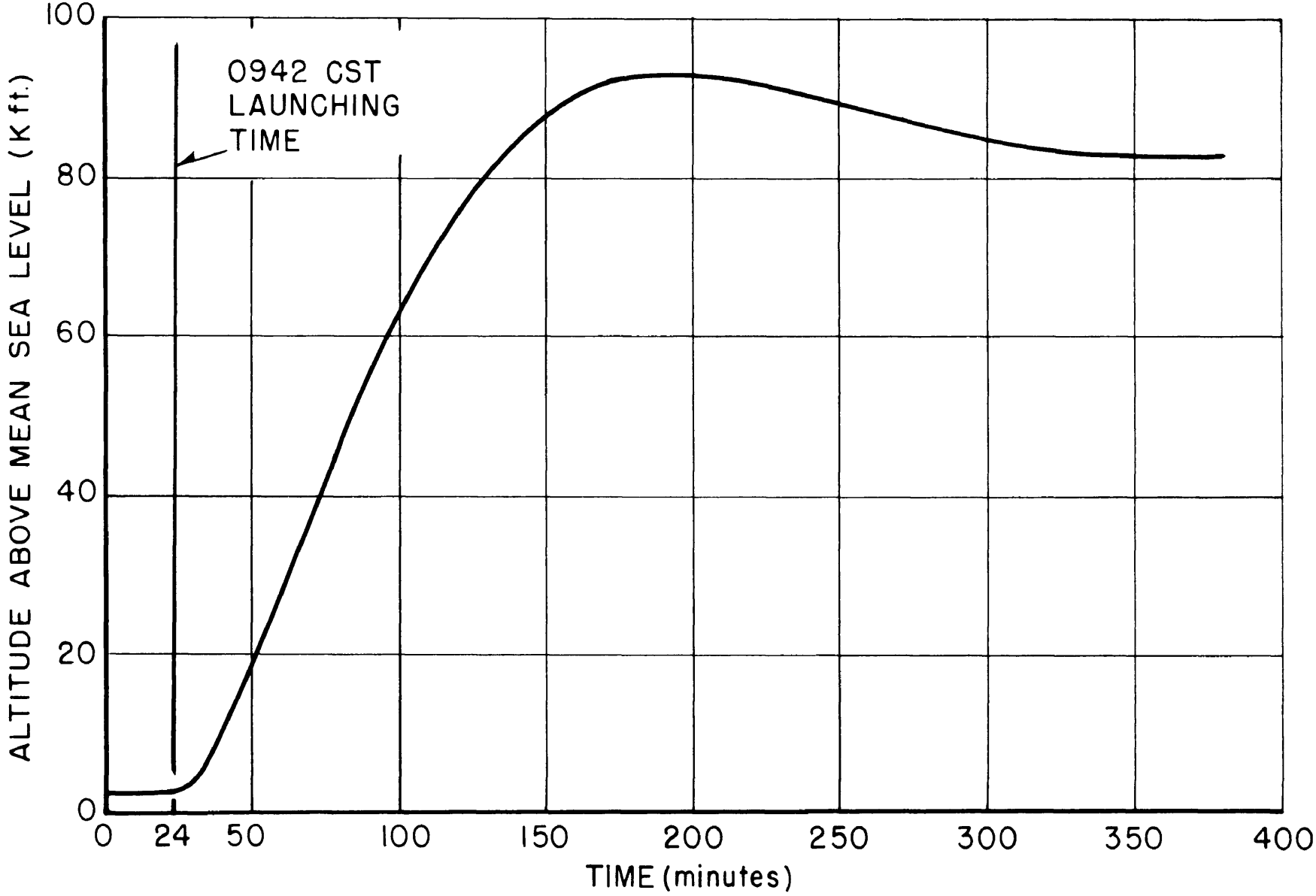
100
80
60
40
20
0
ALTITUDE ABOVE MEAN SEA LEVEL (K ft.)
0942 CST
LAUNCHING
TIME
0
24
50
100
150
200
250
300
350
400
TIME (minutes)

Fig. [illegible]

were brought back to the home laboratory and transcribed onto 12-200' rolls of 12" paper. A sample of this record is shown in Fig. III-3. The major part of the noise which appears on the base line of each channel is due to wow and flutter produced by the tape recorder. In the case of the time channel, some of the noise is due to beats produced between the 400 cps ground timer and leakage modulation of the transmitter by hash from the input side of the 400 cps vibrator appearing on the heater supply (modulation due to heater-cathode leakage in the transmitter oscillator and final amplifier stages) and by 800 cps ripple from the plate and screen supplies (400 cps, full wave). During the time pip and manual indexing periods (a part of such a period is shown at the right hand end of the time channel in Fig. III-3), the ground 400 cps time signal is cut off and the 400 cps discriminator receives no signal. It is characteristic of these discriminators that when a limiting signal in the proper frequency band is not present that a response is obtained from the small cross-modulation products of the other channels, e.g., the difference between the 2nd harmonic of the 1700 cps subcarrier and the 3000 cps subcarrier would be 400 cps. The noise, however, did not interfere with the accurate reduction of the record. On channels 1, 3, 4, 5, and 6 the time and indexing pips and the cosmic-ray pulses can be read through this noise with no trouble. On channel 2 (internal gondola temperature) there is no reason to believe that the time constant of the total heat capacity involved would be such as to yield the type of variation seen on this channel even if a mechanism could be proposed which would impose such a thermal driving function.

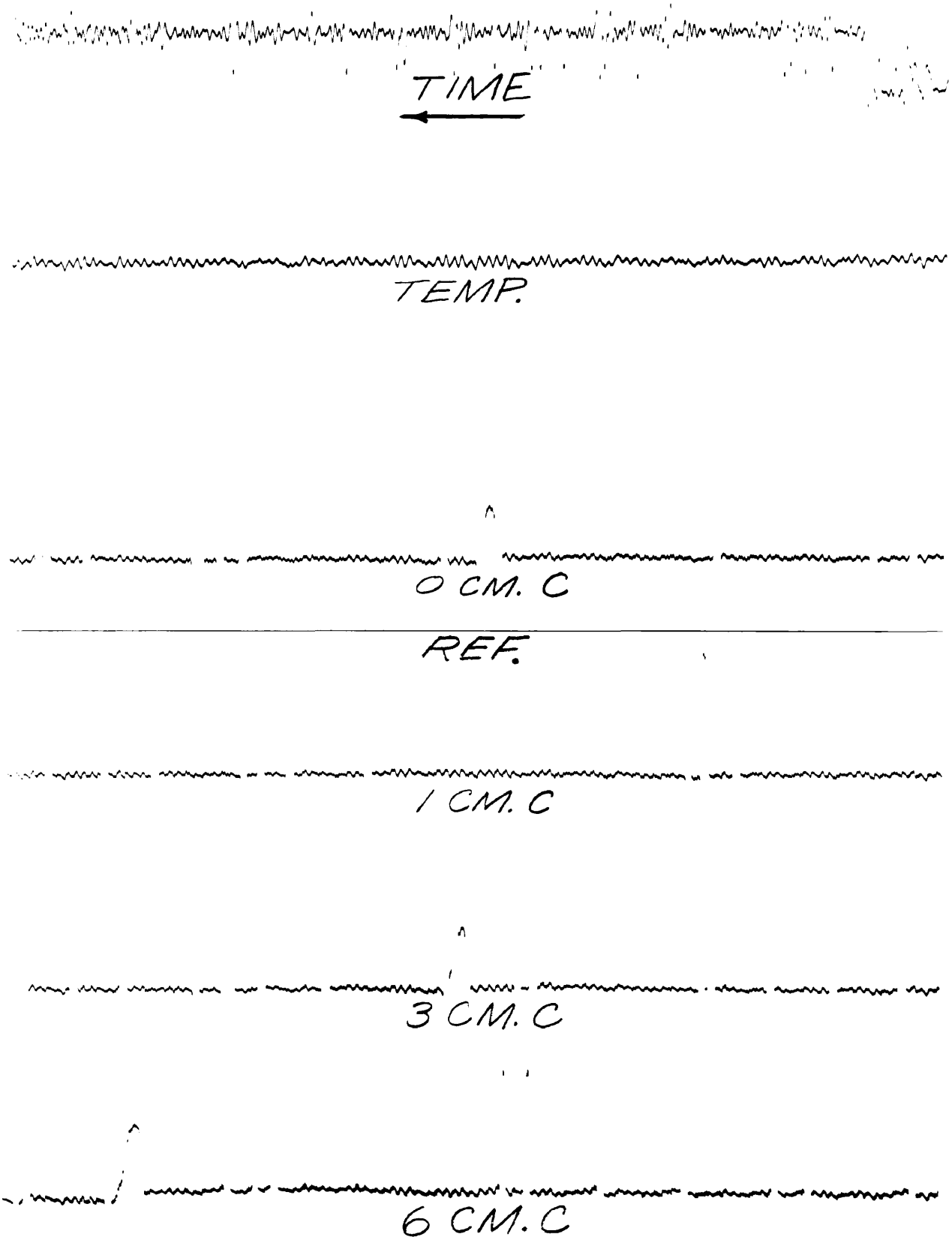

Fig. III-3 PHOTOGRAPH OF TELEMETERING FLIGHT RECORD

Thus the reading of this channel was accomplished by drawing the line which roughly approximated the average value of this noise and determining the distance of this line from the reference line. The record was started 24 minutes before launching and ran for a total of 313 minutes. The minute-by-minute tabulation of this record is given in App. 6 along with the three-point calibration for the temperature channel.

B. Results and Discussion

1. Temperature Measurements.

The thermistor was mounted in an almost air-tight aluminum can. This can served as a radiation shield and at the same time prevented convection currents from rapidly changing the temperature inside the can. The can was mounted at the geometrical center of the cubical gondola and was surrounded by the four cosmic-ray instruments. It is estimated that 85 per cent of the area of the can was facing the cosmic-ray instruments and 15 per cent was facing free space (through the green plastic-cloth gondola covering). It is reasonable to assume that the temperature inside this can was nearly the same as that inside of a typical Geiger counter in any one of the instruments. The curves of temperature vs time and vs altitude are shown in Figs. III-4 and -5. Fig. III-5 also shows the variation of the winter air temperature with altitude for comparison.

2. Cosmic-Ray Telescope Data.

The telescope data (see App. 6) were averaged in ten minute intervals and counting rates vs time curves for the four telescopes are shown in

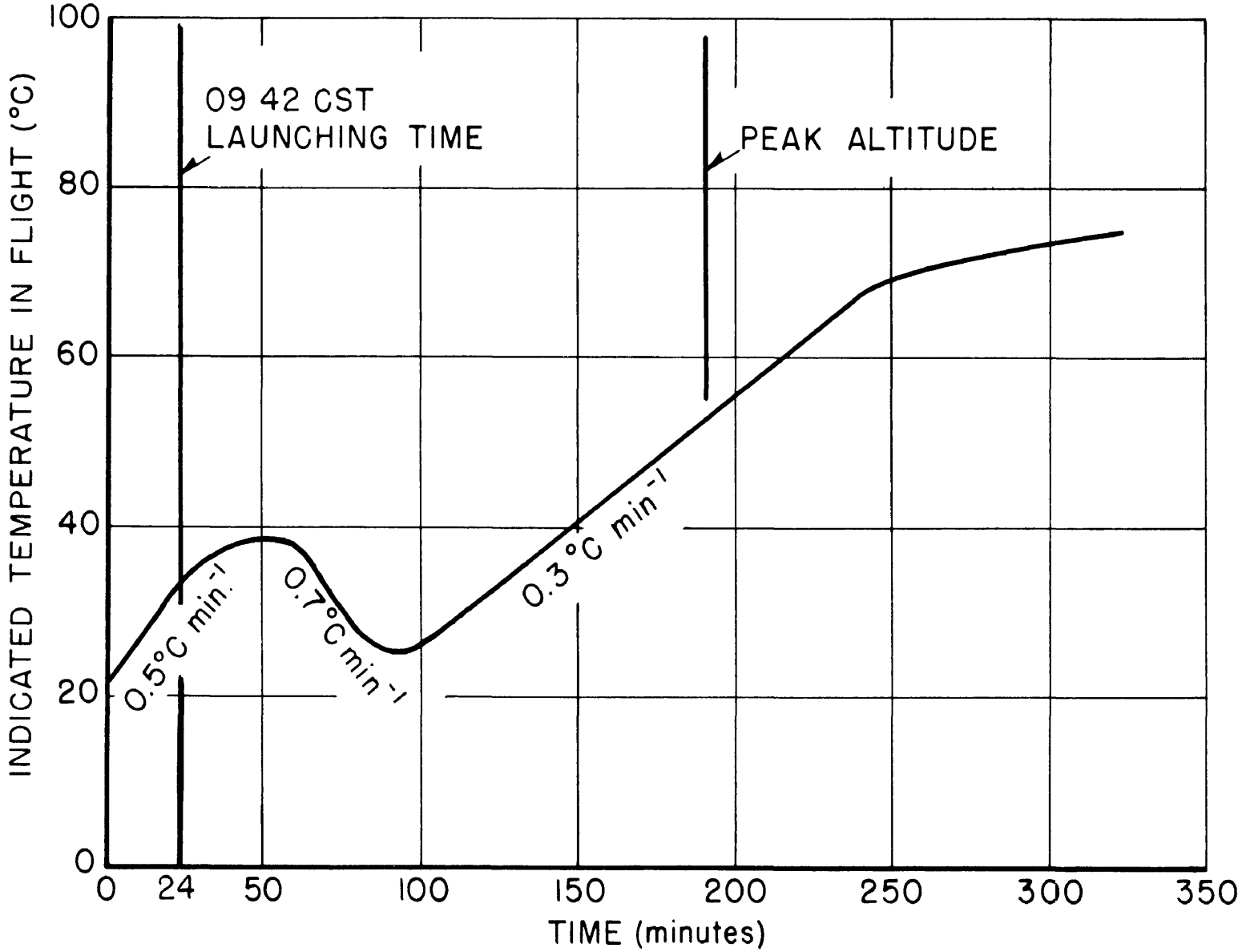
INDICATED TEMPERATURE IN FLIGHT (°C)
100
80
60
40
20
0
09 42 CST
LAUNCHING TIME
PEAK ALTITUDE
0.5°C min⁻¹
0.7°C min⁻¹
0.3 °C min⁻¹
0
24
50
100
150
200
250
300
350
TIME (minutes)

Fig. [illegible]

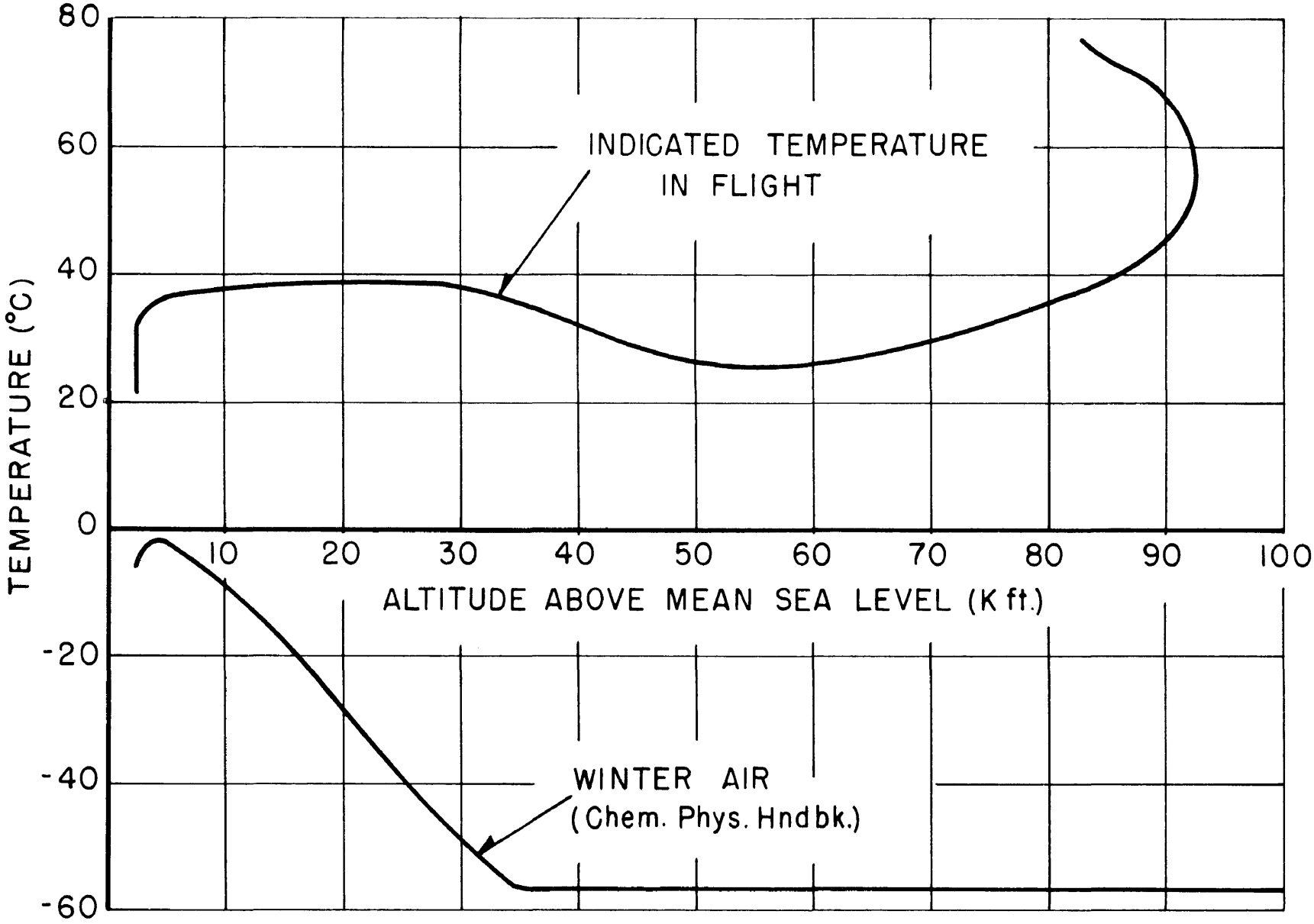

Fig. III-3 INDICATED [illegible]
[illegible] vs [illegible]

Fig. III-6*. These curves are very nearly similar in shape but since each telescope has a different geometric factor, the absolute values of the counting rates are different. The telescope over 6 cm C was the one which had been calibrated against the "perfect" telescope of App. 2 and thus the counting rates of this telescope will be used as a basis for normalizing the counting rates of the other three units. The total number of counts, N_i, (where the subscript indicates the amount of carbon under the particular telescope) in the interval 145 to 310 min. and the ratio N_6/N_i is tabulated below.

i	N_i	N_6/N_i
0	13,714	0.988 ± 0.012
1	12,142	1.116 ± 0.014
3	12,341	1.098 ± 0.014
6	13,552	1

The maximum combined correction for counter dead time and accidental coincidences is less than 1 per cent. This correction is less than the minimum per centage statistical fluctuation and has, therefore, been ignored. The four telescope counting rates were normalized and then averaged. The flight atmospheric pressure vs time curve is shown in Fig. III-7 and from this curve and the computed average counting rates, the curve (see Fig. III-8) of average telescope counting rate vs atmospheric pressure was obtained.

*In these curves and the following work, the errors indicated are the standard deviations attributable to statistical fluctuations.

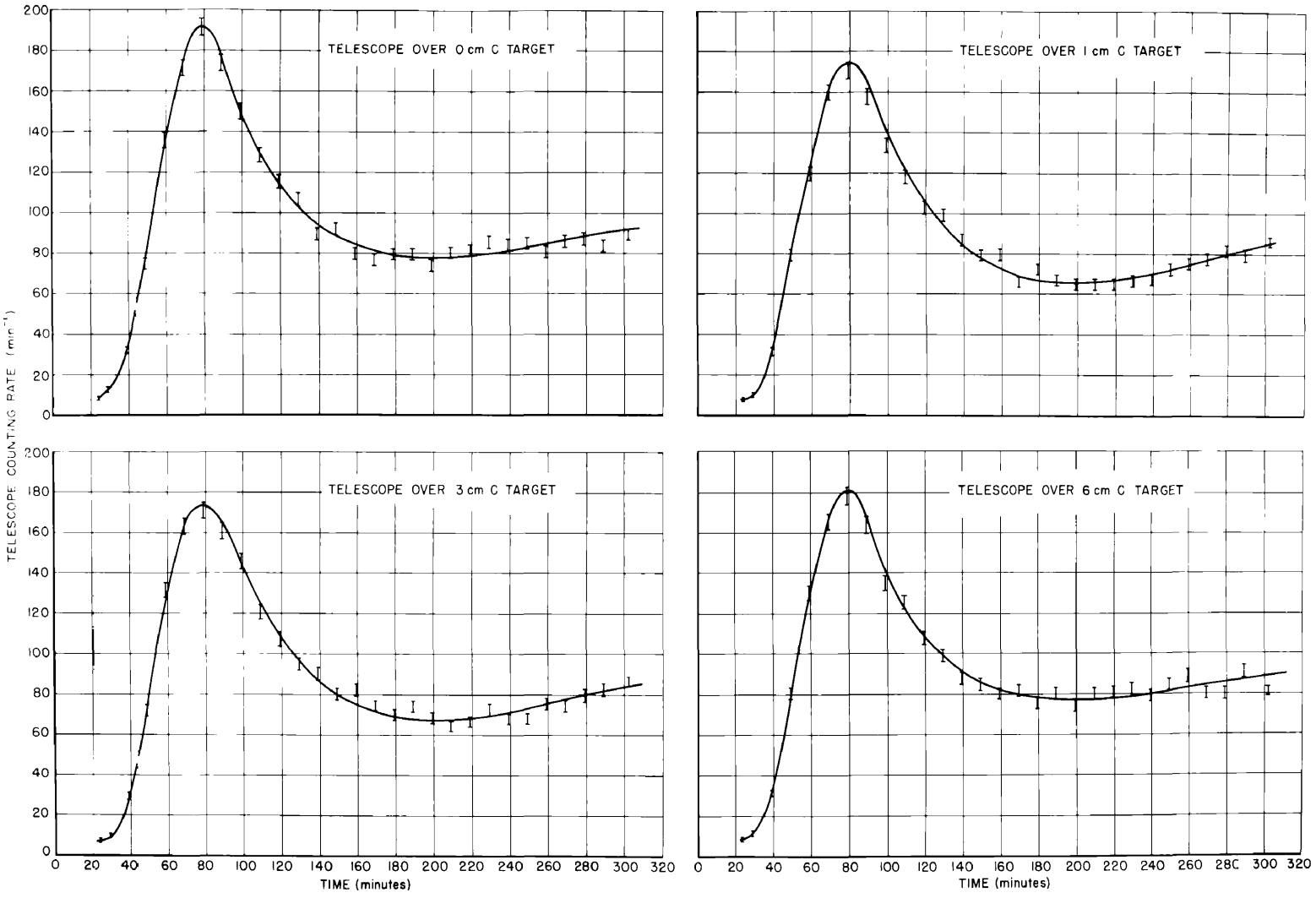

Fig. III-6 COUNTING RATES FOR THE FOUR TELESCOPES vs TIME CURVES

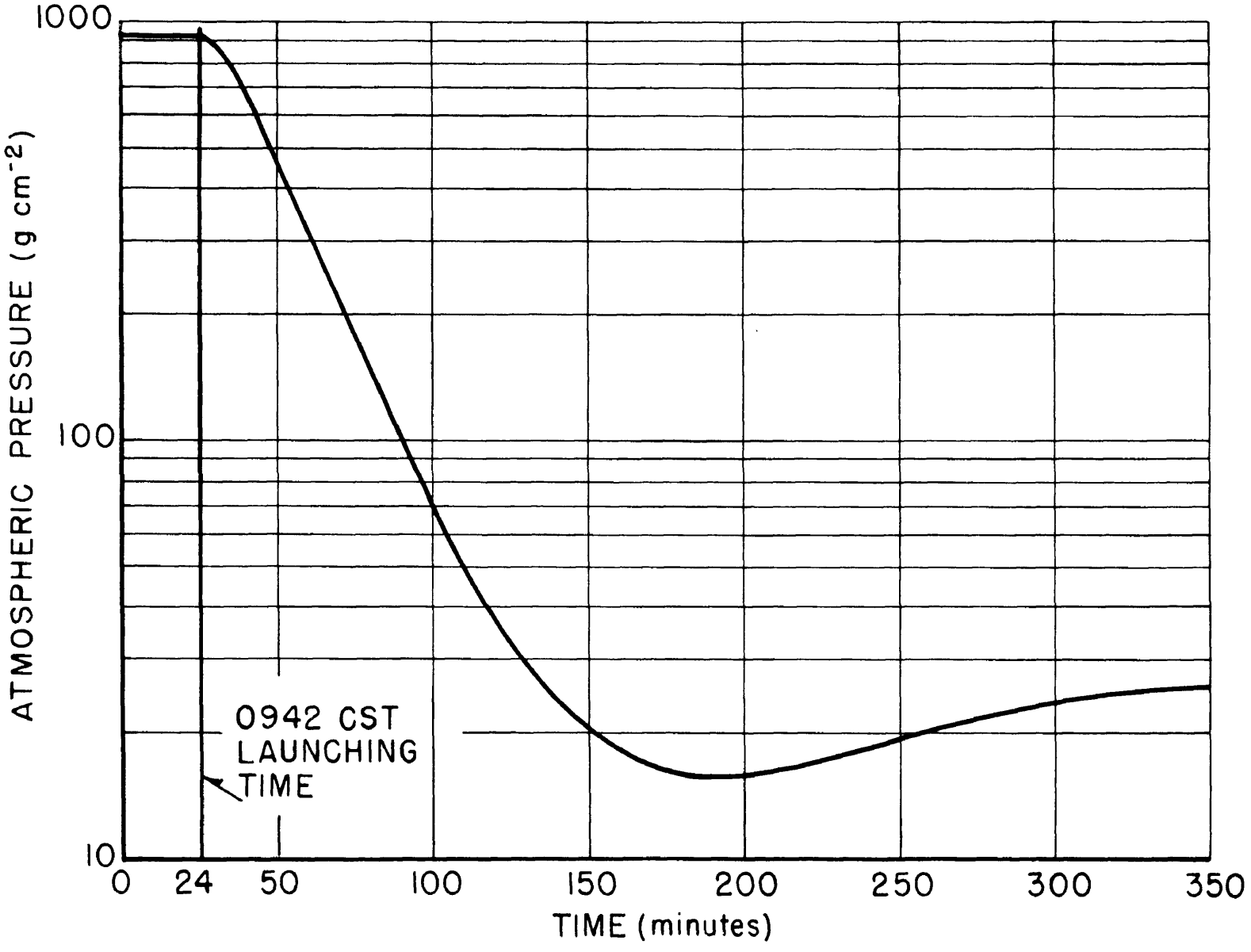
1000
100
10
ATMOSPHERIC PRESSURE (g cm-2)
0942 CST
LAUNCHING
TIME
0
24
50
100
150
200
250
300
350
TIME (minutes)

Fig. [illegible]

Fig. III-8 AVERAGE TELESCOPE COUNTING RATE vs ATMOSPHERIC PRESSURE CURVE

The vertical intensity variation with atmospheric pressure was then found from the average counting rate curve by using the efficiency determined in App. 1, the telescope geometric factor determined in App. 2 and the variation with atmospheric pressure of m in the $\cos^m\theta$ zenith angle dependence as determined by other workers in this field.[1,2,3,4] The resulting curve is shown in Fig. III-9. This curve shows excellent agreement with the work of Beihl et al[5] at $\lambda = 42^\circ$ N geomagnetic latitude. The comparison here is nearly direct since their experiments were made with vertical telescopes which had about the same zenith angle acceptance and were flown at nearly the same geomagnetic latitude as the experiments of the present work. The telescope of Beihl et al contained more absorber in the counter walls ($\sim$1.6 g cm^{-2} Fe as compared with 0.3 g cm^{-2} Al in the present case) but this difference is not noticed in the comparison. This curve also shows substantial agreement with the rocket work of Gangnes et al[6] at $\lambda = 41^\circ$N. In this case, however, the acceptance angle was much greater, the telescopes were inclined at an

---

[1] K. Greisen, Phys. Rev. 61, 212 (1942).

[2] D. J. X. Montgomery, Cosmic Ray Physics, Princeton University Press, Princeton: 1949, p. 169 ff.

[3] W. F. G. Swann, Rev. Mod. Phys. 11, 242 (1939).

[4] J. F. Jenkins, Jr., Bul. Amer. Phys. Soc. 23, No. 3, 1948, Washington meeting, Abstract EA3.

[5] A. T. Beihl, H. V. Neher and W. C. Roesch, Phys. Rev. 76, 914 (1949).

[6] A. V. Gangnes, J. F. Jenkins, Jr., and J. A. Van Allen, Phys. Rev. 75, 57 (1949).

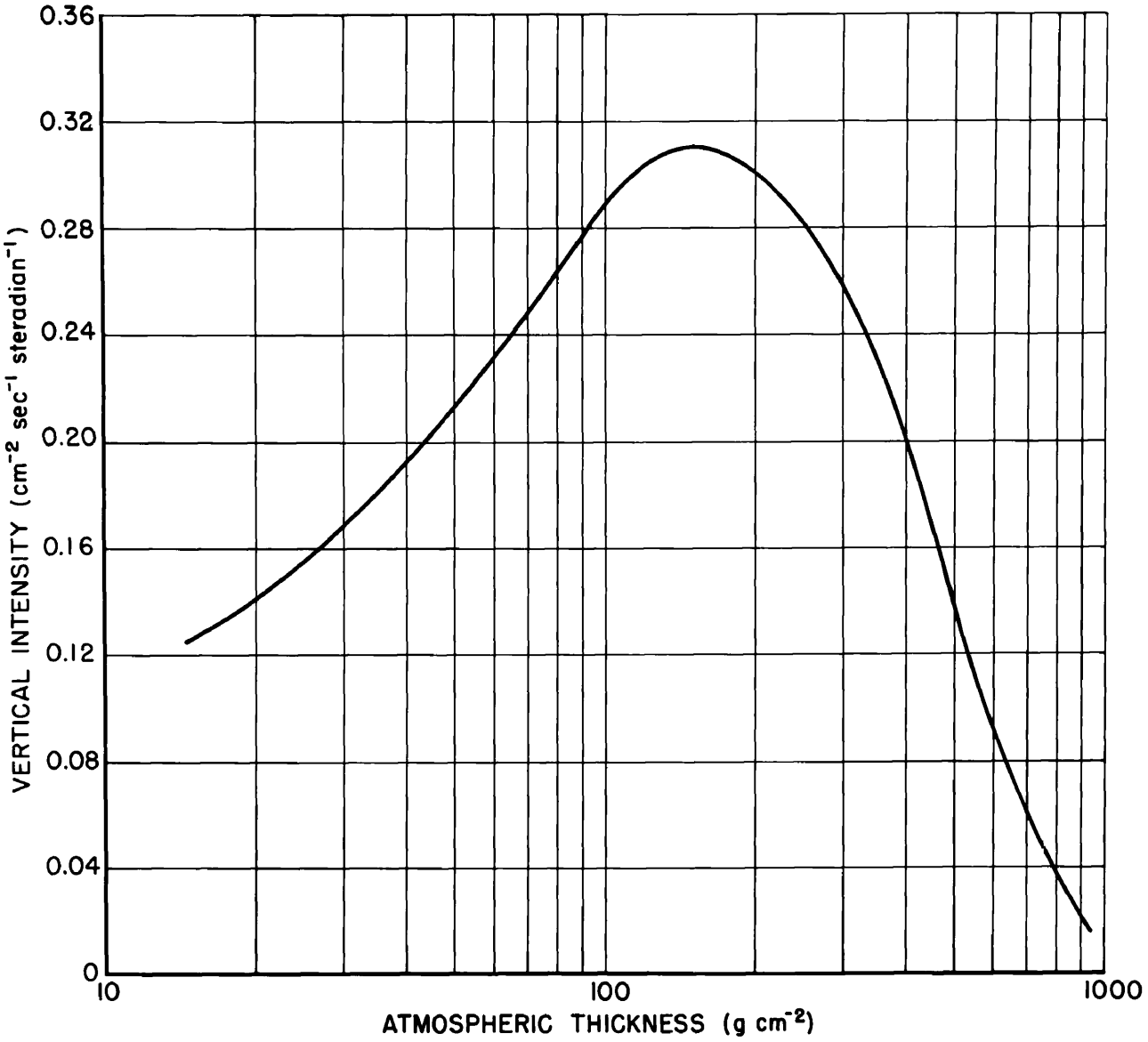

Fig. III-9 VERTICAL INTENSITY vs ATMOSPHERIC PRESSURE CURVE

angle of 45° to the rocket axis and the rocket axis was changing throughout flight. The agreement here is good in the altitude range where $m = 0$ (isotropic distribution of intensity) and at lower altitudes if one assumes that since the rocket was spinning at a constant rate, the average counting rate of the two opposed telescopes is characteristic of the intensity at zenith angle 45°.

3. Cosmic-Ray Burst Data.

The burst event is that event in which three or more ionizing rays trigger a triple coincidence array in coincidence with a telescope event (two will do it but the probability is extremely low). This ionizing radiation must be energetic enough to penetrate at least the 0.03 g cm^{-2} of average path through the brass counter walls of the detector. The interposed targets in the four telescope-burst detector arrays were sheets of graphitic carbon 3/8" thick and of density 1.37 g cm^{-3}. In each of the four arrays a different number of C sheets were used. The numbers used were: 0, 1, 3 and 6 sheets. The effective thickness of each sheet was (see App. 3) $1.06 \cdot 0.375 \cdot 2.54 = 1.01$ cm, thus the target thicknesses will be referred to as 0, 1, 3 and 6 cm.

The number of detected bursts per minute for these four target thicknesses is shown in the histograms of Fig. III-10. It was found by averaging over various sub-intervals within the interval from 140 to 310 min. that the burst rates for any one target thickness were not statistically different. The grand average for this interval is indicated in the figure. The burst rates are proportional to the telescope rates and were, therefore, normalized by the same ratios as were the

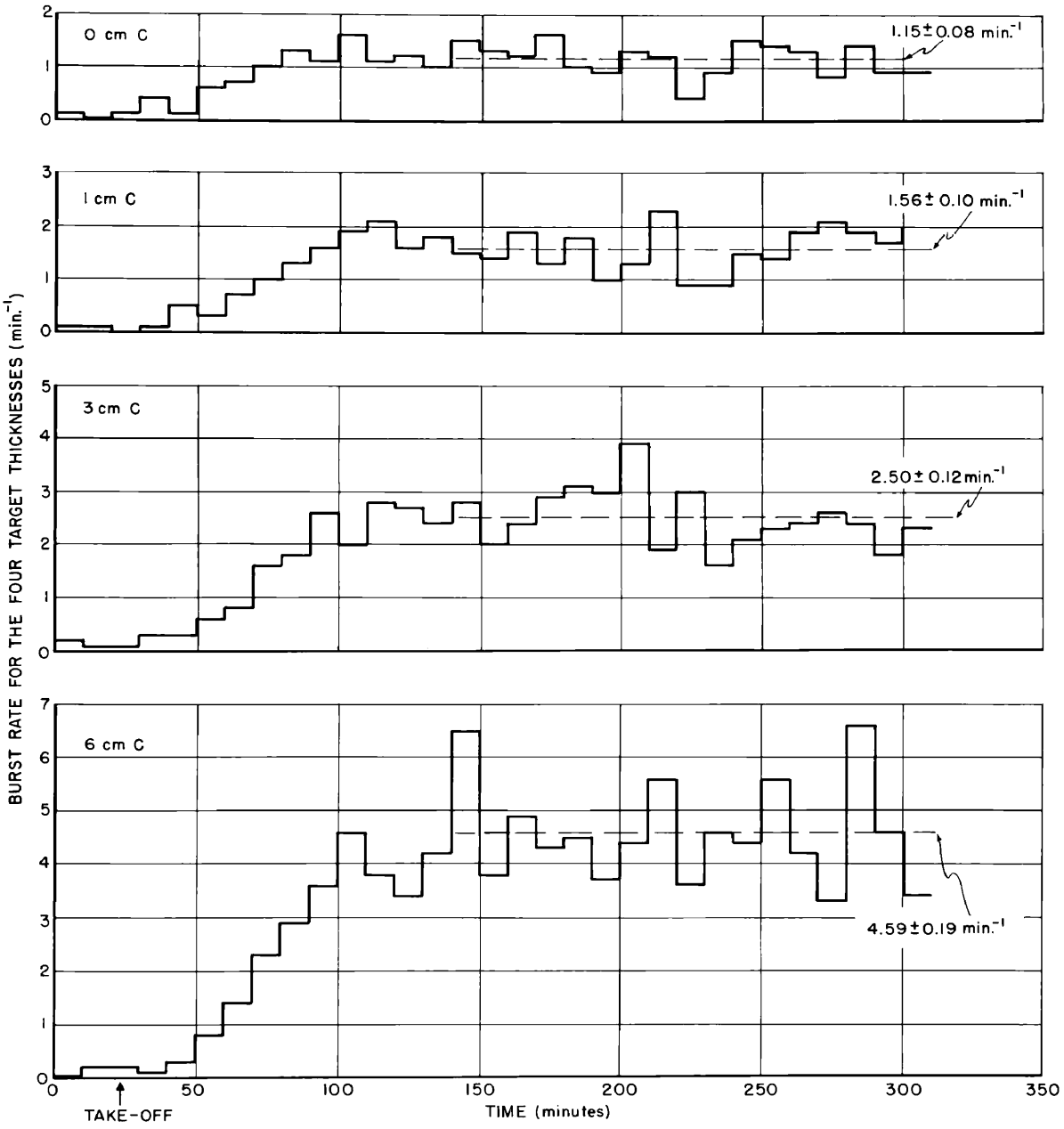

Fig. III-10 BURST RATE FOR THE FOUR CARBON TARGET THICKNESSES vs TIME HISTOGRAMS

the telescopes. These rates were then corrected for counter dead time and counter efficiency. The normalized and corrected burst rates, for the four target thicknesses, are shown as a function of atmospheric pressure in Fig. III-11. The first four low altitude points show the averages of the four sets of data at each altitude since the counting rates were not statistically different. One cannot help but notice the evident flattening of these curves for pressures of less than 100 g cm^{-2}.

At this point it might be well to investigate the mechanisms by which these bursts are produced.

(a) The contribution of knock-on electrons - A process whereby a charged particle traverses the telescope and creates two knock-on electrons in the target and thus proceeds with these electrons into the burst detector would be detected as a burst. In order to estimate the maximum number of this type of event, it is assumed that the knock-on process in the high altitude flux is the same as that for μ mesons at sea level.[1] Brown et al[2] have used a "hard" telescope in coincidence with an interposed segregated array of side counters under various targets to obtain the data tabulated below.

Target	Tde/T	Tef/T
0.34* g cm^{-2} Al	0.0033	0.0038
0.45 g cm^{-2} Wood	0.0041	0.0041
3.8 g cm^{-2} Pb	0.0033	0.0042
15 g cm^{-2} Pb	0.0044	0.0056

*Two 0.11 g cm^{-2} wall Al counters side by side.

[1] F. L. Herford, J. F. I., 249, 449 (1950).

[2] W. W. Brown, A. S. McKay and E. D. Palmatier, Phys. Rev. 76, 506 (1949).

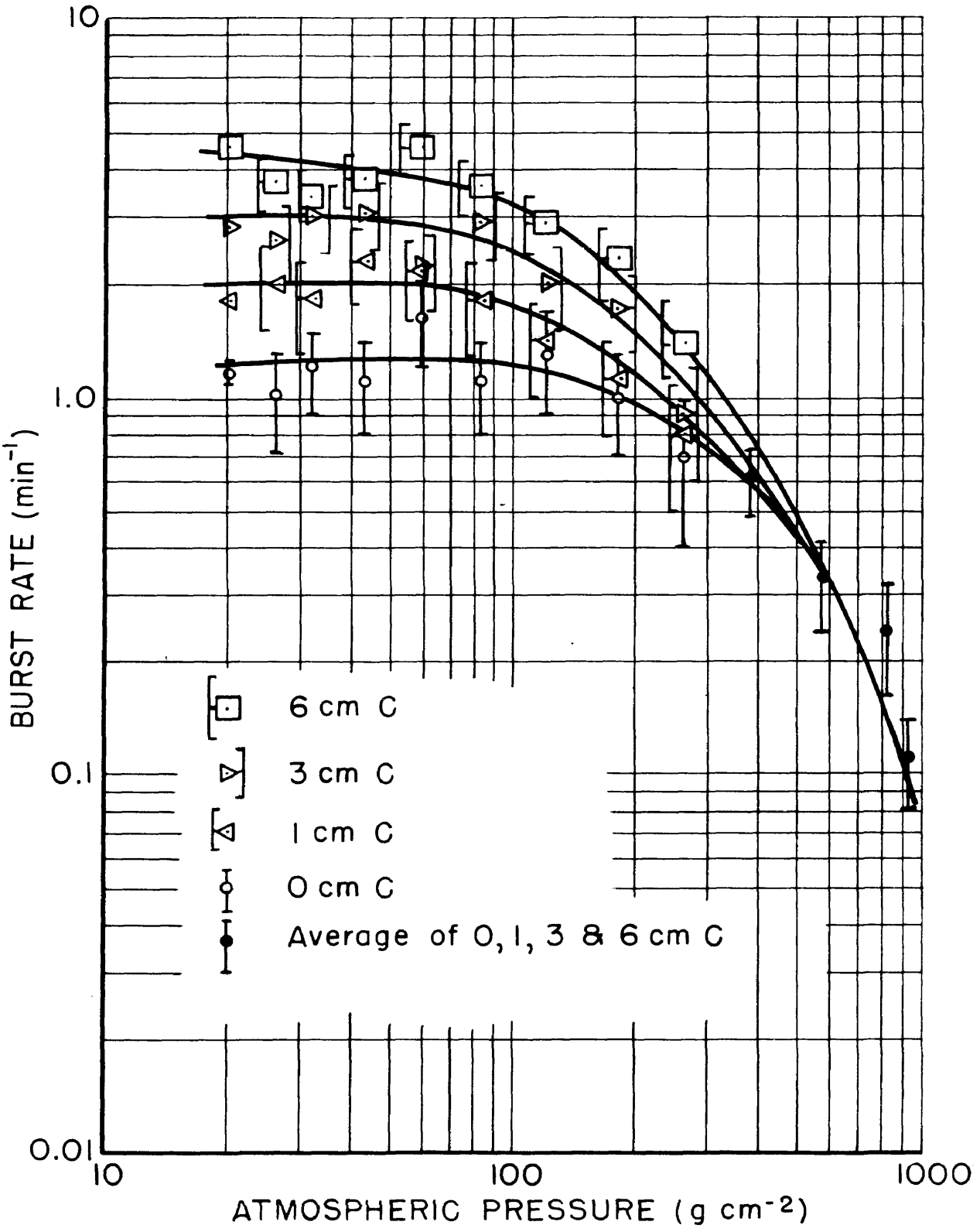

Fig. III-11 vs ATMOS PRES

In this table, T is the telescope event and d, e, and f are side counter events. These results can be compared directly with the balloon-borne equipment of the present experiment since the total target thicknesses are similar* (telescope 0.3 g cm^{-2}Al, 1.37 g cm^{-2} per C sheet or 0.3, 1.4, 4.1 and 8.5gcm^{-2}). The knock-on process exhibits saturation for even the very thin targets so all of the cases of the present experiment will be affected equally. The detection scheme used by Brown et al was rather similar to the burst detector of the present experiment which leads one to believe that the detection efficiency for this event would be the same in both cases. If this is the case, the number of these events should be 0.4 per cent of the telescope events.

This ratio seems reasonable in the light of the ground data. The percentage of bursts per telescope event at 930 g cm^{-2} was 1.3 $\pm$ 0.4.

(b) The zero thickness case - In the case of the bursts produced with no C target it is necessary to assign the role of effective target to the material in the immediate vicinity of the array. The average path through the telescope is 0.3 g cm^{-2}Al and assuming a geometric cross section the number of bursts would be 0.4 per cent of the burst producing flux. Of these, only 20 per cent would be detected (see App. 4) or 0.08 per cent is to be attributed to the material in the telescope. To this is to be added 0.4 per cent attributable to knock-on electrons. The air

*The probability of the knock-on event is proportional to the number of electrons which is given by $N(\rho\ t)\ Z/A$ where N is Avagadro's number and $(\rho\ t)$ is the thickness in g cm^{-2}. Since $Z/A \simeq 0.5$ for all these cases it is only necessary to compare the values of $(\rho\ t)$.

below the telescope cannot account for any measurable part of this production so the only remaining material is that in the three polyethylene high voltage connectors, the 1/16" telescope support plate and the counter end seals. It would seem unlikely any but the uppermost connector would produce bursts that would yield the conditional telescope event and the burst event. If it is assumed that this 30 cm^3 block is mainly composed of carbon and that the flux in approximately 10 per cent of the solid angle of the upper hemisphere could create detectable bursts, then the percentage of bursts per telescope event (assuming geometric cross section) would be 5 per cent. Because of the two-fold increase in distance from the detector of this target over the normal target position, the detector efficiency would be somewhat lower than the normal case (see App. 4). It is estimated that this efficiency would be 15 per cent; thus this contribution is 0.75 per cent.

The remaining mechanism for the "no target" case is that of accidental coincidences. A consideration of all possible modes of generation of the burst event by accidental means shows that at most 0.25 per cent of the telescope rate is attributable to accidentals. A summary of the above findings is tabulated below.

Mechanism	per cent TB/T
Material in telescope	0.08
Knock-ons	0.4
Materials close to telescope	0.75
Accidentals	0.25
T O T A L	1.48

The average burst rate as calculated for the "no target" case over the interval from 140 to 310 min. is 1.15 ± 0.08 min^{-1} and the average associated telescope rate for this same interval 77.9 ± 0.7. The percentage ratio is then 1.48 ± 0.11. The closeness of agreement is fortuitous, of course, but it is indicative of the accountability of the zero thickness bursts.

(c) Electron and photon showers - The electron and photon intensity is a small per centage of the total intensity at 20 g cm^{-2} atmospheric pressure (this will be discussed in a later section). In addition to this fact, the calculations of Rossi and Greisen[1] on multiplicative electron and photon initiated showers show that for even the thickest carbon target ($\sim$1/6 of a radiation length) used in the present experiment the probability is very near zero for this event.

(d) Large zenith angle burst-producing radiation - The events in which burst-producing radiation enters the edge of the target at large zenith angles and produces a burst in which at least one secondary will traverse the telescope are possible burst events. The angular distribution of secondaries with respect to the primary ray is such that in the range $50 \leq \theta' \leq 100^{\circ}$ there are at most 0.05 secondaries per burst per steradian (see Fig. A4-6). It is seen that (see Fig. II-1) these primary rays can enter the edge of the target block over approximately half their total solid angle and produce secondaries which might

---

[1] B. Rossi and K. Greisen, Rev. Mod. Phys. 13, 240 (1941).

traverse the telescope (within the range of θ' indicated above) A reasonable estimate of the volume of target properly disposed for such events is half the telescope tray area by the target thickness or 70 cm^3 for the case of the 6 cm target. The maximum number of secondaries per burst that go through the telescope is $0.05\ (6.4)/\ (13.5)^2 = 0.0065$ (for the solid angle see Fig. II-1). There are $2\pi j/\lambda$ bursts $cm^{-3}\ min^{-1}$ produced by the entire isotropic hemispheric burst-producing flux of directional intensity j $cm^{-2}\ min^{-1}$ steradians^{-1} with mean free path for burst production λ cm. Assuming $j = 6$ and $\lambda = \lambda_{geom.}$ ($60\ g\ cm^{-2}$ or since $\rho = 1.37\ g\ cm^{-3}$ $\lambda_{geom.} = 45$ cm), then $\pi \cdot 6/45 = 0.42$ burst $cm^{-3}\ min^{-1}$ and for the 70 cm^3 block there will be ~ 30 bursts per min. produced. Of these $0.0065 \cdot 30 \simeq 0.2\ min^{-1}$ would give rise to the telescope event. The average number of secondaries of the type required for burst detection is five (see App. 4) and on the average at least three of these five must go off at wide angles to the primary ray and also must be oriented on the lower side of the target in order that an indicated burst event be possible. This reasoning coupled with the calculated detector efficiency of 20 per cent excludes this mechanism as a means of enhancement of the burst rate. It is also seen that the estimated 0.2 min^{-1} is a small contribution to the telescope rate of $\sim 80\ min^{-1}$.

(e) The carbon targets - Consideration of the various mechanisms (a) through (d) listed above shows conclusively that the true burst production rates for the three carbon targets can be obtained by subtraction of the burst rates obtained for the case with no carbon target.

The true burst rate vs atmospheric pressure for 6, 3 and 1 cm C are shown in Figs. III-12, -13 and -14. For atmospheric thicknesses of greater than 75 g cm^{-2} the 6 cm of C case fits a simple exponential with an absorption mean free path of $1/\mu$ = 140 g cm^{-2}. Curves of the same shape are shown in the 3 cm and 1 cm case. In the latter cases the statistics are poor but the curve is seen to fit within the statistical fluctuations. Lord[1] obtains $1/\mu$ = 145 g cm^{-2} for all stars at $\lambda = 28^{\circ}N$ and $54^{\circ}N$ geomagnetic latitudes with a definite flattening at atmospheric thicknesses less than 100 g cm^{-2}. The most dramatic exhibition of this slow increase of burst rate above $\sim$100 g cm^{-2} is shown in the rocket measurements of Van Allen.[2] The case of the Al target (average path 7.1 g cm^{-2}) has been replotted (see Fig. III-15) from the original data on a logarithmic atmospheric pressure scale. The absorption mean free path for atmospheric thicknesses greater than 100 g cm^{-2} is $1/\mu$ = 225 g cm^{-2}. It is quite clear that the burst production curve (and hence the burst producing radiation) does not follow the total intensity curve (compare Figs. III-9 and -11). This fact and the low altitude data (2.6 Kft where the flux is mainly μ mesons) excludes electrons (compare these two curves at the Pfotzer maximum where there are a high per centage of energetic electrons) and μ mesons from the burst producing flux.

---

[1] J. J. Lord, Phys. Rev. 81, 901 (1951).

[2] J. A. Van Allen, Proc. Echo Lake Cosmic Ray Symp., Paper No. 28 (1949).

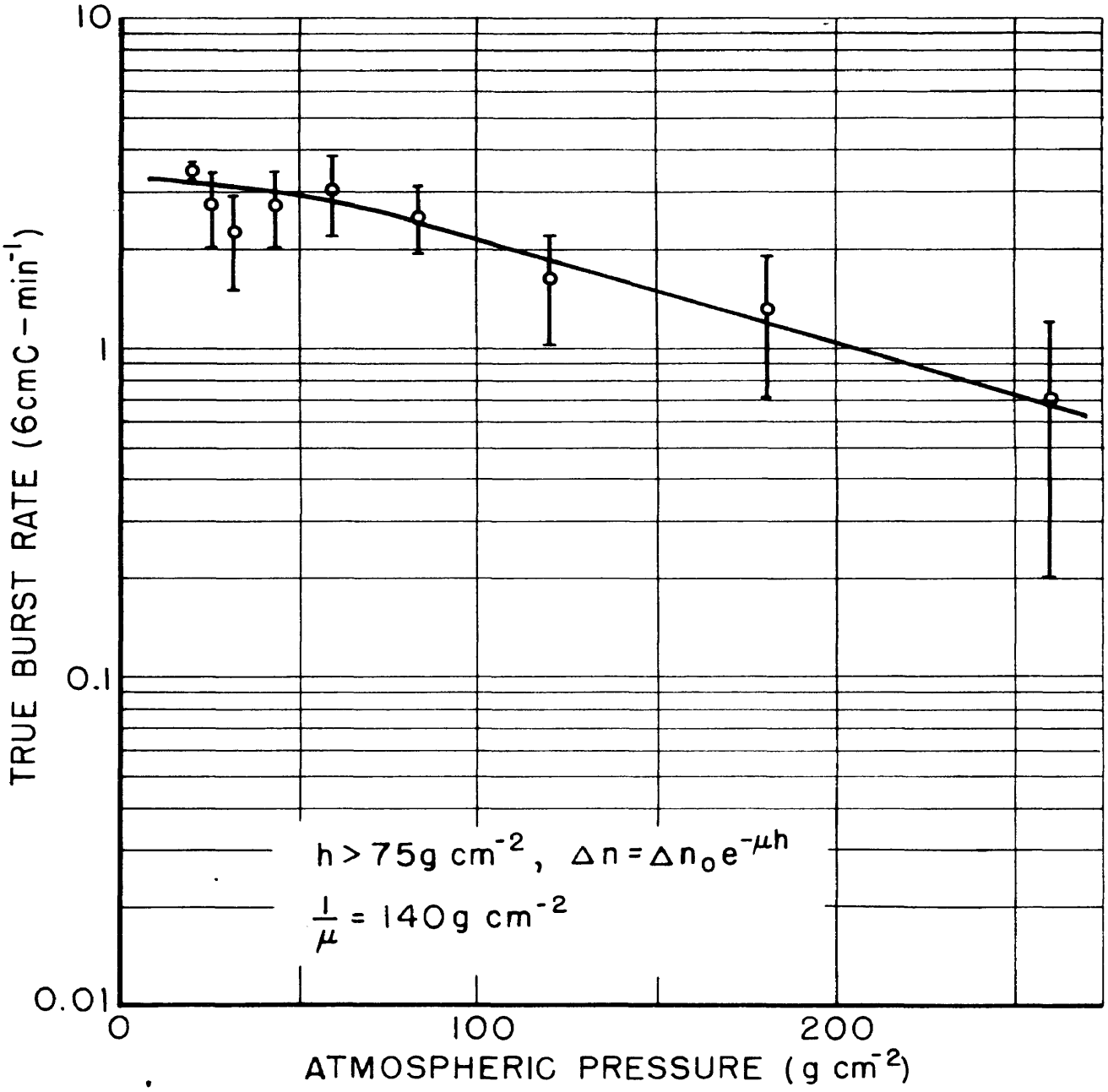

Fig. III-13 TRUE BURST RATE IN 6cm C vs ATMOSPHERIC DEPTH IN C UNITS

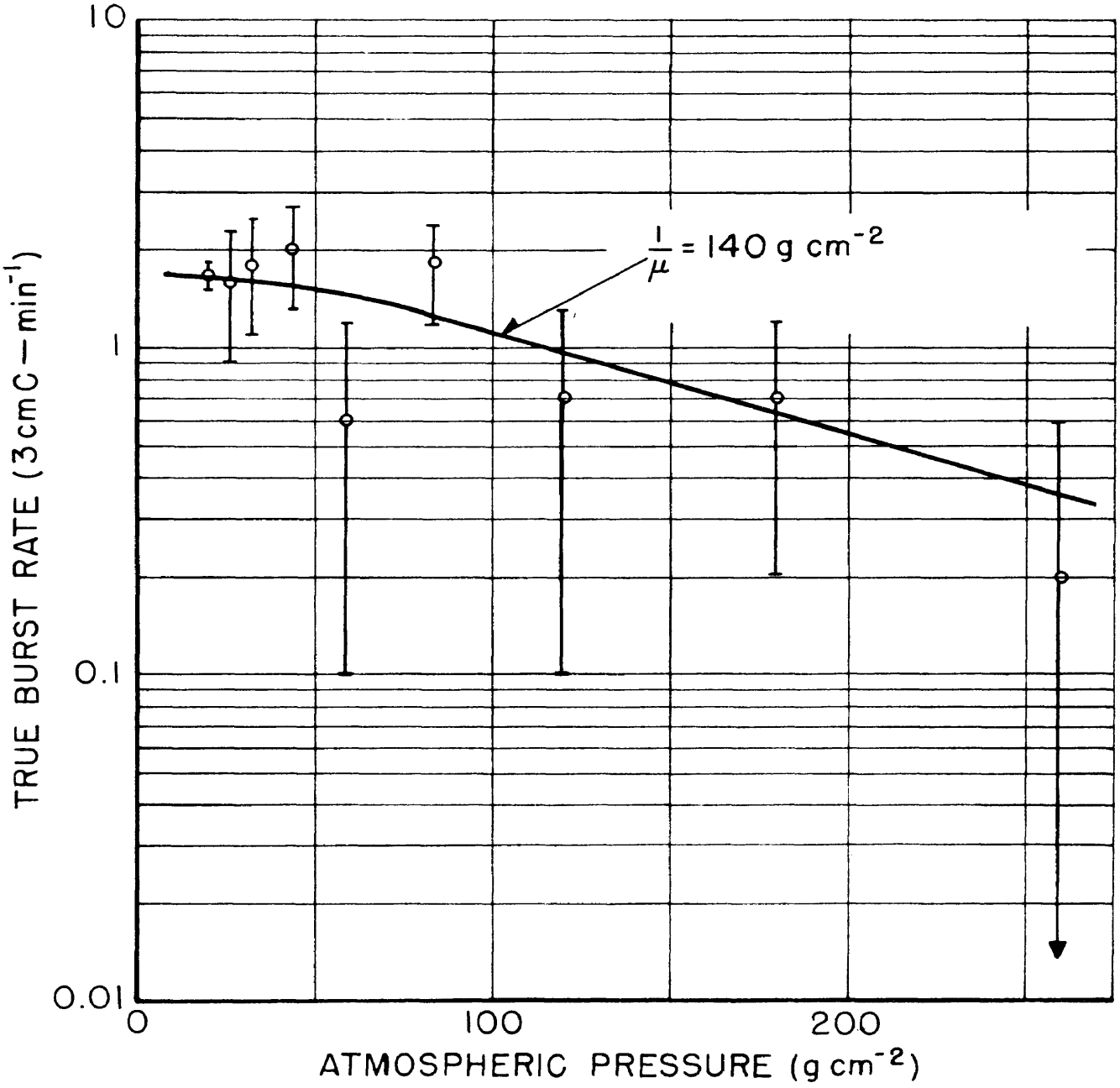
10
1
0.1
0.01
0
100
200
TRUE BURST RATE (3 cm C — min⁻¹)
ATMOSPHERIC PRESSURE (g cm⁻²)
1/μ = 140 g cm⁻²

Fig. III-13

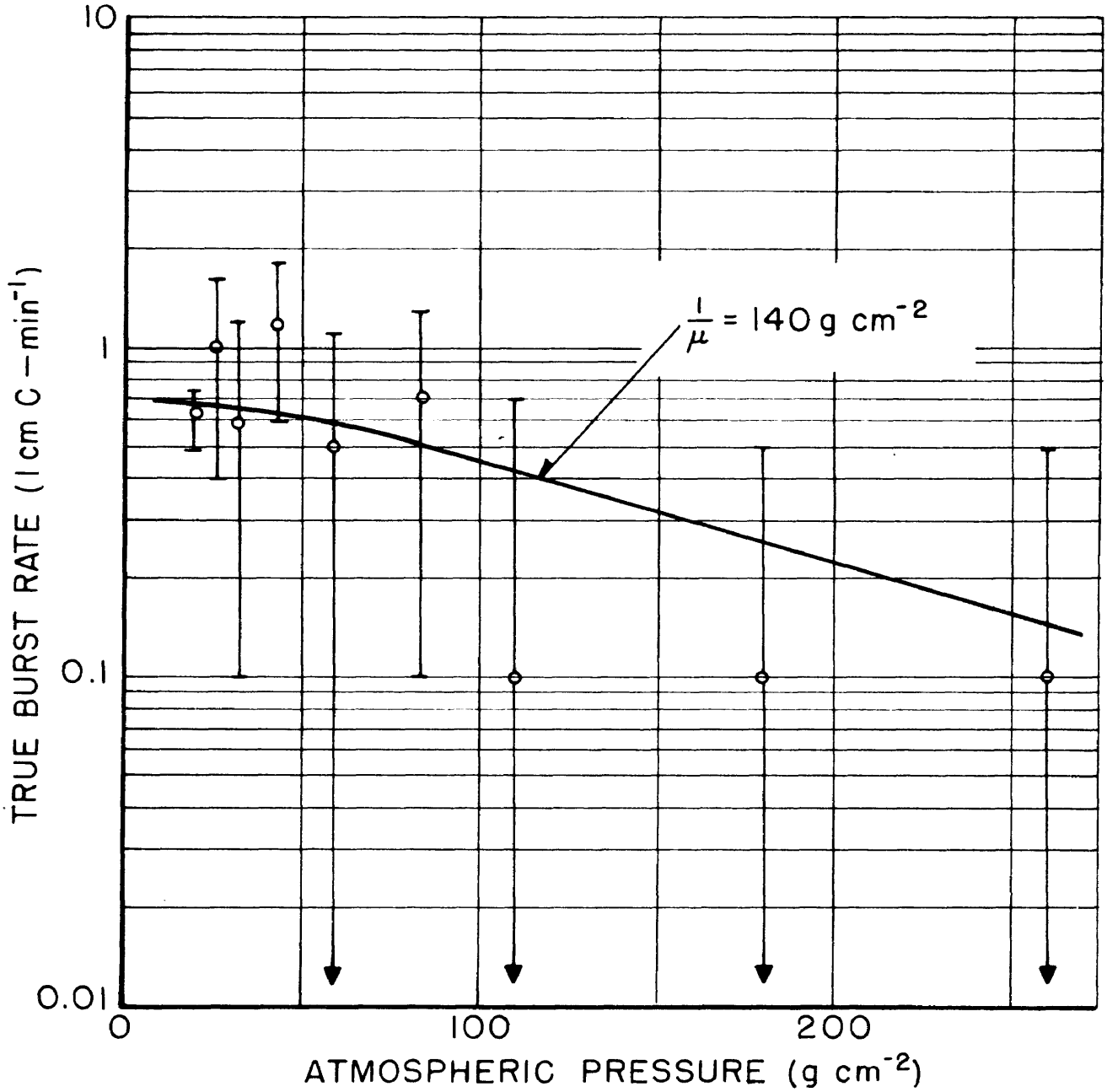

Fig. III-14 TRUE BURST RATE IN 1 cm C VS ATMOSPHERIC PRESSURE

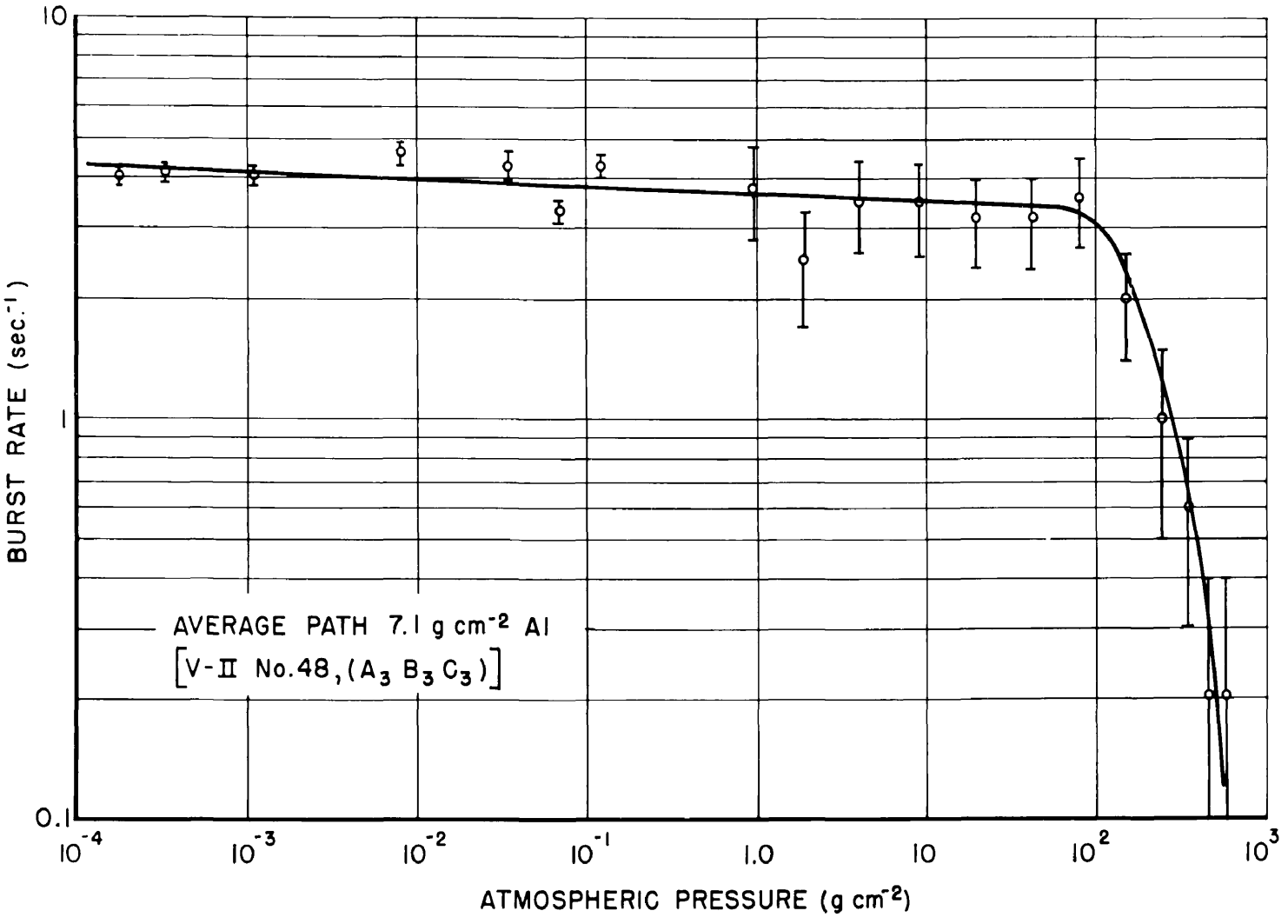

Fig. III-15 BURST RATE IN Al vs ATMOSPHERIC PRESSURE CURVE
(AFTER VAN ALLEN)

The charged, burst producing flux within the atmosphere can now be decomposed into the following possible components: π mesons, protons, α particles and h-nuclei ($Z \geq 3$). It is then seen that the burst data of this experiment is given by

$$\mathfrak{J} = \frac{N}{A_c} \sum_i \sigma_i j_i G_i' \eta_i, \quad i \cong \pi, p, \alpha \text{ and } h \qquad (1)$$

where $\mathfrak{J}$ is the true burst rate per g cm^{-2} of carbon, N is Avagadro's number, A_C is the atomic weight of carbon, σ_i is the cross section of the i^{th} component of the burst producing flux with carbon in cm^2 per atom, j_i is the directional intensity of the i^{th} component of this flux, G_i' is geometric factor of the telescope multiplied by the counter efficiency cubed for the i^{th} component and η_i is the efficiency of the burst detector for the i^{th} component. The values of σ_α and σ_h have been determined for emulsion, glass and brass by Kaplon et al.[1*] These cross sections fit the empirical equation

$$\sigma_{K,T} = \pi(r_K + r_T - 2\Delta r)^2$$

where the subscripts refer to the projectile and the target and $r = 1.45 \cdot 10^{-13} A^{1/3}$ cm, $\Delta r = 1.0 \cdot 10^{-13}$ cm. It will be assumed that this formula also obtains in the cases of carbon and air. The values of G_α' and G_h' should differ only in the intrinsic counter efficiency from $G_p' = (0.963)^3 G(0,m)$ as determined in App. 2.

---

[1] M. F. Kaplon, B. Peters, H. L. Reynolds and D. M. Ritson, Phys. Rev., 85, 295 (1952). Note: In the pages that follow, this work will be referred to as Kaplon et al.

[*] Kaplon et al. have shown that this cross section does not depend strongly on the energy at the projectile in the energy range under consideration since the measurements made at $\lambda = 41^\circ$N and at $\lambda = 55^\circ$N geomagnetic latitude yield the same cross sections.

The counter efficiency is given by the expression

$$\bar{e} = 1 - \exp(-\rho\lambda p)$$

where ρ is the primary specific ionization, λ is the mean path length through the counter and p is the pressure in the counter. The primary specific ionization can be closely approximated by $\rho \propto Z^2$ for this case and the efficiencies are: $\bar{e}_p = 0.963$, $\bar{e}_\alpha = 1.000$ and $\bar{e}_h = 1.000$. Then $G_p(0,m) = G'_\alpha = G'_h$. There is no reason to believe that, over the geometry of the vertical telescopes, the flux of any of the components should differ substantially from an isotropic distribution. It is, therefore, assumed that m = 0 for all the cases at hand and thus $G'_\alpha = G'_h = G(0,0) = 8.2 \pm 0.2$ cm^2 steradian.

At this time, it is well established that the charged primary flux is composed mainly of protons and α particles with a smaller number of heavier nuclei (see Kaplon *et al* and references therein). In particular at $\lambda = 41^\circ$N geomagnetic latitude the components in order of decreasing intensity are: protons, α particles and nuclei of $Z \geq 6$ which are completely stripped of electrons. Measurements near the "top" of the atmosphere (≤ 20 g cm^{-2}) show that the contribution of electrons and photons to the total intensity is a very small per centage of this intensity.[1] Davis *et al*[2] obtain $j_\alpha = 0.043 \pm 0.004$ (cm^2 sec steradian)$^{-1}$ at an atmospheric pressure

---

[1] J. G. Wilson, Progress in Cosmic Ray Physics, North-Holland Publishing Company, Amsterdam; Interscience Publishers, Inc. New York, 1952, pp. 194, 256, 288, 324 and 348.

[2] L. R. Davis, H. M. Caulk, C. Y. Johnson, G. J. Perlow and C. A. Schroeder, Bul. Amer. Phys. Soc., 27 No. 3, 1952, Washington Meeting, Abstract Z2.

of 9 g cm^{-2} in the vertical direction at $\lambda = 55^{\circ}N$ geomagnetic latitude. The corrected $j_{0,\alpha}$ at the top of the atmosphere is

$$j_{0,\alpha} = j_{\alpha} e^{h/\lambda_a} = 0.053 \pm .005 \text{ (cm}^2 \text{ sec steradian)}^{-1}$$

where $\lambda_a = 44.5$ g cm^{-2} as calculated for α particles in air from the formula of Kaplon et al. From the integral energy spectrum for α particles given by Kaplon et al, the ratio of the intensity at $\lambda = 41^{\circ}N$ to that at $\lambda = 55^{\circ}N$ is 0.38. Thus, using the j_{α} of Davis et al corrected to the "top" of the atmosphere, $j_{0,\alpha} = 0.020 \pm 0.002$ (cm^2 sec steradian)$^{-1}$ at $\lambda = 41^{\circ}N$. Then at 20 g cm^{-2} atmospheric pressure,

$$j_{20,\alpha} = j_{0,\alpha} e^{-20/44.5} = 0.013 \pm 0.001 \text{ (cm}^2 \text{ sec steradian)}^{-1} .$$

The data of Kaplon et al give

$$j_{0,h} = (8.3 \pm 0.9) \cdot 10^{-4} \text{ (cm}^2 \text{ sec steradian)}^{-1}$$

at $\lambda = 41^{\circ}N$ and at 20 g cm^{-2},

$$j_{20,h} = j_{0,h} e^{-20/25} = (3.8 \pm 0.4) \cdot 10^{-4} \text{ (cm}^2 \text{ sec steradian)}^{-1} .$$

At 20 g cm^{-2} the counting rates are obtained by multiplying these intensities by $60 G' = 60 (8.2 \pm 0.2)$ cm^2 steradian sec min^{-1} and $n_{\alpha} = 6.4 \pm 0.5$ min^{-1} and $n_h = 0.19 \pm 0.02$ min^{-1}. The total average counting rate over the period from 140 to 310 min was $n_T' = (77.0 \pm 0.7)$ min^{-1} and when the counter efficiency correction is applied this becomes,

$$n_T = [n_T' - (n_\alpha + n_h)]\,(0.963)^{-3} + n_\alpha + n_h = (85.4 \pm 0.9)\ \text{min}^{-1}$$

where n_T includes μ mesons, π mesons (the number of π mesons should be small because of π-μ decay, since even $5 \cdot 10^9$ ev π mesons would traverse $\sim$ 270 m, on the average, before decaying into μ mesons), protons, α particles and h-nuclei. This counting rate also includes the atmospheric albedo of which only the re-entrant albedo could cause the burst events while all the albedo could add to the telescope events. Little is known about the atmospheric albedo. In a recent experiment, Winckler[1] measured the albedo of charged particles for which $\beta \geq 0.7$ at 17 g cm^{-2} atmospheric pressure in the vertical direction. These particles were energetic enough to traverse 25 g cm^{-2} of lucite interposed in a telescope of approximately the same geometric factor as the ones of the present experiment. His results show no detectable albedo (within statistical fluctuations) for these particles. In addition to this, the showers produced by the flux at large zenith angles in the atmosphere below the telescope must be included. A comparison of the ground telescope data with the high altitude data (tabulated below) allow the establishment of a lower limit for particle energies in these showers that could cause the telescope event. The relative

Atmospheric Pressure (g cm^{-2})	n_o(min^{-1})	n_1(min^{-1})	n_3(min^{-1})	n_6(min^{-1})
PAFB-930	0.127 ± 0.008	0.101 ± 0.006	0.107 ± 0.007	0.128 ± 0.007
HAFB-890	0.136 ± 0.008	0.111 ± 0.008	0.118 ± 0.007	0.123 ± 0.006
Flight-20	77.9 ± 0.7	69.0 ± 0.6	70.1 ± 0.6	77.0 ± 0.7

[1] J. R. Winckler, Phys. Rev. 85, 1054 (1952)

telescope rates are seen to be the same at low and high altitudes so the albedo particle lower energy limit can be established by the greatest thickness of absorber below the telescopes. This thickness is 9.4 g cm^{-2} (8.2 g cm^{-2} C + 0.75 g cm^{-2} wood + 0.40 g cm^{-2} Al). The lower energy bound is then $KE_\mu > 40$ Mev and $KE_p > 100$ Mev. The condition $\beta \geq 0.7$ (Winckler's data[1]) establishes an upper limit of $KE_\mu < 40$ Mev and $KE_p < 400$ Mev. The μ meson albedo is ruled out since the upper and lower bounds meet but the proton albedo in the range $100 < KE_p < 400$ Mev could exist. However, the experimental differential energy distribution for shower protons given by Camerini et al[2] shows that the number per star (burst) in the range $0 < W' < 1100$ Mev ($W' = KE + M_o c^2$) is ~ 200 times the number per star in the range $1100 < W' < 1400$ Mev. In the light of these data, it is hard to believe that if an unmeasurable number were detected below the lower energy bound that more would be detected in the range $100 < KE_p < 400$ Mev. On the basis of the above arguments and experimental facts, it is reasonable to assume that the vertical albedo does not measurably effect the telescope counting rates.

The efficiency of the burst detector has been calculated (see App. 4) for an isotropically distributed proton and π meson flux, over the upper hemisphere, of energies $\geq 4.5 \cdot 10^9$ ev. It is felt that the weakest argument in this calculation is the form of the multiplicity

---

[1] J. R. Winckler, Phys. Rev. 85, 1054 (1952)

[2] Wilson, op.cit. p. 24

distribution. However, the upper bound of multiplicity selected is a very reasonable one both on theoretical and experimental grounds. If a more nearly accurate form of this distribution were known one could obtain the efficiency, $\eta_{(\pi + p)}$, by using the difference distribution in M^* (see App. 4, Fig. A 4 - 9) histogram obtained in this calculation. Two arbitrary distributions are shown in the following table and the efficiencies for these distributions are computed to illustrate the point. The histogram values have been divided by 10 so that the tabulated results read directly in per cent efficiency in $\Delta M = 1$ at M.

M	Histogram Values	Distribution No. 1	$\Delta\eta_1$	Distribution No. 2	$\Delta\eta_2$
0	0	0	0	0.835	0
1	0	0.75	0	0.835	0
2	0	1.50	0	0.835	0
3	0.6	2.23	1.338	0.835	0.501
4	0.9	1.83	1.647	0.835	0.752
5	1.9	1.50	2.850	1.670	3.173
6	2.5	1.10	2.750	1.670	4.175
7	4.0	0.73	2.920	0.835	3.340
8	4.2	0.36	1.512	0.835	3.507
9	5.7	0	0	0.835	4.760
TOTAL	19.8 %	10.00	13.0 %	10.0	20.2 %

The best estimate of the form of the multiplicity distribution, from the experimental data available at the present time, is that each value of M has equal probability in the range $0 \leq M \leq 9$ and zero probability for $M > 9$. The value of the efficiency for this distribution is $\eta_{(\pi + p)} = 0.198 \pm 0.013$ and this value will be used in the present calculations.

---

*M is the multiplicity of near minimum and minimum ionization particles, i.e., those particles which could traverse the remaining target from the point where the burst was produced and proceed outside the target for possible detection.

For the flux of particles $Z \geq 2$ the median energy is $3 \cdot 10^9$ ev per nucleon for $\lambda = 41^\circ N$ as taken from the integral energy spectrum of Kaplon et al. The maximum number of charged π mesons generated by an α particle of this energy interacting with a C nucleus is calculated from the curve of Pickup and Voyvoidic[1], to be 10 and the mean number is calculated to be 5. From a consideration of charge conservation, the maximum number of charged nucleons produced would be 2 + 6 = 8. It is estimated from the emulsion work of Camerini et al[2] that, on the average, approximately half the total number of protons involved in the catastrophic event will be energetic enough to escape the target and contribute to the burst events of the present experiment. It is true that this estimate is based on emulsion bursts and not on carbon bursts, but for lack of the proper data this is the best estimate that can be made at the present time. On this basis the mean number of charged particles having near minimum or minimum ionization energies is $5\pi + 4p$ or 9 in all. If it is considered that the four nucleons of the α particle act more or less in an independent manner, then these bursts should not only contain more particles on the average but should have three times the angular spread ($3 \cdot 10^9$ ev as compared to $10 \cdot 10^9$ ev) of the average proton initiated burst.

---

[1] E. Pickup and L. Voyvoidic, Phys. Rev., 84, 1190 (1951)

[2] U. Camerini, J. H. Davis, P. H. Fowler, C. Franzinetti, W. O. Lock, H. Muirhead, D. H. Perkins and G. Yekutieli, Nuclear Transmutations Produced by Cosmic Ray Particles of Great Energy, Part VI. Experimental Results on Meson Production, Phil. Mag., 42, 1241 (1951).

In the calculation of the efficiency of the burst detector array for proton primary rays, a large number of bursts were not detected because the angular spread of the secondaries was such as to place the path of many of the secondary rays outside of the burst detector array. The burst detector efficiency would then remain the same as in the case of proton primaries since the density of burst particles per unit area of the detector is nearly the same. In the case of the h-nuclei the average atomic weight is ~ 14 and the median energy is given by the integral energy spectrum of Kaplon *et al* as $4.5 \cdot 10^9$ ev per nucleon. The maximum number of π mesons is 41 and the mean number is 20.5. From charge considerations, the maximum number of protons would be $7 + 6 = 13$. By the reasoning followed in the case of α particles (see above), the mean number of charged particles that will produce the burst event is $20.5\pi + 6.5p$ or 27 in all. The angular spread is about twice that of the primary proton case ($4.5 \cdot 10^9$ ev as compared with $10 \cdot 10^9$). The density of burst particles per unit area of the detector is, then, ~ 3 times that of the primary proton case. The efficiency can be approximated by

$$\eta \simeq (1 - e^{-\rho A})^3$$

for this triple coincidence type detector (thus the exponent 3) where ρ is the burst density and A is the detector area. Then, since it has been calculated that

$$\eta_{(\pi + p)} = 0.20$$

$$\eta_{(\pi + p)} = 0.2 \simeq (1 - e^{-\rho A})^3$$

and it is found that

$$\eta_h \simeq (1 - e^{-3\rho A})^3 \simeq 0.8 \quad .$$

Equation (1) is now restated in a more convenient form and the data from above is tabulated below.

$$\mathcal{F} = \frac{N}{A_c} \sum_i \sigma_i \, n_i \, \eta_i \quad , \quad i \stackrel{?}{=} (\pi + p), \alpha \text{ and } h \qquad (1)'$$

i	$\sigma_i(cm^2)$	$n_i(min^{-1})$	η_i
$(\pi + p)$	$\bar{\sigma}_{(\pi + p)}$	$n_{(\pi + p)}$	0.20 ± 0.01
α	$41.3 \cdot 10^{-26}$	6.4 ± 0.5	0.2
h	$74.1 \cdot 10^{-26}$	0.19 ± 0.02	0.8

$$n_{(\pi + p)} = n_T - n_\alpha - n_h - n_\mu = (78.8 \pm 0.9) - n_\mu \ min^{-1}$$

$A_c/N = 1.98 \cdot 10^{-23}$ grams of C per atom.

From the slope of the average burst rate at 20 g cm^{-2} atmospheric pressure vs thickness of carbon target curve of Fig. III-16 and the density of the carbon used, it is found that:

$$\mathcal{F} = \frac{(0.56 \pm 0.04)}{1.37} = (0.41 \pm 0.02) \frac{\text{bursts}}{\text{min}} \text{ per g cm}^{-2} \text{ C.}$$

By rearranging Eq. (1)':

$$\begin{aligned} \bar{\sigma}_{(\pi + p)} n_{(\pi + p)} \eta_{(\pi + p)} &= 1.98 \, \mathcal{F} \cdot 10^{-23} - \sigma_\alpha n_\alpha \eta_\alpha - \sigma_h n_h \eta_h \\ &= \left[(812 \pm 40) - (53 \pm 4) - (11 \pm 1)\right] \cdot 10^{-26} \\ &= (748 \pm 40) \cdot 10^{-26} \ cm^2 \ min^{-1} \quad .* \end{aligned}$$

*It is to be noted that the terms for $i = \alpha$ and h are $\sim 7\%$ of the major term and hence the cross section will not be highly dependent on the assumptions leading to the choice of η_α and η_h.

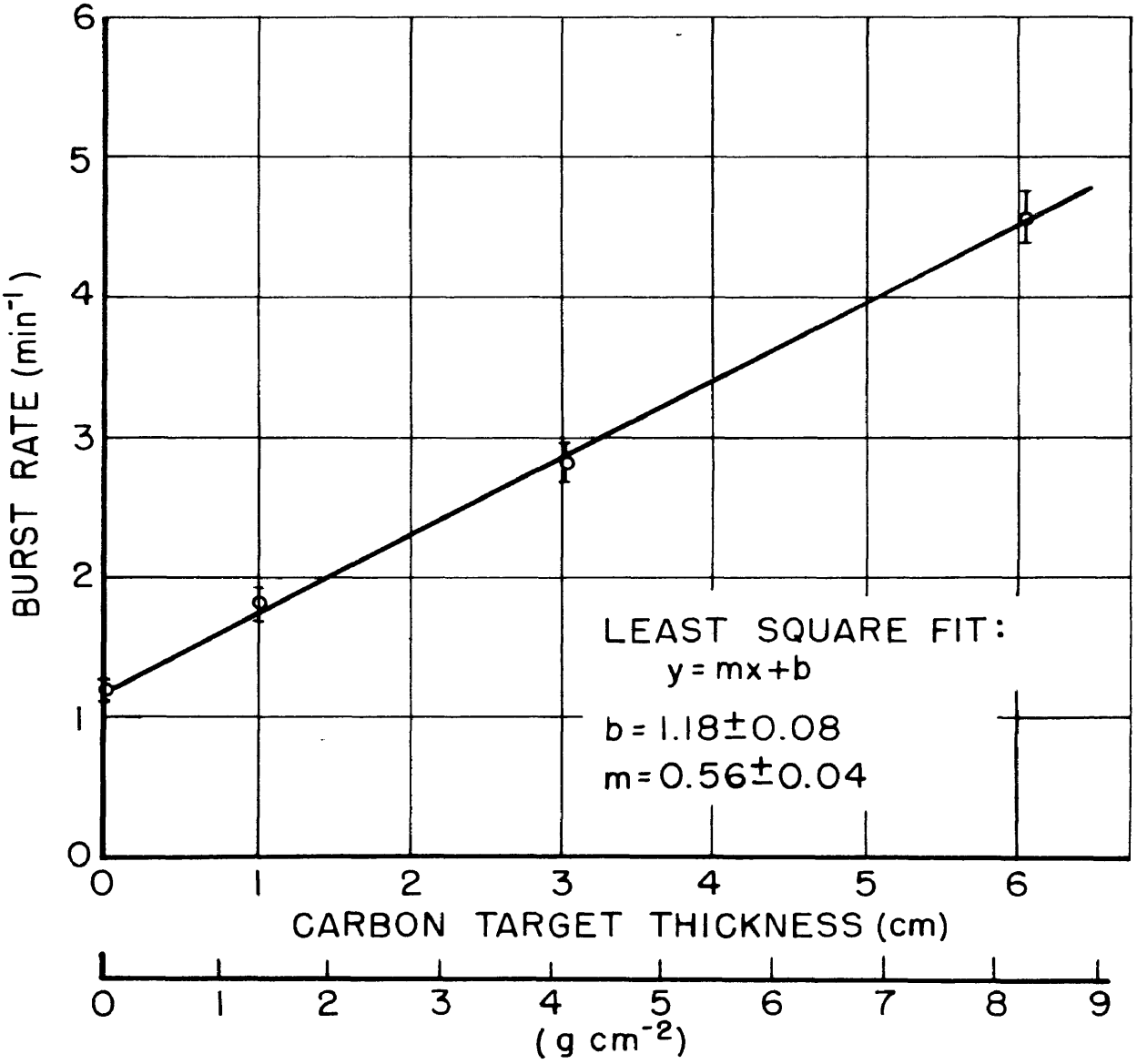

Fig. [illegible] (140 to 510 min. or ~ [illegible] atmospheric pressure) vs [illegible]

The best estimate of the μ meson intensity is that given by Rossi[1] at $\lambda = 50^{\circ}N$ geomagnetic latitude. His value at 20 g cm^{-2} atmospheric pressure is 0.018 $(cm^2 \text{ sec steradian})^{-1}$. The latitude effect from $\lambda = 50^{\circ}N$ to $\lambda = 41^{\circ}N$ is 0.5 as given by Van Allen and Singer[2] and the μ meson counting rate is then:

$$n_{\mu} = jG \cdot 60 = 0.018 \cdot 0.5 \cdot 8.2 \cdot 60 = 4.4 \text{ min}^{-1}.$$

Then

$$n_{(\pi + p)} = (78.8 \pm 0.9) - 4.4 = (74.4 \pm 0.9) \text{ min}^{-1} .$$

The best value of $\sigma\eta$ is then,

$$\bar{\sigma}_{(\pi + p)} \; \eta_{(\pi + p)} = \frac{(748 \pm 40)}{(74.4 \pm 0.9)} \cdot 10^{-26} = (10 \pm 1) \cdot 10^{-26} \text{ cm}^2.$$

The calculated value of $\eta_{(\pi + p)}$ is (0.20 ± 0.01) and hence,

$$\bar{\sigma}_{(\pi + p)} = \frac{(10 \pm 1)}{(0.20 \pm 0.01)} \cdot 10^{-26} = (50 \pm 6) \cdot 10^{-26} \text{ cm}^2$$

is the best value of $\bar{\sigma}_{(\pi + p)}$ that can be obtained from the experimental results with the present knowledge of $\eta_{(\pi + p)}$ and n_{μ}. Bounds for $\eta_{(\pi + p)}$ can be established in the following manner: it is clear that the absolute bounds are given by,

$$0 < \eta_{(\pi + p)} \leq 1 \quad .$$

---

[1] B. Rossi, Rev. Mod. Phys., 20, 537 (1948)

[2] J. A. Van Allen and S. F. Singer, Phys. Rev., 78, 819 (1950)

The upper bound can be lowered by considering that the distribution in M is all contained in M = 9 thus giving an upper bound of 0.57 (see Fig. A4-9). The lower bound can be increased by considering the calculated mean number of π mesons (2) and that of the total number of protons (6 + 1 = 7) at least 2 might contribute to the burst event. This procedure would concentrate the entire distribution of M = 4 and the lower bound would then be 0.09. The practical bounds are then:

$$0.1 < \eta_{(\pi + p)} < 0.6 \quad .$$

Using these practical limits on η, the value of σ must lie in the range

$$17 \cdot 10^{-26} < \bar{\sigma}_{(\pi + p)} < 100 \cdot 10^{-26} \text{ cm}^2 \quad .$$

C. Conclusions

1. The result of this experiment yields the values*

$$\bar{\sigma}_{(\pi + p)} \eta_{(\pi + p)} n_{(\pi + p)} = (748 \pm 40) \cdot 10^{-26} \text{ cm}^2 \text{ min}^{-1}$$

and

$$n_{(\pi + p)} + n_{\mu} = (78.8 \pm 0.9) \text{ min}^{-1} \quad .$$

2. From the present data available on the μ meson intensity vs altitude, the best estimate at 20 g cm^{-2} atmospheric pressure is $n_{\mu} = 4.4 \text{ min}^{-1}$. Using this figure, the product $\sigma\eta$ is determined to be

---

*The indicated errors are the standard deviations attributable to statistical fluctuations.

$$\bar{\sigma}_{(\pi + p)} \quad \eta_{(\pi + p)} = (10 \pm 1) \cdot 10^{-26} \text{ cm}^2 \quad .$$

There is no means by which the effect of π mesons can be separated from the experimental data but because of π-μ decay it is thought that the above values are characteristic of the proton component.

3. The value of $\eta_{(\pi + p)}$ as calculated in App. 4 is based on data obtained from emulsion studies of bursts at high altitudes. It is, however, believed that the general character of the carbon bursts is the same as that of the emulsion bursts of low multiplicity. For the information used in the calculation, care was taken to sort the available data of other workers in such a way as to select only the events where the sum of the near minimum and minimum ionization tracks in the emulsion was less than ten. It is felt that the major uncertainty in this calculation is in the form of the multiplicity distribution since the only information available was based on a small total number of events (approximately 50). The calculated value of the burst detector efficiency is:

$$\eta_{(\pi + p)} = (0.20 \pm 0.01) \quad .$$

By selecting two limiting practical distributions in multiplicity the practical bounds for the efficiency are established as:

$$0.1 < \eta_{(\pi + p)} < 0.6 \quad .$$

Then the best value of the cross section is,

$$\sigma_{(\pi + p)} = (50 \pm 6) \cdot 10^{-26} \text{ cm}^2$$

and the estimated bounding values are,

$$17 \cdot 10^{-26} < \bar{\sigma}_{(\pi + p)} < 100 \cdot 10^{-26} \text{ cm}^2 .$$

4. The empirical formula of Kaplon et al, for the cross section of nuclei of $Z \geq 2$ interacting with other nuclei, would yield the value:

$$\sigma_p = \pi(r_p + r_c - 2\Delta r)^2 = 25 \cdot 10^{-26} \text{ cm}^2 .$$

The overlap, Δr, in this case is $1.0 \cdot 10^{-13}$ cm. From this point of view, the geometric cross section for the interaction of a proton with a carbon nucleus would be given by:

$$\sigma_{p_g} = \pi(r_p + r_c)^2 = 72 \cdot 10^{-26} \text{ cm}^2 .$$

The best value of $\bar{\sigma}_{(\pi + p)}$ from this experiment yields a value for the overlap of:

$$\Delta r = (0.4 \pm 0.01) \cdot 10^{-13} \text{ cm} .$$

5. In the light of the well established continued decrease of the near vertical intensity from 20 g cm^{-2} to 1 g cm^{-2} atmospheric pressure (rocket measurements to 10^{-4} g cm^{-2}) and with the assumption that the cross section is a constant for the range of particle energies involved, one can only conclude that the vertical burst producing intensity (and therefore the number of bursts produced by this flux) must also show an appreciable decrease in this interval. The available burst data at very high altitudes has been obtained with detectors which yield the average burst rate produced by the flux in the upper hemisphere. The highest of these measurements (the data obtained by Van Allen shown in Fig. III-15) actually shows an increase in

the burst rate of $\sim$20 per cent from 50 g cm^{-2} to 1 g cm^{-2} atmospheric pressure. It is seen that the vertical data and the data giving the average over the hemisphere are only compatible through the assumption of an intensity distribution which increases with increasing zenith angle, from the vertical direction, in the very high atmosphere. It is felt that this is a confirmation of the findings of Van Allen[1] which have been obtained by a different method.

6. The previously quoted albedo measurements of Winckler (see p. 68) and the results of the present experiment indicate that the near vertical upward moving albedo is of an amount no larger than the statistical errors of both of these experiments. In the present work this would be in the order of 2 per cent of the telescope rate at 20 g cm^{-2} altitude or 1.5 min^{-1}.

---

[1] J. A. Van Allen, Proc. Echo Lake Cosmic Ray Symp. Paper No. 53a (1949). Van Allen's experimentally determined intensity distribution is $j = j_0(1 + B \sin \theta)$.

APPENDIX 1

Experimental Determination of the Intrinsic Efficiency of the Victoreen 1B85 Geiger Counter

The intrinsic efficiency of four typical 1B85 counter tubes was measured in a telescope configuration similar to that used in the actual balloon flight telescopes. The experimental equipment (see Fig. A1-1) consisted of ten 1B85 counter tubes, two Rossi type triple-coincidence circuits (resolving time, $\tau \simeq 12\,\mu$sec) and a double channel Brush amplifier and recorder. The ten counters were arranged in a five-fold vertical telescope in trays of two each. Counter trays 1, 3 and 5 were connected to one Rossi triple-coincidence circuit and trays 2 and 4 were connected to two grids of the other Rossi triples circuit. The input to the third grid of the second triples circuit was supplied from the output of the inverter-amplifier which received an input pulse whenever an output pulse appeared at the plates of the first triples circuit. The output pulses of each Rossi triples circuit was then fed into a separate pulse-broadening circuit and thence to the input of each Brush amplifier and recorder.

It is seen that, using the above system, three-fold coincidences were recorded in one channel and five-fold coincidences were recorded in the other. If the intrinsic efficiency of the four counters in trays 2 and 4 were each 100 per cent, the number of five-fold coincidences, N_5, would equal the number of three-fold coincidences, N_3, at any time excluding the possibility of counter dead time, side showers

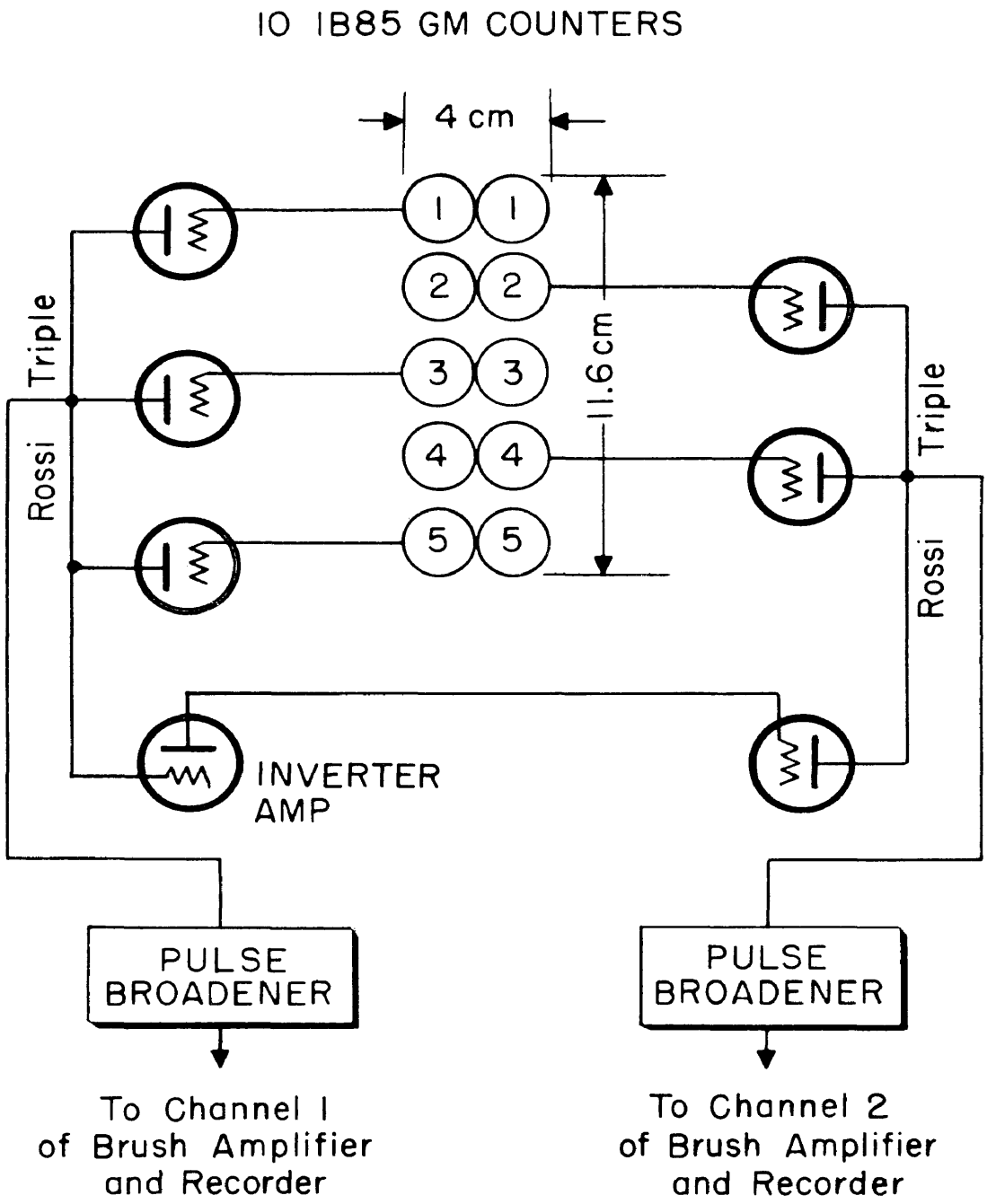
10 1B85 GM COUNTERS
4 cm
11.6 cm
1 1
2 2
3 3
4 4
5 5
Triple
Rossi
Triple
Rossi
INVERTER AMP
PULSE BROADENER
PULSE BROADENER
To Channel 1 of Brush Amplifier and Recorder
To Channel 2 of Brush Amplifier and Recorder

and accidental coincidences within the resolving time of the system. The ratio N_5/N_3 is then a measure of the intrinsic efficiency of the trays 2 and 4 in coincidence. The manner in which this ratio is related to the intrinsic efficiency is shown in the following development.

The recorded counting rate of a cosmic ray telescope n_r, made up of r trays, can be calculated as

$$n_r = e_R \int_{\Omega}\int_{A} \prod_{i=1}^{r} e_{D_i} \prod_{i=1}^{r} e_{T_i} j \; \vec{dA} \cdot \vec{d\Omega}$$

where e_R is the recorder efficiency, $(1 - e_{D_i})$ is the inefficiency of the i^{th} tray due to counter dead time, e_{T_i} is the intrinsic efficiency of the counters in the i^{th} tray, j is the directional intensity of the cosmic ray flux, $\vec{dA}$ is an element of area, $\vec{d\Omega}$ is an element of solid angle and the integrations are to be carried out over the geometry of the telescope. It is noted that the e_i are the independent probabilities that the passage of a charged particle through the counters of the i^{th} tray produces a usable output from the tray. Assuming that, on the average, counters of the same type have the same dead time and the same intrinsic efficiency and that these average values are not sensitive to the geometry of the telescope, the integrals can be simplified to give:

$$n_r = e_R \, \bar{e}_D^{\,r} \, \bar{e}_T^{\,r} \int_{\Omega}\int_{A} j \; \vec{dA} \cdot \vec{d\Omega} \quad .$$

For the time interval τ the number of counts obtained will be

$$N_r = n_r \tau$$

and if similar recording systems are used

$$\frac{N_5}{N_3} = \frac{\bar{e}_D^{\,5}\ \bar{e}_T^{\,5}}{\bar{e}_D^{\,3}\ \bar{e}_T^{\,3}} = \bar{e}_D^{\,2}\ \bar{e}_T^{\,2}$$

since the flux through the three-fold telescope is certainly equal to that through the five-fold telescope. The intrinsic efficiency can now be found from

$$\bar{e}_T = \bar{e}_D^{-1}\left[\frac{N_5}{N_3}\right]^{\frac{1}{2}}$$

since the values of all the parameters can be determined experimentally.

In the above calculation the values of N are the true number of counts for each telescope. The experimental values found for the number of telescope counts will include accidental coincidences and coincidences due to side showers. The magnitude of the accidental coincidence rate can be estimated as follows:

$$a_5 < a_3 \simeq 2\tau\left[2n_2n_1\right] + (\text{terms in } \tau^2)$$

where a_5 and a_3 are the accidental five-fold and three-fold coincidence rates, τ is the resolving time of the Rossi circuits, n_2 is the genuine double coincidence rate of trays 1 and 3 or 3 and 5 (thus the factor of two) and n_1 is the individual tray rate.[1] The measured values are: $\tau = 12.5\mu$ sec, $n_2 \simeq 0.2$ sec^{-1} and $n_1 \simeq 2$ sec^{-1}. Thus the estimated accidental rate is

$$a_3 = 20\cdot10^{-6}\ \text{sec}^{-1}$$

---

[1] L. Janossy, Cosmic Rays, Oxford, 1948, p. 48.

The magnitude of the side shower coincidence rate is more difficult to estimate. In the experiments of Wei and Montgomery[1] on narrow showers it was found that shielding out the side showers from their double coincidence vertical shower detector did not decrease the rate as established without the shield. Any decrease was, therefore, within the magnitude of the statistical fluctuation assigned to the double coincidence rate (0.150 ± 0.008 min^{-1}). In the vertical direction the ratio of double to triple coincidences was 7 with the same geometry. It can be estimated from these figures that the greatest rate of triple coincidences due to side showers was 0.0023 min^{-1} for their geometry. In the case at hand the area to be considered is about 1/3 of that in the case cited above. It can be concluded that a fair estimate of the maximum side shower coincidence rate applicable here is less than 0.0007 min^{-7} or $12 \cdot 10^{-6}$ sec^{-1}. This estimated value is more nearly correct for three-fold coincidences than for five-fold coincidences since it would be lower for the latter.

The statistical fluctuation, $\sigma_{\bar{e}_T}$, to be assigned to the calculated intrinsic efficiency can be determined in the following manner: in a series of N_3 independent trials in which the probability for the five-fold coincidence event is p in every trial, the probability that this event will occur exactly N_5 times is given by

$$P_{N_3}(N_5) = \binom{N_3}{N_5} p^{N_5} (1-p)^{(N_3 - N_5)}$$

---

[1] J. Wei and C. G. Montgomery, Phys. Rev. 76, 1488 (1949).

where $N_5 \leq N_3$ and $\binom{N_3}{N_5}$ are the binomial coefficients, then the most probable number of successes will be given by[1] $N_5 \leq (N_3+1)\, p \leq N_5+1$ and for large values of N_3 this can be approximated by $N_5 = N_3 p$; the standard deviation, σ_p, will be given by[2]

$$\sigma_p = \sqrt{N_3 p(1-p)} \quad .$$

then

$$p \pm \sigma_p = \frac{N_5}{N_3} \pm \sqrt{N_5\left(1 - \frac{N_5}{N_3}\right)} \quad . \tag{1}$$

but

$$\frac{N_5}{N_3} = \bar{e}_D^{\,2} \quad \bar{e}_T^{\,2}$$

and

$$\sigma_{\bar{e}_T} = \sigma_p \frac{\partial \bar{e}_T}{\partial N_5} = \frac{1}{2\,\bar{e}_D} \sqrt{\frac{1}{N_3}\left(1 - \frac{N_5}{N_3}\right)} \quad .$$

Thus

$$\bar{e}_T \pm \sigma_{\bar{e}_T} = \bar{e}_D^{-1} \left[\sqrt{\frac{N_5}{N_3}} \pm \frac{1}{2} \sqrt{\frac{1}{N_3}\left(1 - \frac{N_5}{N_3}\right)} \right] \tag{2}$$

The value of $\bar{e}_D$ can be calculated, from the dead time as given by the manufacturer of the 1B85 (100μ sec) and the counting rate of the tray (2 sec^{-1}), after the method of Janossy:[3]

---

[1] J. V. Uspensky, Introduction to Mathematical Probability, McGraw-Hill, New York: 1937, p. 48 ff.

[2] Ibid., p. 175.

[3] Janossy, op. cit. p. 41.

$$\bar{e}_D = \exp[-n_1 \tau_D] \simeq (1 - n_1 \tau_D) \ .$$

Thus, $\bar{e}_D = 0.9998$ and $\bar{e}_D = 1.0002$.

The uncorrected numbers of three-fold and five-fold coincidences as obtained in the above described experiment are tabulated below:

N'_3	N'_5	Time sec
5293	4906	109,620

The estimated maximum correction for accidental and side shower coincidences is:

$$A + S = (a + s)\, t \leq 32 \cdot 10^6 \cdot 10^5 = 3.2 \ .$$

The intrinsic efficiency as calculated from Eq. (2) above is then

$$\bar{e}_T = 0.963 \pm 0.001 \ .$$

APPENDIX 2

Calculation of The Cosmic Ray Telescope Geometric Factor

The counting rate, n, of a cosmic ray telescope composed of r identical counters of absolute average efficiency, $\bar{e}$, and fixed in space relative to a flux of charged particles of directional intensity j is given by:

$$n = \bar{e}^{r} \int_{\Omega} \int_{A} j \, \vec{dA} \cdot \vec{d\Omega} \qquad (1)$$

where dA is the element of area, $d\Omega$ is the element of solid angle and the integrations are to be carried out over the geometry of the telescope. In order to compare the measurements of various observers in this field, it is desirable to reduce the counting rates in a given direction to directional intensities. It is the object of this calculation to determine the so-called geometric factor, G, of the telescopes used in the experimental balloon flight equipment so that the directional intensities may readily be obtained from the counting rate data found experimentally.

It has been shown by Greisen[1] that under the assumption that $j(\theta)$ varies linearly with θ over the small range of angle subtended by the diameters of the counters, the directional intensities are proportional to the counting rates. The error caused by the above assumption is small, e.g. if[1,2]

---

[1] K. Greisen, Phys. Rev. 61, 212 (1942).

[2] See also D.J.X. Montgomery, Cosmic Ray Physics, Princeton University Press, Princeton: 1949, p. 169 ff.

$$j(\theta) = j(0)\cos^m\theta, \quad 0 \leq \theta \leq \frac{\pi}{2}$$

$$j(\theta) = 0 \quad , \quad \frac{\pi}{2} < \theta \leq \pi$$

for $m = 2$ and $\theta_o = 0$ (see Fig. A2-1)

$$\frac{\text{correct average intensity over the diameter}}{\text{assumed average intensity over the diameter}} = 1 + \frac{1}{6}\left(\frac{a}{S}\right)^2(\tan^2\theta_o - 1)$$

and for the geometry in question $a \simeq 2$ cm and $s \simeq 8$ cm and the correction is approximately .99. This correction is nearer unity for smaller values of m and since the range of m to be covered is $0 \leq m \leq 2$ [1] the above assumption is valid.

In order to simplify the calculation still further, it is assumed that the cylindrical counters can be replaced by plane detectors of the same length and of width equal to the counter diameter. As seen from Fig. A2-2, if the intensity varies in a linear manner along the counter diameter, the correction factor is simply β/γ where

$$\sin\beta = \tan\gamma = a/S .$$

For the actual geometry $\beta/\gamma \simeq 1.03$.

Using the $\cos^m\theta$ relationship for the directional intensity variation with zenith angle and the above assumptions and facts, Eq. (1) can be simplified by the following artifice (with reference to Fig. A2-1):

$$j(\theta) = j(\theta_o)\frac{\cos^m\theta}{\cos^m\theta_o} = j(\theta_o)\cos^m\alpha \qquad (2)$$

---

[1] J. F. Jenkins, Jr., Bul. Amer. Phys. Soc. 23, No. 3 (1948) Washington Meeting, Abstract EA3.

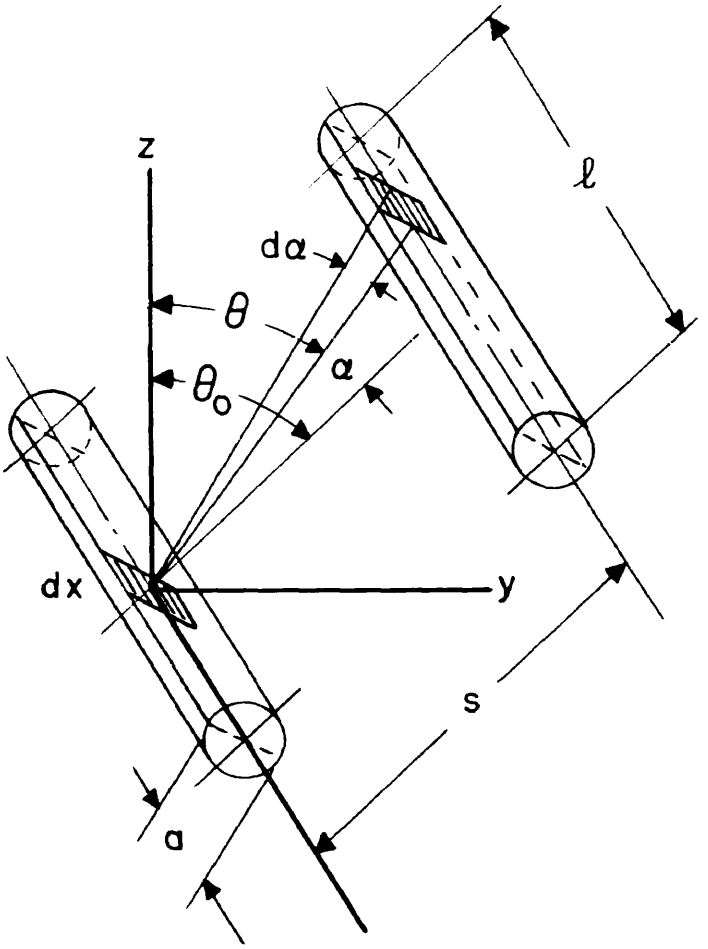

Fig. A3-1 [illegible]

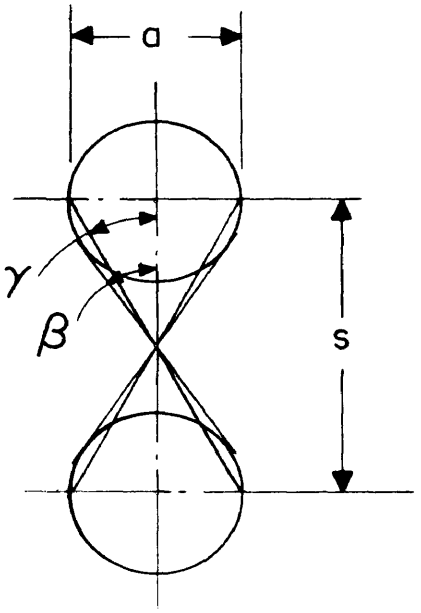

Fig. A3-2 [illegible]

then $n(\theta_o) = \bar{e}^{r}\int\int j(\theta) f(\alpha, x)\, d\alpha\, dx = \bar{e}^{r} j(\theta_o)\iint \cos^{m}\alpha\, f(\alpha,x)\, d\alpha\, dx$

or $$G(\theta_o,m) = \frac{n(\theta_o)}{\bar{e}^{r} j(\theta_o)} = \iint \cos^{m}\alpha\, f(\alpha, x)\, d\alpha\, dx \qquad (3)$$

since the integrals are functions of only the telescope geometry. The expression $f(\alpha, x)d\alpha\, dx$ is just $\vec{dA}\cdot\vec{d\Omega}$ and this is seen, from Fig. A2-1, to be

$$f(\alpha, x) = \frac{a^2\cos^2\alpha}{S} .$$

Substitution in (3) yields

$$G(\theta_o,m) = \frac{a^2}{S}\iint \cos^{(m+2)}\alpha\, d\alpha\, dx$$

integrating once we have

$$G(\theta_o,m) = \frac{2a^2}{S}\int_o^{\tan^{-1}\frac{\ell}{S}} (\ell - S\tan\alpha)\cos^{(m+2)}\alpha\, d\alpha$$

The geometry is such that ℓ is not great enough to ignore the flux through the circular ends of the counters, hence, the end correction

$$\Delta G = \frac{\pi a^3}{2S}\int_o^{\tan^{-1}\frac{\ell}{S}} \cos^{(m+1)}\alpha \sin\alpha\, d\alpha = \frac{\pi a^3}{2S(m+2)}\left[1 - \left(\frac{S^2}{S^2+\ell^2}\right)^{\frac{m+2}{2}}\right] \qquad (4)$$

must be made. The complete geometric factor for a component telescope, the counting axis of which lies at zenith angle θ_o, is thus,

$$G(\theta_o,m) = \frac{2a^2\beta}{S\gamma}\int_o^{\tan^{-1}\frac{\ell}{S}} (\ell - S\tan\alpha)\cos^{(m+2)}\alpha\, d\alpha + \frac{\pi a^3}{2S(m+2)}\left[1 - \left(\frac{S^2}{S^2+\ell^2}\right)^{\frac{m+2}{2}}\right] \qquad (5)$$

Consider now the geometrically perfect vertical telescope (see Fig. A2-3) made up of component telescopes having the following dimensions and counting axis angles:

$$a = 1.91 \text{ cm}^{*,**}$$

$$\ell = 5.92 \text{ cm}^{**,1}$$

$$S_1 = 8.00 \text{ cm}$$

$$S_2 = 8.24 \text{ cm}$$

$$\theta_1 = 0$$

$$\theta_2 = \pm 14.5^{\circ}$$

$$\frac{\beta_1}{\gamma_1} = \frac{\beta_2}{\gamma_2} = 1.03.$$

Calculation of $G(\theta_i,m)$ from Eq. (5) yields (where i refers to the i^{th} component telescope):

for $(A_1 B_1 C_1)$ or $(A_2 B_2 C_2)$***

$$G(0,2) = 1.848 \text{ cm}^2 \text{ steradians}$$

$$G(0,1) = 1.919 \text{ cm}^2 \text{ steradians}$$

$$G(0,0) = 1.996 \text{ cm}^2 \text{ steradians}$$

---

*In accordance with the universal findings of other workers, the effective diameter has been taken as the internal diameter of the metal wall of the counter.

**The counters used in this telescope were Victoreen 1B85 Thyrodes.

***Notation after the algebra of Boole; thus, A + B means A and/or B and AB means A with B.

[1]Private communication. Effective length determined experimentally for 1B85 Thyrodes by L. H. Meredith, State University of Iowa, Sept. 1951, after the method of J. C. Street and R. H. Woodward, Phys. Rev. 46, 1029 (1934).

ACCURATE MODEL

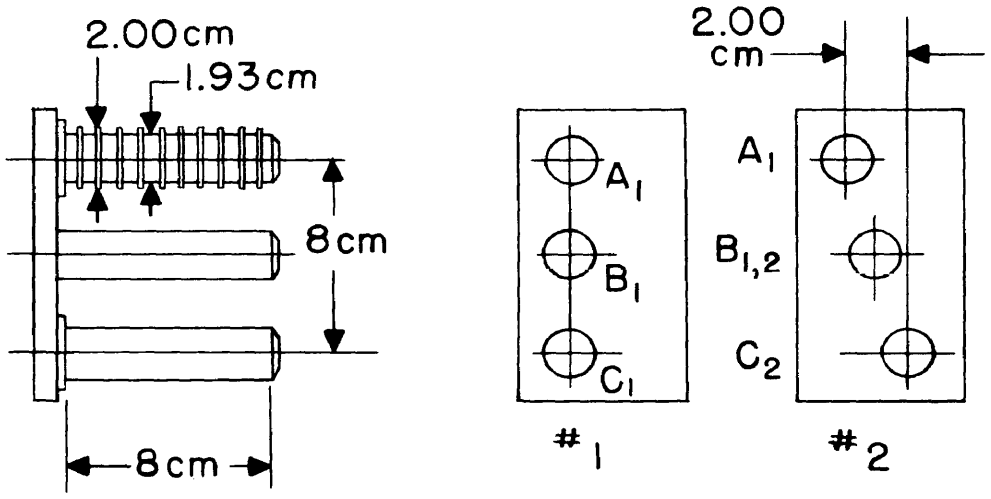

side view

end view

FIG. B-2 [illegible]

"PRODUCTION" MODEL

(defect exaggerated)

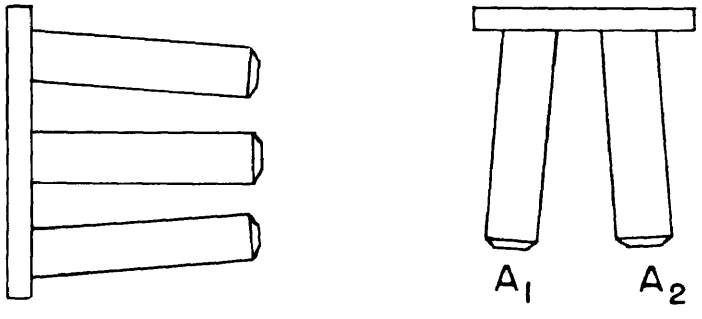

side view

top view

FIG. B-3 [illegible]

$$G(14.5^{\circ},2) = 1.795 \text{ cm}^2 \text{ steradians}$$

$$G(14.5^{\circ},1) = 1.863 \text{ cm}^2 \text{ steradians}$$

$$G(14.5^{\circ},0) = 1.938 \text{ cm}^2 \text{ steradians}$$

By generalizing Eq. (2)

$$G(\theta_o,m) = \sum_i G(\theta_i,m) \frac{\cos^m\theta_i}{\cos^m\theta_o} ,$$

the above components can be combined to give the geometric factors for the complete vertical ($\theta_o = 0$) telescope for $m = 2$, $m = 1$, and $m = 0$:

for $(A_1 + A_2)$ $(B_1 + B_2)$ $(C_1 + C_2)$ or more simply (ABC)

$$G(0,2) = 7.059 \text{ cm}^2 \text{ steradians}$$

$$G(0,1) = 7.446 \text{ cm}^2 \text{ steradians}$$

$$G(0,0) = 7.871 \text{ cm}^2 \text{ steradians.}^1$$

It is seen that the value of G for this narrow, vertical telescope does not change by more than $\pm$ 5 per cent in going from a $\cos^2\theta$ to a hemispheric isotropic distribution of $j(\theta)$.

The geometry of the eight "production" model telescopes is subject to the various misalignments shown exaggerated in Fig. A2-4. Even if the alignments were perfect and the dimensions were accurately known, the gap between the tubes B_1 and B_2 could never be closed and in any calculation of the geometric factor it would be necessary to take the

---

[1] Compare H. E. Newell, Jr. and E. C. Pressly, Rev. Sci. Inst. 20 568 (1949). Using their graphs, $G(0,0) = 7.84$ cm^2 steradians and $G(0,2) = 6.94$ cm^2 steradians.

size of this gap into account. This type of defect involves the application of a rather difficult graphical computation to obtain the correct geometric factor. In lieu of producing telescopes with the counter tubes accurately aligned and with dimensions accurately known and finally carrying out the complex graphical computation to correct for the gap between B_1 and B_2, the component telescopes of one such telescope were made (see Fig. A2-3) and the eight "production" models were calibrated against the combined components. Now since the eight "production" models were of nearly the same geometry and also of nearly the same geometry as the special telescope shown in Fig. A2-3, and since, if the counting rate of the special telescope and of one "production" model were obtained at the same time in essentially the same location, the two would be exposed to the same average cosmic ray flux, it follows that the ratio of the counting rates would be equal to the ratio of the geometric factors. Thus it was determined that for the special telescope

$$n_{A_1B_1C_1} = 0.0198 \pm 0.0007 \text{ sec}^{-1}$$

$$n_{A_2B_2C_2} = 0.0190 \pm 0.0007 \text{ sec}^{-1}$$

$$n_{A_1B_{12}C_2} = 0.0178 \pm 0.0007 \text{ sec}^{-1}$$

$$n_{A_2B_{12}C_1} = 0.0168 \pm 0.0007 \text{ sec}^{-1}$$

and the sum of these $n_{ABC} = 0.0734 \pm 0.0014 \text{ sec}^{-1}$. For telescope No. 8

of the "production" models, $n'_{ABC} = 0.0766 \pm 0.0009$ sec^{-1}. The geometric factor at sea level (m = 2) for the special telescope, as computed above, is G = 7.059 cm^2 steradians which yields a geometric factor at sea level for No. 8 of $G_8 = (7.35 \pm .16)$ cm^2 steradians. The errors indicated in the above data and computations are the standard deviations attributable to statistical fluctuations.

APPENDIX 3

Calculation of the Effective Thickness of Target Under the Cosmic Ray Telescopes

The thickness of target presented to each ray at zenith angle θ through the telescope will vary with θ. It then becomes necessary to determine the effective or weighted mean thickness of target for all such possible rays.

Consider a target which is an infinite flat slab of an homogenous isotropic material of thickness t. The path length through the slab at any zenith angle θ is then $t/\cos\theta$. If this slab is placed below a telescope with known geometry, the effective thickness, $\bar{t}$, can be calculated in the following manner (see App. 2):

$$\bar{t} = \frac{\int_{\Omega}\int_{A} j(\theta)\,\frac{t}{\cos\theta}\,\vec{dA}\cdot\vec{d\Omega}}{\int_{\Omega}\int_{A} j(\theta)\,\vec{dA}\cdot\vec{d\Omega}}$$

but from Eq. (2) App. 2

$$\cos\theta = \cos\theta_i \cos\alpha$$

substituting in Eqs. (3) and (4) App. 2

$$\bar{t} = \frac{\sum_i \frac{2a^2 t j(\theta_i)}{S_i \cos\theta_i} \int_0^{\tan^{-1}\frac{\ell}{S_i}} \left[\frac{\beta_i}{\gamma_i}\left(\ell - S_i\tan\alpha\right)\cos^{(m+1)}\alpha + \frac{\pi a}{4}\cos^{m}\alpha\sin\alpha\right] d\alpha}{\sum_i \frac{2a^2 j(\theta_i)}{S_i} \int_0^{\tan^{-1}\frac{\ell}{S_i}} \left[\frac{\beta_i}{\gamma_i}\left(\ell - S_i\tan\alpha\right)\cos^{(m+2)}\alpha + \frac{\pi a}{4}\cos^{(m+1)}\alpha\sin\alpha\right] d\alpha}$$

but

$$j(\theta_i) = j(\theta_o)\,\frac{\cos^{m}\theta_i}{\cos^{m}\theta_o}$$

or

$$\bar{t} = \frac{\frac{t}{\cos\theta_o} \sum_i \frac{\cos^{(m-1)}\theta_i}{\cos^{(m-1)}\theta_o} G\left(\theta_i, (m-1)\right)}{G(\theta_o, m)}$$

but for a vertical telescope $\theta_o = 0$ and hence,

$$\frac{\bar{t}}{t} = \frac{G\left(0,(m-1)\right)}{G(0,m)}$$

It is noted that only the case m = 0 must be computed from the telescope geometry since the cases for m = 1 and m = 2 can be obtained from the value of G for m = 0, m = 1 and m = 2 as computed in App. 2. The computed value of G(0,-1) using the telescope dimensions given in App. 2 is 8.325. The values of $\bar{t}/t$ vs m and G are shown in the table below.[1]

Table A3-1

m	$G(0,m)$ cm^2 steradians	$\frac{\bar{t}}{t} = \frac{G\left(0,(m-1)\right)}{G(0,m)}$
0	7.871	1.058
1	7.446	1.057
2	7.059	1.055

[1] Compare M. A. Pomerantz and E. E. Witmer, J.F.I. 246, 293 (1948).

APPENDIX 4

Calculation of the Efficiency of the Burst Detector Array

The burst detector is essentially a plane array composed of nine contiguous Geiger counters, 2.54 cm outside diameter, .025 cm brass wall and of approximately 40 cm effective length. These counters are connected in groups of three such that a burst event is indicated by the triple coincidence of one or more counters of each of the three groups. In addition, the counters are interlaced in such a manner as to interpose one counter from each of two of the groups between each two counters of the third group. The area of the detector is that of a rectangle 23 cm x 40 cm, placed at such a distance below the telescope so as to fill completely the aperture of the telescope.

Since the data collected in this experiment can only give the product of the burst detector efficiency by the burst production cross section, it is necessary to know the detection efficiency in order that the cross section can be determined.

Consider (see Fig. A4-1) the primary ray which enters the plane of the condensed target at the point (x_o, y_o) at zenith angle θ and azimuth angle φ. In general this ray produces M "daughter rays" which make angles θ_i' and φ_i' with the primary, where $1 \leq i \leq M$, and some of these daughters will go through the detector plane. In this simple picture the target has been condensed on the c.g. plane of the target and the detector is considered as plane strips of width equal to the counter diameter and of length equal to the effective length of the counter. It is seen that if the distribution in θ' and the

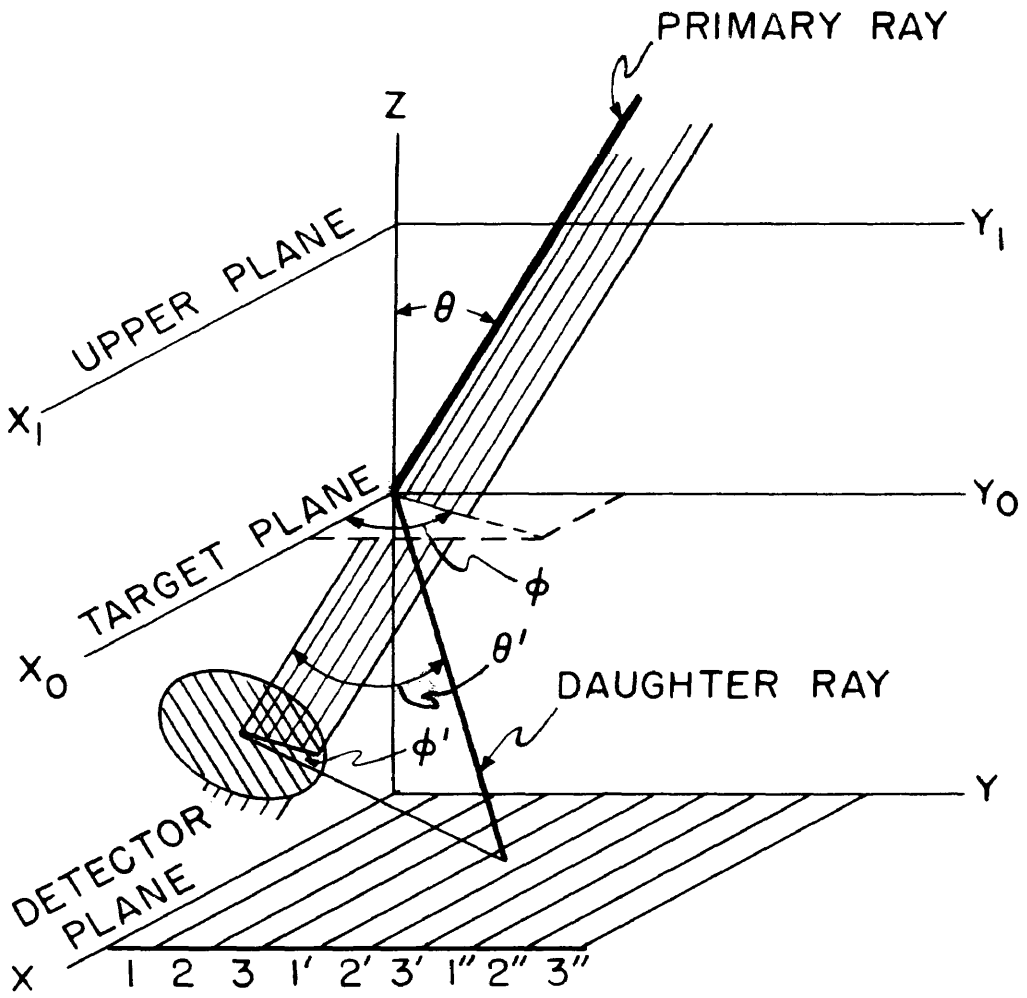

Fig. A4-1 GEOMETRIC RELATIONS FOR PRIMARY AND DAUGHTER RAYS

distribution in M of the daughters is known, the detector efficiency can be calculated, in principle at least, for a given geometry of the defining telescope and the burst detector array. After much consideration of this problem, it was determined that solution of the integrals involved in this calculation would be obtained only through the use of very tedious and complex numerical methods.

As an alternate method of solution, the statistical experiment, described below, was devised and carried out.

A twice-scale model (see Fig. A4-2) of the telescope and burst detector array was made in such a way that the telescope was fixed in the correct manner with respect to the burst detector. This arrangement was mounted on a table in a manner so as to allow complete freedom of motion in the x,y plane within the bounds of the geometry (see Fig. A4-1). A plate was fixed to this table such that the upper surface of the plate was in the position which would be assumed by the c.g. of the actual target. In the center of this plate a special set of double gimbaled rings (see Fig. A4-3) was mounted, on which could be measured the double set of azimuth and zenith angles (θ , φ) and (θ', φ'). An extendable pointer was fixed on the lower side of the inside gimbal so that the exact position of entry of a daughter ray on the detector plane could easily be determined. The upper face of the box, shown in Fig. A4-3, which served as the telescope, was made of clear plastic, one surface of which had been frosted, and a grid was ruled upon the frosted side, with rulings parallel to the x and y axes. On the upper side of the inside gimbal and on the axis of the extendable pointer,

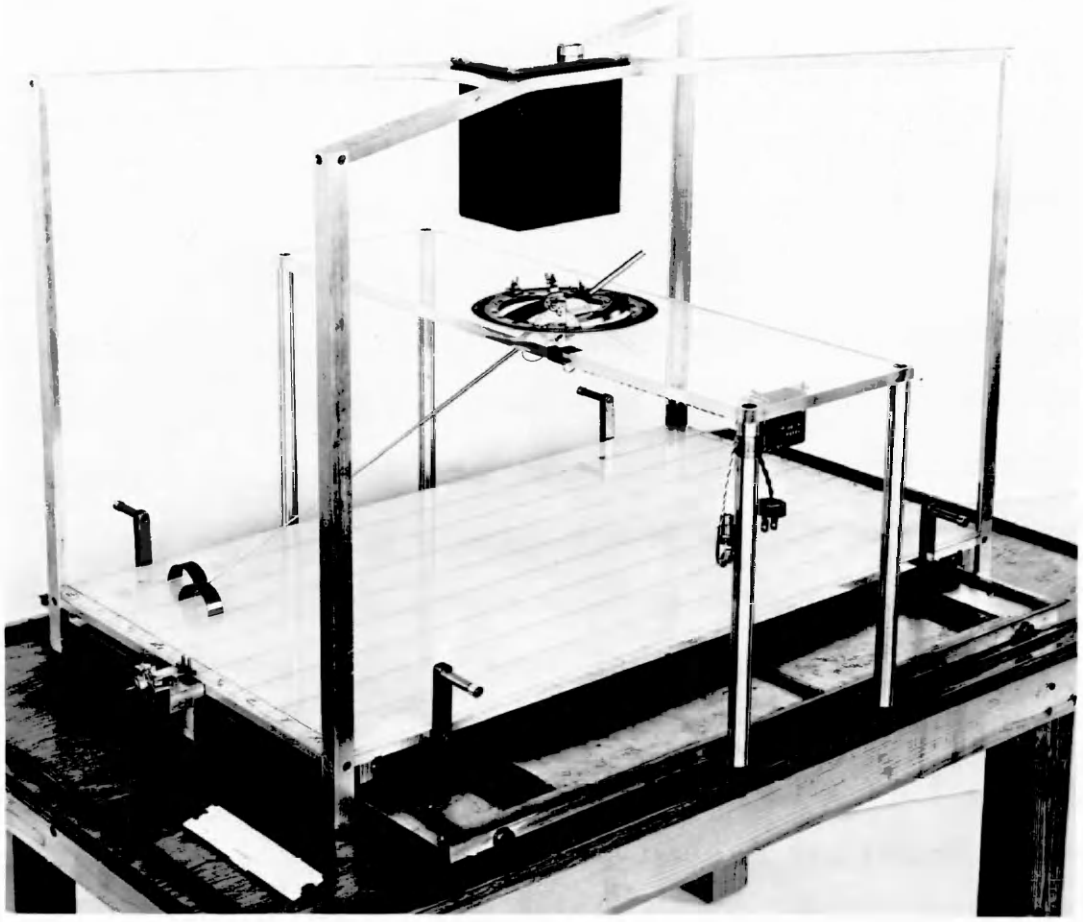

Fig. A4-2 PHOTOGRAPH OF TWICE SCALE TELESCOPE-TARGET-BURST DETECTOR SIMULATOR

Fig. A4-3 PHOTOGRAPH SHOWING THE PROTRACTORS FOR THE DOUBLE SET OF AZIMUTH AND ZENITH ANGLES AND THE GRID ON THE UPPER PLANE OF THE TELESCOPE

a brass tube was mounted which contained a small light source and a piece of glass tubing (see Fig. A4-4). The light pattern, which was obtained through the exit hole in the upper end of the brass tube, formed a "bull's eye" on the frosted surface of the ruled grid at the top of the telescope box.

The rulings on the grid were divided into 99 spaces in each direction. The rings, which measured φ and φ', had fastened to them circular scales dividing each circle into 200 equal parts. These were marked from 0 to 100 in each direction. The edge of each ring was provided with a thin circular plate, the center of which was on a gimbal axis. These plates were marked off in 100 equal divisions over half the circumference and thus provided a means of measuring θ and θ'.

With the above instrument, it is possible to examine any set of primary and daughter rays which might be of interest in the actual experiment. The cosmic ray phenomenon is purely a random one, hence directions and positions of possible primary rays can be obtained by choosing the coordinates x_1, y_1, θ, and φ from their integral distribution functions in a completely random manner. Once a primary ray has been defined, the number of daughter rays to be produced by it can be determined by random selection of M from the integral distribution function for M. The same procedure can then be followed for each of the M values of θ' and φ'. The termination of each set of daughter rays thus defined by x_1, y_1, θ, φ, M and the M values of θ and φ', on the detector plane will determine whether or not a coincidence

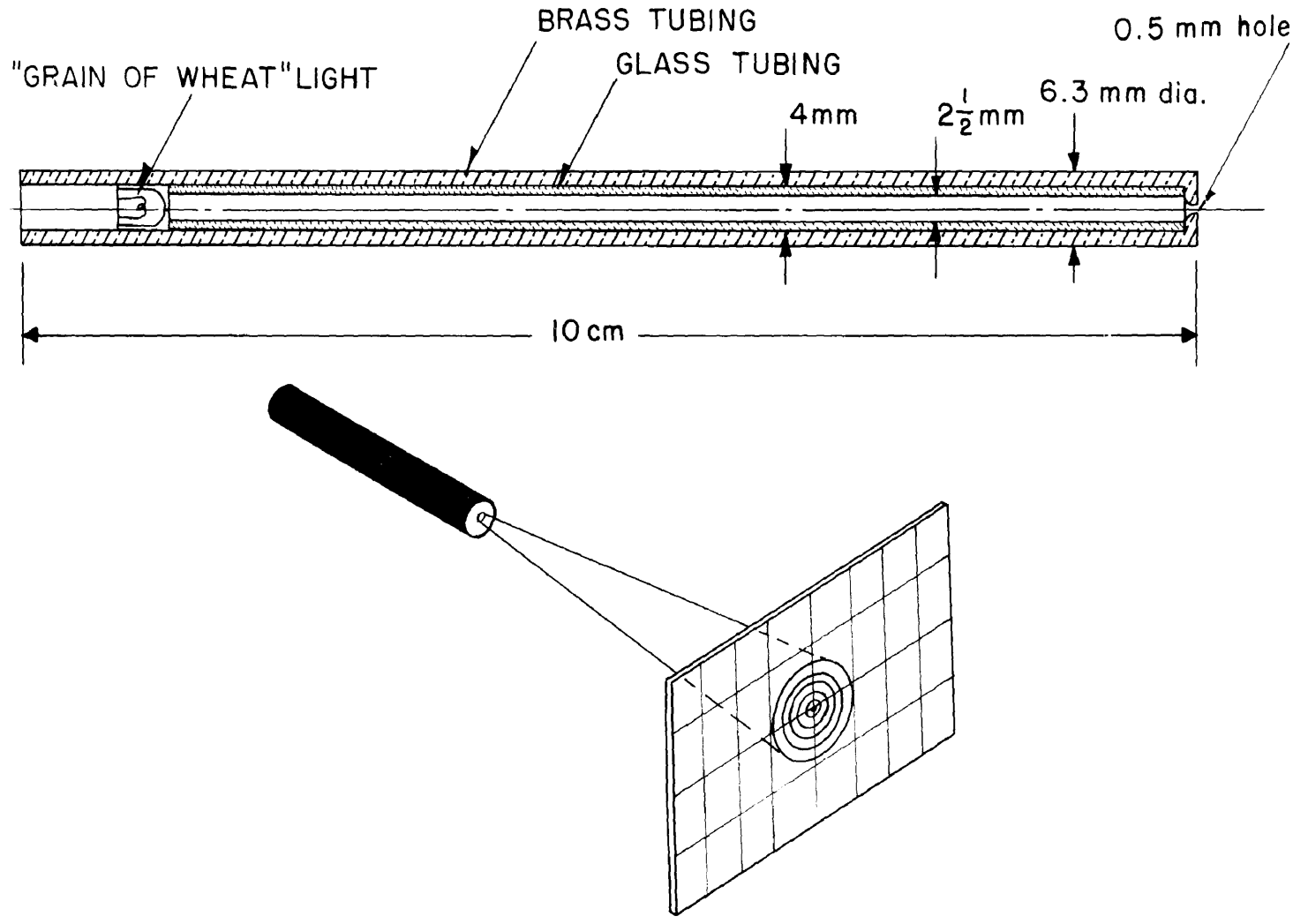

Fig. A4-4 OPTICAL POINTER FOR THE PRIMARY RAY

has been obtained and hence whether or not the burst in question has been counted. Thus the ratio of the number of bursts counted to the number of bursts produced will be the efficiency of detection of bursts.

The actual cosmic ray experiment was done at high altitudes. A flux which is isotropically distributed over the upper hemisphere and zero over the lower hemisphere was therefore selected for the primary rays. It was then possible to take, for the coordinates x_1 and y_1, numbers from 00 to 99 inclusive from a table of random numbers.[1] The numbers for φ and each of the M values of φ' were taken in a similar manner with the exception that a third digit was needed in each case to determine whether the counting should proceed in a clockwise (even digit) or counter-clockwise (odd digit) direction on the circular scale (which was divided 0 to 99 clockwise and 1 to 100 counter-clockwise). The numbers for θ had to be weighted by a factor $\sin\theta\cos\theta$ and thus the integral distribution function $\sin^2\theta$ was normalized to 99 at θ_{max} (telescope cutoff) and the abscissa was expanded such that the interval $0 \leq \theta \leq 90^\circ$ was equal to the interval $0 \leq \theta \leq$ 50 divisions (see Fig. A4-5). Hence the values θ were determined by taking a random number from 00 to 99, entering the curve of Fig. A4-5 at this number from the ordinate and finding the value of the abscissa. There is little information on the distributions in

---

[1] M. G. Kendall and B. Babington Smith, Tracts for Computers No. XXIV, Tables of Random Sampling Numbers, Department of Statistics, Univ. of London, University College, Cambridge Univ. Press, 1946.

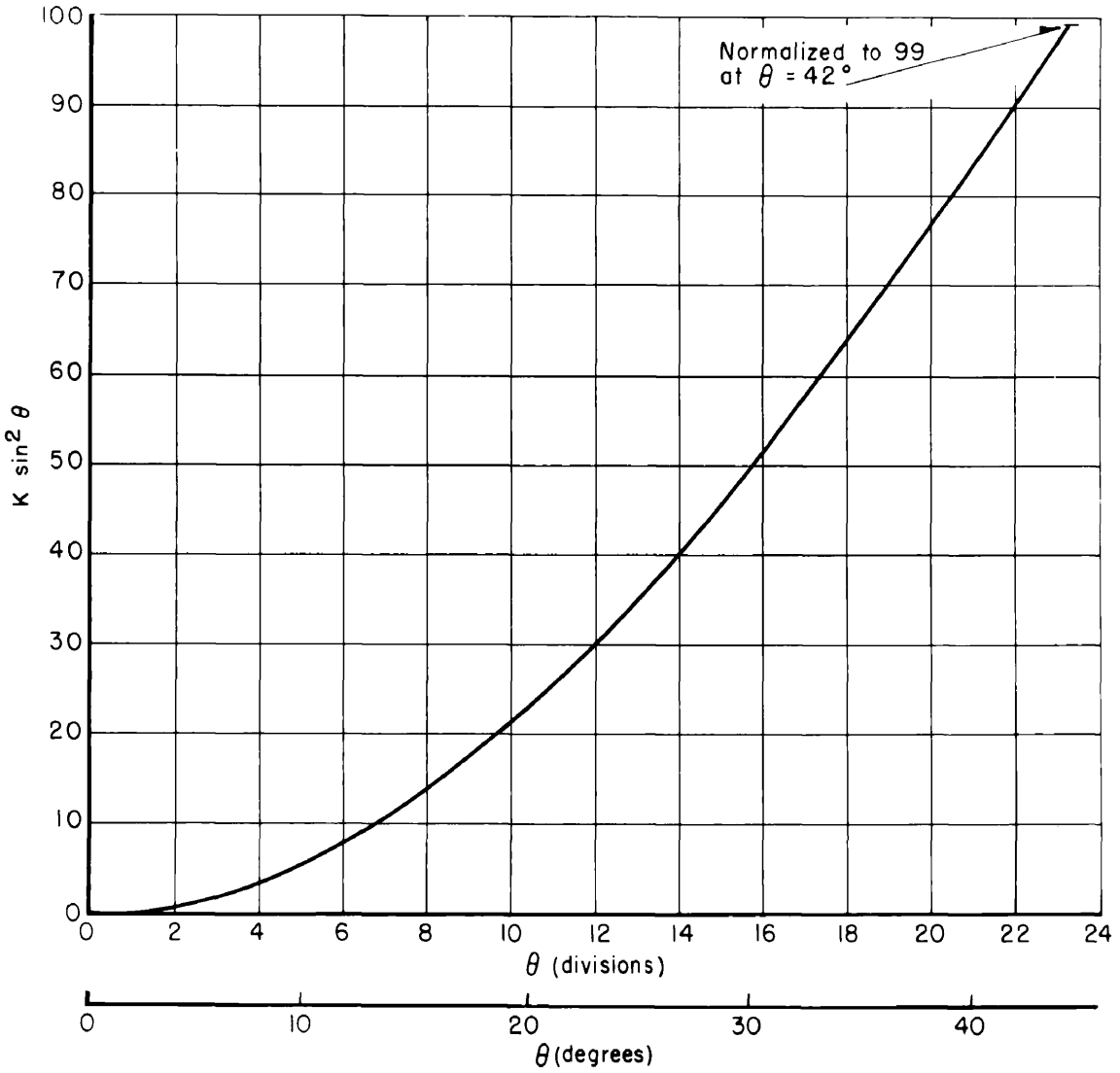

Fig. A4-5 RELATIVE NUMBER OF PRIMARY RAYS WITH ANGLES LESS THAN Θ vs Θ WITHIN THE ZENITH ANGLE BOUNDARY OF THE TELESCOPE

θ' and M; however, in the high altitude nuclear emulsion studies of Camerini et al[1] there are several experimental curves which show the angular distributions of several types of daughter particles with respect to the primary particle for various multiplicities. The shape of each of these curves is similar. By selecting the types of daughter particles appropriate for detection in the above described burst detector array (no short, heavy prongs) and limiting, to a reasonable number,[2*] the multiplicity of daughters that might be produced in a carbon target, a composite angular distribution curve was obtained (see Fig. A4-6). The integral angular distribution curve (the integral of this composite curve) was then normalized to 99 and the abscissa expanded such that the interval $0 \leq \theta' \leq 180^{\circ}$ was equal to the interval $0 \leq \theta' \leq 100$ divisions (see Fig. A4-7). Values for θ' were then obtained as in the previous case of θ. An histogram in the work of Camerini et al[1] shows a flat distribution of shower multiplicities out to 6 and zero beyond for primary particles of

---

[1] U. Camerini, J. H. Davies, P. H. Fowler, C. Franzinetti, W. O. Lock, H. Muirhead, D. H. Perkins and G. Yekutieli, Nuclear Transmutations Produced by Cosmic Ray Particles of Great Energy, Part VI. Experimental Results on Meson Production, Phil. Mag. 42, 1241 (1951).

[2] E. Pickup and L. Voyvoidic, Phys. Rev. 84, 1190 (1951).

*From the work of Pickup and Voyvodic[2], it is computed that the maximum number of charged pions would be 4 for an incoming 10^{10} ev proton (median energy at geomagnetic latitude 41°N) and that a maximum of 7 charge nucleons could be obtained from a carbon nucleus. These values are in good agreement with the experimental findings of Camerini et al.[1]

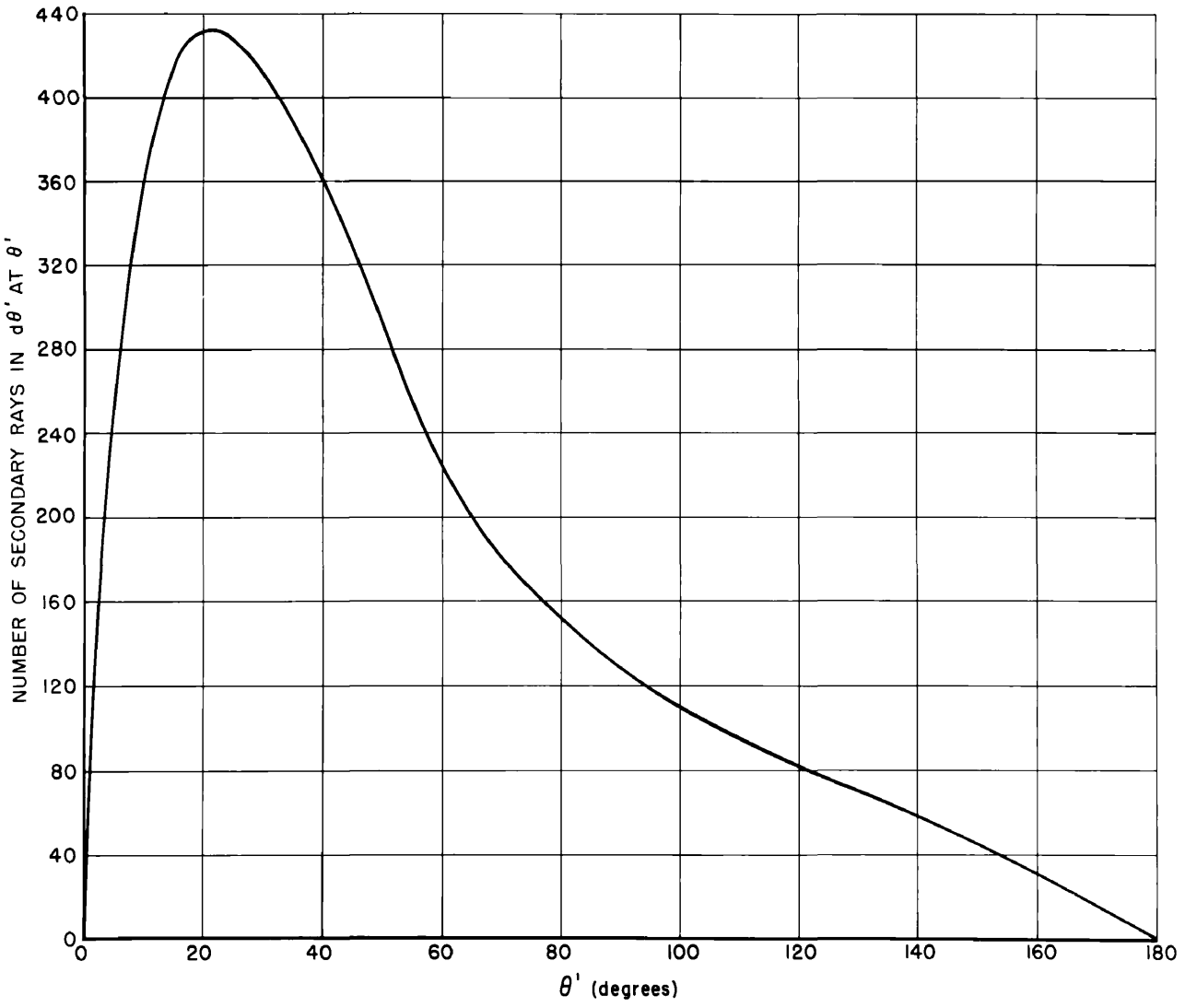

Fig. A4-6 NUMBER OF SECONDARY (DAUGHTER) RAYS IN dΘ' AT Θ' vs Θ'

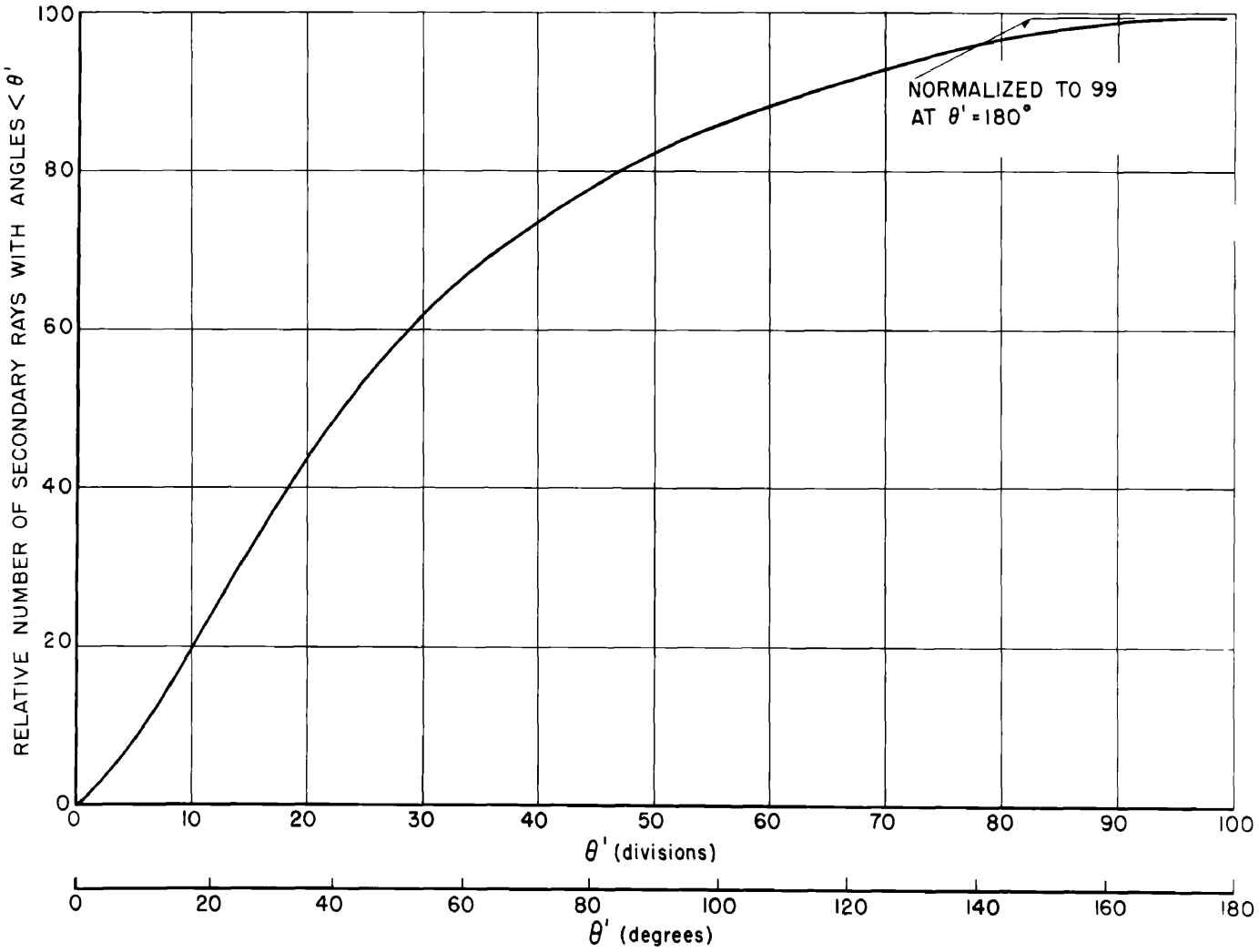

Fig. A4-7 RELATIVE NUMBER OF SECONDARY (DAUGHTER) RAYS WITH ANGLES LESS THAN Θ' vs Θ'

energy $4.3 \cdot 10^9$ ev (the magnetic cut off energy at $\lambda = 41^{\circ}N$ is $4.5 \cdot 10^9$ ev, thus this particular histogram fitted best the energy range for the area in which the balloon flights were to be made) and by using various data obtained in this work it was determined that the distribution function for M could be assumed to be flat for $0 \leq M \leq 9$ in the primary energy range to be considered. The values for M were then obtained from random numbers from 0 to 9 inclusive since each possible value of M was to be given equal weight. Fig. A4-8 shows the method by which the random number tables were read.

At low angles of entry to the detector plane, the approximation of plane strip detectors was not good enough. These cases, however, were taken care of by placing two short hemi-cylinders to represent the actual counters near the end of the extendable pointer.

The detector plane was made in such a way that the distance from the detector plane to the c.g. of the target plane was variable in three steps in order to investigate the sensitivity of the detection efficiency to small changes in the detector plane efficiency. These three levels were 0, 2.5 and 5 cm on the twice scale model or 0, 1.25 and 2.5 cm for the actual cosmic-ray instrument (0 cm was the actual level used in the flight instrument, the other levels, 1.25 and 2.5 cm, were closer to the c.g. of the target plane).

The results of the statistical experiment are shown in the following table:

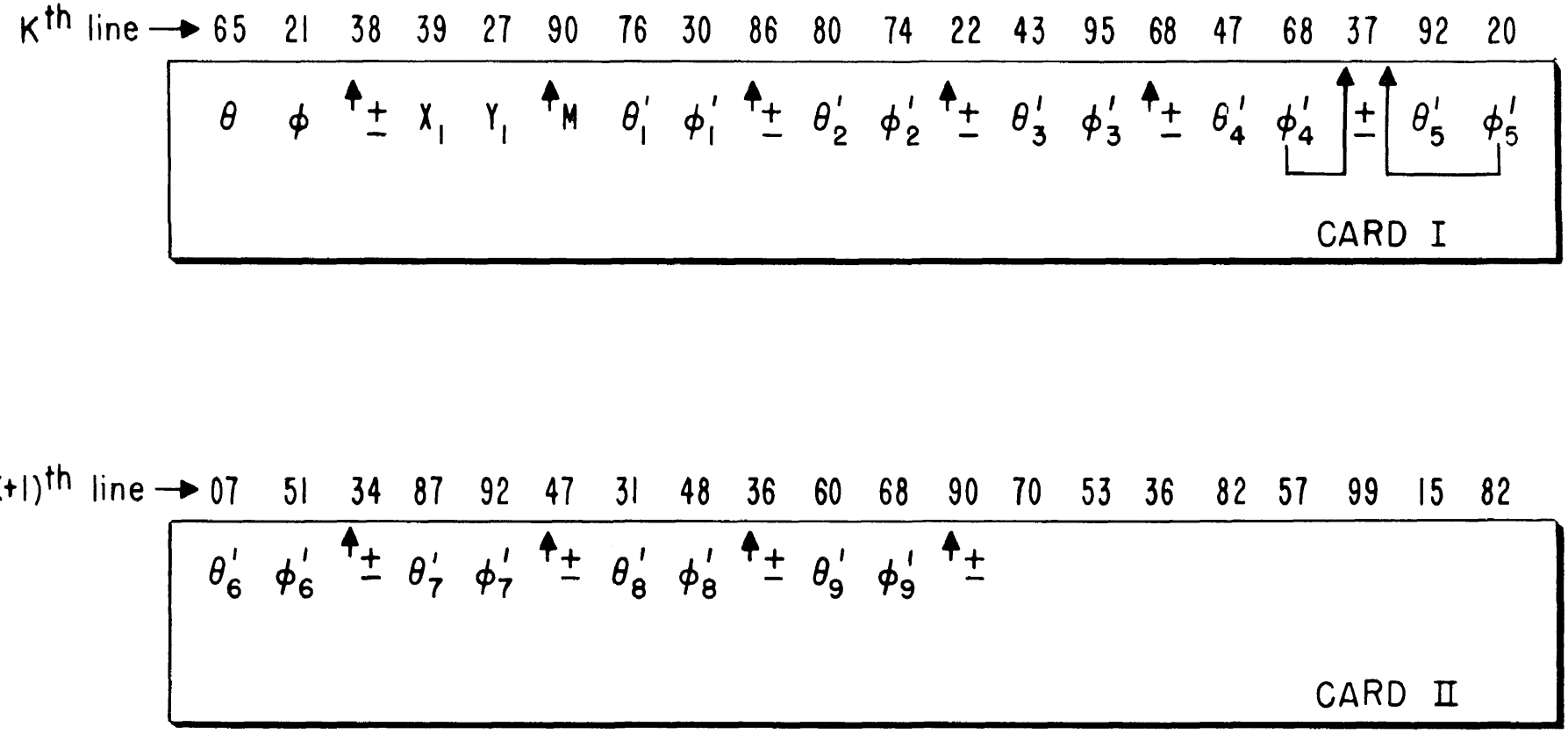

NOTE: Plus = even = clockwise , minus = odd = counterclockwise

Level (twice scale) cm	No. of primary rays	No. of triple coincidences	Efficiency*
0	1000	198	0.198 ± 0.013
2.5	1000	210	0.210 ± 0.013
5	1000	238	0.238 ± 0.013

The efficiencies are statistically the same but an increase is suggested by the trend from the lowest to the highest level. However, the eight instruments had been constructed with the burst detector array at the level zero and the gain, if any, did not justify the work of moving them.

Fig. A4-9 shows the differential distribution of triple coincidences, i.e. the number of triple coincidences in $\Delta M = 1$ at M vs M, for the 0 cm level. It is to be noted that the histogram of Fig. A4-9 can be used to investigate other possible distributions in M in the range $0 \leq M \leq 9$.

* The errors indicated are the standard deviations (see App. 1, Eq. (1)).

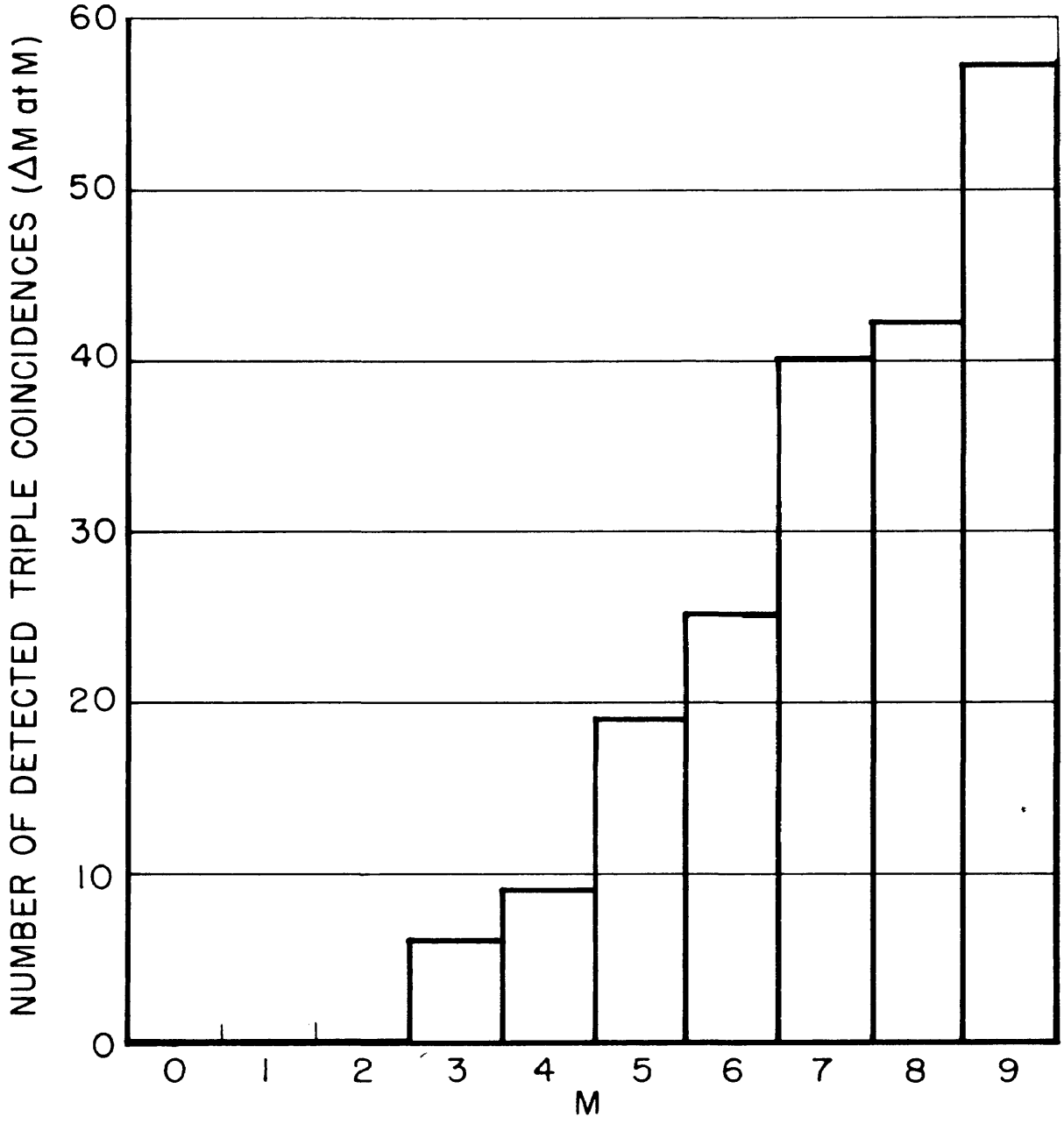
NUMBER OF DETECTED TRIPLE COINCIDENCES (ΔM at M)
60
50
40
30
20
10
0
0 1 2 3 4 5 6 7 8 9
M

APPENDIX 5

Duration Time of Recorded Output Pulses

For maximum ease of reducing the recorded data, the output pulses should be as long as is compatible with good resolution. Since the recorded events will follow a Poisson distribution, the probability that N events will occur in time t is given by

$$P(N,t) = \frac{(\lambda t)^N}{N!} e^{-\lambda t}$$

where

$$P(N,t) = 1.$$

Now

$$\bar{N} = \sum_{N=0}^{\infty} N P(N,t) = \lambda t e^{-\lambda t} \sum_{N=0}^{\infty} \frac{(\lambda t)^{(N-1)}}{(N-1)!}$$

or $\bar{N} = \lambda t e^{-\lambda t} e^{\lambda t} = \lambda t$

then $\lambda = \bar{N}/t = \bar{n}$, the average time rate of events. Thus:

$$P(N,t) = \frac{(\bar{n}t)^N}{N!} e^{-\bar{n}t}$$

and the probability that no event will occur in time τ is

$$P(0,\tau) = e^{-\bar{n}\tau}.$$

But then, τ is just the recording time that must be allowed for each event with probability $P(0,\tau)$ that other events will not intefere with the readability of the record.

In this case if $P = 0.9$ then $\bar{n}\tau = 0.1$. The expected maximum telescope counting rate was calculated to be 3 sec^{-1} (this is the counting rate that would be expected at the Pfofzer maximum at $\lambda = 41^{\circ}N$ from a telescope of geometric factor of about 7 cm^2 steradians) and the maximum burst rate would be 20 per cent of this value. Hence:

$$\tau_T = \frac{1}{10} \cdot \frac{1}{3} = \frac{1}{30} \text{ sec}$$

$$\tau_B = \frac{1}{10} \cdot \frac{1}{.2 \cdot 3} = \frac{1}{6} \text{ sec}$$

It is considered that 0.05 inches is an adequate resolution distance on the final record for large pulses with a definite character. Using the pulse width determined above, it is seen that in order to resolve completely 90 per cent of the telescope counts, the recording must be made at 3 in/sec. Assuming that the reader can separate no more than two events which may overlap, the resolution efficiency can be calculated from the theorem of total probability. The probability for the mutually exclusive events $N \geq 2$ to fail to occur in the interval τ is given by

$$P = 1 - \sum_{N=2}^{\infty} P(N,\tau) = \sum_{N=0}^{1} P(N,\tau)$$

since $\sum_{N=0}^{\infty} P(N,\tau) = 1$. Thus in the case at hand $\bar{n}\tau = .1$ and $P = 0.995$. Satisfactory resolution will then be obtained if the above values of τ_T and τ_B are used for the telemetered pulse widths.

The output pulse from each thyratron will be of the form $\Delta V = - Ve^{-t/RC}$ where V is approximately 75 v assuming full recovery

of the thyratron circuit prior to the initiation of the event in question. This 75 v exponential pulse can then be differentiated and the resulting positive overshoot can be diode clipped to give a tall saw tooth pulse. This pulse can now be clipped at a low negative voltage level to obtain a nearly rectangular wave form. With an appropriate selection of time constants and clipping voltages, the resulting output pulses (after diode mixing) are shown in Fig. A5-1. It is seen, from the figure, that one is able to pick out easily the type of event which has occurred even though two types of event are recorded on each channel.

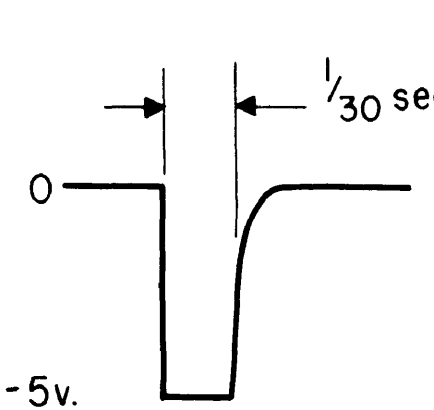

TELESCOPE EVENT

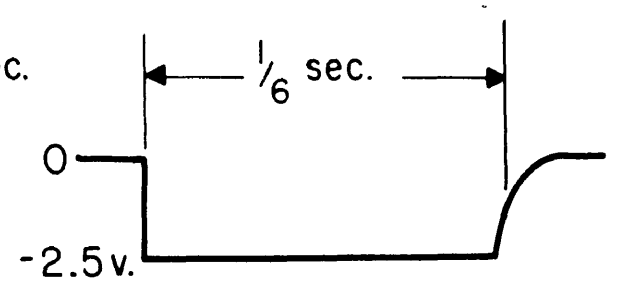

BASIC BURST EVENT

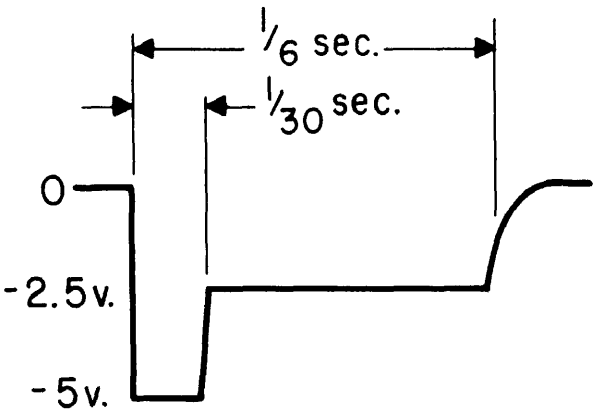

BURST EVENT

(composed by mixing the telescope event with the basic burst event through diodes)

Burst event followed by a telescope event

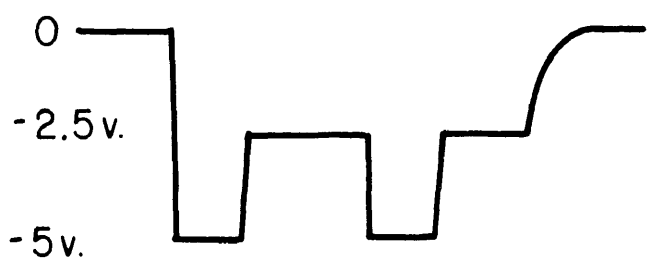

Burst event followed by a burst event

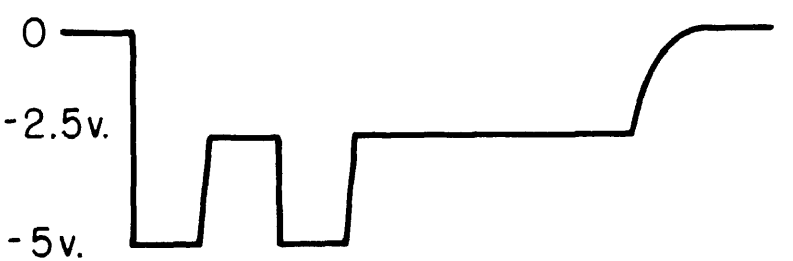

Fig. 5-1

APPENDIX 6

Tabulation of Indexing Times, Flight Data and Frequency Calibration of Temperature Channel

Table A6-1 - Indexing Times

Approximate Time of Index Pip - C.S.T.	Time on Record - Minutes -
0942	23.95 (Take off)
0949	30.95
1020	59.92
1049.5	89.45
1119.5	119.44
1147.5	148.38
1218.5	178.38
1248.5	208.43
1318.5	238.43
1348.5	267.43
1417.5	297.44

Table A6-2 - Flight Data

Legend

Ch. 1 - End of Time Interval, min.

Ch. 2 - Internal Gondola Temperature, inches.

Ch. 3 - 0 cm C - T and B

Ch. 4 - 1 cm C - T and B

Ch. 5 - 3 cm C - T and B

Ch. 6 - 6 cm C - T and B

T - Telescope Counting Rate, $min.^{-1}$

B - Burst Detector Counting Rate, $min.^{-1}$

		Ch. 3		Ch. 4		Ch. 5		Ch. 6	
Ch. 1	Ch. 2	T	B	T	B	T	B	T	B
1	3.00	12	0	5	0	7	0	9	0
2	3.02	4	0	8	1	3	0	11	0
3	3.04	11	0	14	0	4	1	6	0
4	3.06	9	0	6	0	8	0	8	0
5	3.07	9	0	9	0	11	0	9	0
6	3.08	6	0	5	0	9	1	5	0
7	3.10	10	0	3	0	9	0	6	0
8	3.10	8	1	10	0	13	0	11	0
9	3.11	8	0	3	0	11	0	13	0
10	3.11	4	0	11	0	8	0	7	0
11	3.12	11	0	14	1	5	0	8	0
12	3.11	7	0	9	0	4	0	5	0
13	3.14	10	0	10	0	3	0	5	0
14	3.14	12	0	3	0	6	0	4	0
15	3.18	7	0	7	0	6	1	17	0
16	3.19	6	0	9	0	5	0	9	0
17	3.18	16	0	9	0	9	0	10	0
18	3.20	9	0	5	0	10	0	11	1
19	3.20	2	0	3	0	5	0	10	0
20	3.21	5	0	10	0	6	0	8	1

Ch. 1	Ch. 2	Ch. 3		Ch. 4		Ch. 5		Ch. 6	
		T	B	T	B	T	B	T	B
21	3.23	10	0	5	0	6	0	11	0
22	3.22	8	0	5	0	5	0	8	0
23	3.24	9	0	8	0	7	0	7	0
24	3.25	6	0	8	0	11	0	5	0
25	3.28	8	0	7	0	6	0	12	0
26	3.29	5	0	6	0	10	1	8	0
27	3.29	9	0	8	0	9	0	14	0
28	3.31	12	1	7	0	9	0	9	2
29	3.32	16	0	8	0	9	0	16	0
30	3.32	22	0	16	0	5	0	15	0
31	3.31	15	2	12	1	8	1	8	0
32	3.29	15	0	13	0	17	0	14	0
33	3.25	16	1	11	0	11	0	8	0
34	3.27	11	0	12	0	8	0	9	0
35	3.29	11	0	19	0	20	1	33	0
36	3.28	23	0	22	0	18	0	17	0
37	3.29	32	0	14	1	14	1	20	0
38	3.29	26	0	30	0	16	0	22	0
39	3.30	31	1	23	0	34	0	20	1
40	3.31	33	0	29	0	28	0	25	0
41	3.29	27	0	30	0	29	1	35	0
42	3.32	44	0	39	0	36	0	41	0
43	3.31	50	0	44	0	39	0	40	0
44	3.31	43	0	52	0	57	0	62	1
45	3.30	59	0	38	2	57	2	43	0
46	3.30	61	1	59	1	50	0	69	1
47	3.30	63	0	67	1	56	0	66	0
48	3.31	69	0	83	0	52	0	80	0
49	3.31	69	0	78	1	66	0	68	0
50	3.31	82	0	77	0	74	0	77	1
51	3.31	72	1	84	0	71	0	88	0
52	3.32	75	0	97	0	90	0	88	1
53	3.32	94	1	101	0	105	1	98	0
54	3.33	105	1	107	1	95	2	125	1
55	3.33	108	2	96	0	120	0	92	0
56	3.30	107	1	123	2	117	0	116	0
57	3.31	118	0	99	0	128	0	117	3
58	3.31	127	0	105	0	122	1	133	0
59	3.32	141	0	108	0	136	1	134	1
60	3.30	133	0	136	0	131	1	138	2

Ch. 1	Ch. 2	Ch. 3		Ch. 4		Ch. 5		Ch. 6	
		T	B	T	B	T	B	T	B
61	3.32	157	0	110	1	125	0	148	3
62	3.31	154	1	147	1	130	1	134	1
63	3.31	147	1	149	0	153	1	140	2
64	3.30	162	1	120	1	151	1	149	2
65	3.29	148	0	147	0	159	0	147	0
66	3.28	160	1	154	1	154	1	147	1
67	3.28	160	2	159	2	164	0	150	3
68	3.27	165	0	153	1	157	1	171	1
69	3.25	202	0	182	0	155	3	167	0
70	3.24	178	1	162	0	170	0	160	1
71	3.21	168	2	137	1	163	2	182	3
72	3.19	168	0	178	1	164	3	176	1
73	3.18	185	0	170	1	174	2	179	4
74	3.17	174	2	154	2	168	0	166	1
75	3.16	189	1	168	1	165	1	184	1
76	3.15	199	1	157	1	164	1	160	6
77	3.15	209	0	161	0	176	3	181	2
78	3.14	176	1	164	0	172	2	186	1
79	3.13	180	1	169	3	179	0	193	1
80	3.11	178	2	176	0	167	2	181	3
81	3.10	183	1	181	2	168	0	174	1
82	3.07	196	0	179	1	177	1	173	1
83	3.07	191	1	168	2	174	1	179	1
84	3.06	212	0	182	2	165	4	168	5
85	3.08	191	2	167	1	168	3	177	7
86	3.08	205	1	183	2	174	2	180	3
87	3.05	190	0	160	0	167	2	168	4
88	3.07	181	4	151	1	160	1	186	2
89	3.09	156	2	166	1	162	2	163	2
90	3.11	159	2	147	1	172	2	155	3
91	3.10	185	1	166	0	163	3	143	1
92	3.10	182	1	138	1	164	2	154	6
93	3.13	136	1	153	1	153	2	174	9
94	3.14	151	4	143	2	155	4	132	4
95	3.10	177	0	131	4	149	3	139	2
96	3.14	163	1	143	3	157	2	135	4
97	3.15	174	0	155	2	160	3	132	2
98	3.13	152	0	134	2	158	2	157	8
99	3.14	140	2	131	1	136	1	132	0
100	3.16	144	1	118	0	140	4	138	0

		Ch. 3		Ch. 4		Ch. 5		Ch. 6	
Ch. 1	Ch. 2	T	B	T	B	T	B	T	B
101	3.12	140	1	131	2	144	1	137	1
102	3.12	128	2	131	1	142	2	134	0
103	3.13	122	3	137	0	133	2	113	3
104	3.14	156	1	121	2	133	3	128	7
105	3.13	138	2	138	1	120	1	134	6
106	3.13	121	1	109	1	130	3	127	6
107	3.15	132	0	137	4	128	2	111	4
108	3.16	124	4	108	2	118	4	131	5
109	3.13	136	1	119	3	108	1	127	8
110	3.13	134	1	121	3	126	1	119	6
111	3.12	121	2	107	1	130	1	135	3
112	3.12	132	1	107	1	116	2	132	5
113	3.19	126	0	108	2	120	3	115	5
114	3.19	115	2	121	4	108	0	119	6
115	3.19	116	0	104	0	107	7	126	4
116	3.14	110	2	108	1	107	4	97	4
117	3.19	115	2	95	4	117	1	122	4
118	3.18	108	1	102	1	100	3	100	4
119	3.18	135	0	129	4	111	4	119	3
120	3.20	112	1	93	3	118	3	107	1
121	3.25	129	0	96	1	107	4	107	2
122	3.28	94	0	120	2	102	2	98	5
123	3.30	108	1	78	1	95	4	94	6
124	3.30	120	5	97	1	104	3	103	3
125	3.31	112	1	90	2	98	3	110	3
126	3.33	117	1	96	0	105	3	96	3
127	3.35	104	2	90	4	102	2	98	4
128	3.33	110	1	107	2	109	2	104	4
129	3.36	116	1	99	1	92	2	96	4
130	3.35	110	0	93	2	86	2	123	0
131	3.30	114	1	97	1	98	2	111	8
132	3.34	104	0	90	2	93	1	84	0
133	3.32	91	1	84	1	78	1	80	6
134	3.36	83	0	82	4	83	3	84	9
135	3.35	108	2	101	2	100	3	121	4
136	3.36	85	1	82	1	92	1	83	0
137	3.30	93	0	88	2	95	2	90	5
138	3.36	85	1	85	3	88	1	90	2
139	3.40	96	2	75	2	102	2	82	2
140	3.42	85	2	96	0	74	7	82	6

Ch. 1	Ch. 2	Ch. 3		Ch. 4		Ch. 5		Ch. 6	
		T	B	T	B	T	B	T	B
141	3.33	83	0	78	2	83	3	86	6
142	3.28	85	1	93	1	81	1	92	9
143	3.33	93	2	81	0	91	1	76	6
144	3.28	77	1	87	2	90	3	70	9
145	3.33	79	2	78	3	78	3	89	5
146	3.38	79	1	82	2	81	0	71	6
147	3.39	90	1	76	0	71	2	98	6
148	3.42	84	4	90	1	92	3	68	5
149	3.41	94	1	89	1	83	4	93	5
150	3.36	88	2	75	3	83	1	83	8
151	3.34	120	1	78	0	88	1	87	0
152	3.36	101	2	60	1	76	4	89	4
153	3.35	103	0	65	2	59	1	89	0
154	3.38	76	4	97	0	84	0	78	1
155	3.39	83	2	66	1	83	4	94	7
156	3.38	84	1	72	2	88	2	77	3
157	3.37	64	0	94	2	76	5	72	8
158	3.39	94	2	81	2	77	0	83	1
159	3.40	74	0	82	2	71	1	73	7
160	3.40	74	1	84	2	86	2	82	7
161	3.42	80	1	77	2	83	4	81	1
162	3.45	86	3	72	0	92	0	89	5
163	3.46	73	3	91	5	88	4	77	5
164	3.48	82	3	77	2	73	2	73	6
165	3.50	71	1	63	1	63	2	76	3
166	3.50	82	0	62	2	78	4	76	2
167	3.50	83	0	53	3	76	0	84	3
168	3.50	80	0	67	1	82	1	83	9
169	3.52	87	0	65	3	66	3	87	6
170	3.52	75	1	71	0	68	4	74	9
171	3.52	68	1	72	1	61	2	67	4
172	3.55	78	3	69	0	77	3	91	2
173	3.57	77	2	58	0	83	2	86	3
174	3.50	62	3	77	2	86	0	93	4
175	3.45	82	2	73	5	73	2	80	3
176	3.44	79	0	58	0	69	5	77	9
177	3.43	73	0	64	1	62	3	88	3
178	3.43	78	2	88	1	67	0	72	5
179	3.43	93	1	63	1	81	6	75	8
180	3.51	72	2	80	2	74	6	69	2

Ch. 1	Ch. 2	Ch. 3		Ch. 4		Ch. 5		Ch. 6	
		T	B	T	B	T	B	T	B
181	3.57	77	0	67	2	72	3	70	5
182	3.57	93	0	81	2	57	2	82	0
183	3.58	66	2	86	2	69	4	74	4
184	3.53	78	1	62	1	71	2	66	4
185	3.58	72	1	69	1	74	5	71	2
186	3.58	83	0	68	0	76	4	84	9
187	3.59	83	1	61	1	75	3	83	4
188	3.60	78	3	81	4	68	5	86	5
189	3.62	73	1	63	2	79	1	76	8
190	3.60	76	1	65	3	59	2	78	4
191	3.63	81	1	75	0	74	1	72	1
192	3.64	86	1	75	1	74	5	92	8
193	3.66	77	0	55	3	83	1	81	1
194	3.67	83	1	56	2	75	1	78	4
195	3.69	83	2	63	1	62	3	79	4
196	3.69	68	0	62	1	69	8	71	3
197	3.68	89	0	67	0	53	2	73	1
198	3.69	55	2	59	1	75	3	68	1
199	3.71	74	1	75	0	67	3	86	9
200	3.70	73	1	59	1	56	3	76	5
201	3.69	67	0	67	0	69	4	79	1
202	3.71	68	2	69	1	76	5	77	2
203	3.69	69	3	74	2	74	2	66	3
204	3.58	87	0	54	2	79	8	69	8
205	3.58	75	2	68	0	58	5	87	4
206	3.59	73	2	53	1	70	2	73	1
207	3.58	99	2	76	2	75	4	81	5
208	3.59	68	1	52	0	73	3	67	9
209	3.58	79	1	58	0	61	1	85	5
210	3.59	76	0	67	4	68	5	94	6
211	3.60	87	3	57	4	59	1	76	2
212	3.61	91	0	62	1	53	4	74	1
213	3.61	68	1	74	4	56	1	82	9
214	3.59	83	2	78	3	64	2	82	1
215	3.60	78	2	58	1	83	3	92	9
216	3.61	91	1	65	2	55	2	91	8
217	3.60	70	1	67	4	65	3	86	6
218	3.62	83	1	64	1	82	0	83	10
219	3.62	82	1	52	1	67	2	88	3
220	3.62	81	0	74	2	63	1	77	7

Ch. 1	Ch. 2	Ch. 3		Ch. 4		Ch. 5		Ch. 6	
		T	B	T	B	T	B	T	B
221	3.64	92	2	68	0	53	3	75	0
222	3.64	73	0	67	0	65	2	73	8
223	3.66	73	0	65	4	71	4	75	0
224	3.65	88	1	66	2	61	2	69	6
225	3.68	79	0	75	0	60	1	83	4
226	3.69	86	0	69	3	54	5	80	9
227	3.68	83	0	59	0	83	2	98	1
228	3.70	92	1	62	0	82	3	93	4
229	3.69	70	0	72	0	75	5	94	2
230	3.70	89	0	53	0	71	3	76	2
231	3.71	85	0	73	1	83	2	74	7
232	3.73	98	1	69	1	80	2	67	8
233	3.73	84	0	65	1	59	0	73	2
234	3.74	87	1	66	1	78	4	86	0
235	3.71	63	0	67	0	55	1	75	2
236	3.73	84	0	65	0	72	0	89	2
237	3.71	94	2	72	0	54	2	87	6
238	3.72	91	1	64	1	75	2	95	11
239	3.65	79	1	65	4	70	1	81	5
240	3.80	71	3	71	0	74	2	69	3
241	3.81	77	2	72	1	68	2	78	0
242	3.79	95	1	60	3	75	6	67	9
243	3.80	98	3	71	2	73	0	66	8
244	3.79	76	3	63	3	61	1	85	4
245	3.79	91	1	83	1	61	0	76	3
246	3.81	78	2	81	0	73	4	67	7
247	3.81	93	1	60	2	69	2	96	5
248	3.80	84	1	67	0	70	1	98	6
249	3.81	91	0	76	2	63	2	95	2
250	3.78	69	1	73	1	65	3	84	0
251	3.80	76	1	62	0	60	2	87	4
252	3.81	95	2	76	1	68	2	84	4
253	3.80	86	0	69	1	81	3	88	5
254	3.81	82	2	76	2	68	1	74	9
255	3.80	78	0	71	0	78	3	90	1
256	3.82	67	1	73	0	82	3	98	5
257	3.83	74	1	80	3	83	0	93	5
258	3.81	98	3	64	3	81	1	81	9
259	3.82	90	3	73	1	63	3	85	7
260	3.83	87	1	76	3	65	5	73	7